TOXIC SUBSTANCES FROM COAL COMBUSTION
A Comprehensive Assessment

Quarterly Report

Reporting Period Start Date: 07/01/1999 End Date: 09/30/1999

Principal Authors:
CLSenior, T Panagiotou (1); FE Huggins (2)
GP Huffman, N Yap (2); JOL Wendt, W Seames (3)
MR Ames (4); AF Sarofim, J Lighty (5)
A Kolker R Finkelman CA Palmer SJ Mroczkowsky (6)
JJ Helble, R Mamani-Paco (7)

Report Issue Date: 11/01/1999

DE-AC22-95PC95101--15

(1) Physical Sciences Inc
20 New England Business Center
Andover, MA 01810-1077
(2) University of Kentucky
Lexington, KY 40506-0059
(3) University of Arizona
Tucson, AZ 85721
(4) Massachusetts Institute of Technology
Cambridge, MA 02139
(5) University of Utah
Salt Lake City, UT 84112
(6) U.S. Geological Survey
Reston, VA 20192
(7) University of Connecticut
Storrs, CT 06269

TABLE OF CONTENTS

LIST OF FIGURES

LIST OF FIGURES (Continued)

LIST OF FIGURES (Continued)

LIST OF FIGURES (Continued)

LIST OF TABLES

LIST OF TABLES (Continued)

ABSTRACT

The Clean Air Act Amendments of 1990 identify a number of hazardous air pollutants (HAPs) as candidates for regulation. Should regulations be imposed on HAP emissions from coal-fired power plants, a sound understanding of the fundamental principles controlling the formation and partitioning of toxic species during coal combustion will be needed. With support from the Federal Energy Technology Center (FETC), the Electric Power Research Institute, and VTT (Finland), Physical Sciences Inc. (PSI) has teamed with researchers from USGS, MIT, the University of Arizona (UA), the University of Kentucky (UK), the University of Connecticut (UC), the University of Utah (UU) and the University of North Dakota Energy and Environmental Research Center (EERC) to develop a broadly applicable emissions model useful to regulators and utility planners. The new Toxics Partitioning Engineering Model (ToPEM) will be applicable to all combustion conditions including new fuels and coal blends, low-NO_x combustion systems, and new power generation plants. Development of ToPEM will be based on PSI's existing Engineering Model for Ash Formation (EMAF).

This report covers the reporting period from 1 July 1999 to 30 September 1999. During this period the MIT INAA procedures were revised to improve the quality of the analytical results. Two steps have been taken to reduce the analytical errors. A new nitric acid leaching procedure, modified from ASTM procedure D2492, section 7.3.1 for determination of pyritic sulfur, was developed by USGS and validated. To date, analytical results have been returned for all but the last complete round of the four-step leaching procedure. USGS analysts in Denver have halted development of the cold vapor atomic fluorescence technique for mercury analysis procedure in favor of a new direct analyzer for Hg that the USGS is in the process of acquiring. Since early June, emphasis at USGS has been placed on microanalysis of clay minerals in project coals in preparation for use of the Stanford/USGS SHRIMP RG Ion Microprobe during August 1999. The SHRIMP-RG data confirm that Cr is present at concentrations of about 20 to 120 ppm, just below the electron microprobe detection limits (100 to 200 ppm), as suspected from Phase I microprobe work and previous studies of clay mineral separates. The University of Utah has started trial runs on the drop tube furnace to ensure that the gas analysis system is working properly and that the flow pattern within the furnace is laminar and direct. A third set of ASTM samples will be prepared at the University of Utah for the Phase I and Phase II coals. This time the INAA counting time will be optimized for the elements in which we are interested, guided by the results from the first two samples. The iodated charcoal which was used by MIT for vapor phase Hg collection was tested to see whether it collected other vapor phase metals. A second set of tests were performed at PSI using the entrained flow reactor (EFR). The University of Arizona's pilot-scale downflow laboratory combustion furnace was used to test the partitioning of toxic metals in the baseline experiments for the Phase II North Dakota lignite and the Pittsburgh seam bituminous coal at baghouse inlet sampling conditions. In addition, baseline data were collected on combustion of the Phase I Kentucky Elkhorn/Hazard bituminous coal. Emphasis at the University of Kentucky was placed on (1) collection of new Hg XAFS data for various sorbents, and (2) on collection of XAFS and other data for arsenic, sulfur, chromium and selenium in two baseline ash samples from the University of Arizona combustion unit. A preliminary interpretation of the mercury data is given in this report. Revision was made to the matrix for the intial experiments on mercury-ash interactions to be conducted at EERC. The

overall goal of this effort is to collect data which will allow us to model the interactions of mercury and fly ash (specifically, adsorption of Hg^0 and Hg^{+2} and oxidation of Hg^0) in the air heater and particulate control device of a coal-fired power plant. The simple mass balance model for emissions of mercury from coal-fired power plants was revised to further test our current understanding of mercury transformations in flue gas. Improvements were made to the model for major element vaporization. The method for predicting vaporization of major elements predicts the total amount vaporized within a factor of two.

SECTION 1

EXECUTIVE SUMMARY

1. EXECUTIVE SUMMARY

The technical objectives of this project are:

a) To identify the effect of the mode-of-occurrence of toxic elements in coal on the partitioning of these elements among vapor, submicron fume, and fly ash during the combustion of pulverized coal,

b) To identify the mechanisms governing the post-vaporization interaction of toxic elements and major minerals or unburnt char,

c) To determine the effect of combustion environment (i.e., fuel rich or fuel lean) on the partitioning of trace elements among vapor, submicron fume, and fly ash during the combustion of pulverized coal,

d) To model the partitioning of toxic elements among various chemical species in the vapor phase and between the vapor phase and complex aluminosilicate melts,

e) To develop the new Toxics Partitioning Engineering Model (ToPEM), applicable to all combustion conditions including new fuels and coal blends, low-NO_x combustion systems, and new power generation plants.

A description of the work plan for accomplishing these objectives is presented in Section 2.1 of this report.

During this period the MIT INAA procedures were revised to improve the quality of the analytical results. Two steps have been taken to reduce the analytical errors. Estimates are included in this report on the reduction in errors of individual elements that are expected, based on these changes.

Incomplete pyrite extraction in the USGS leaching procedure has been noted previously. As a result, a new nitric acid leaching procedure, modified from ASTM procedure D2492, section 7.3.1 for determination of pyritic sulfur, was developed and validated. For the Ohio 5/6/7 coal it is clear from the preliminary leaching data that iron and arsenic are strongly associated with pyrite, as in many bituminous coals, consistent with microprobe date for pyrite. A much smaller pyrite association is indicated for Fe and As in the two low rank coals. These coals show a large HCl-leachable fraction we have previously interpreted as arsenate. For Cr, a significant HF-leachable fraction is shown for each of the coals, consistent with ion probe data for Cr in illite, reported in the section on microanalysis. However, each of the coals has significant (30 to 65%) unleached Cr, indicating an organic association for this fraction. For the other elements reported- potassium shows a strong silicate association- as it is a major component of illite/smectite. Sodium shows a significant ion-exchangeable component, especially in the low rank coals. Cobalt, uranium and scandium show mixed affinities that are dominated by organic, silicate, or HCl-leachable forms. USGS analysts in Denver have halted development of the cold vapor atomic fluorescence technique for mercury analysis procedure in favor of a new direct

analyzer for Hg that the USGS is in the process of acquiring. Since early June, emphasis at USGS has been placed on microanalysis of clay minerals in project coals in preparation for use of the Stanford/USGS SHRIMP RG Ion Microprobe during August 1999. The SHRIMP- RG data confirm that Cr is present at concentrations of about 20 to 120 ppm, just below the electron microprobe detection limits (100 to 200 ppm), as suspected from Phase I microprobe work and previous studies of clay mineral separates.

The University of Utah has started trial runs on the drop tube furnace to ensure that the gas analysis system is working properly and that the flow pattern within the furnace is laminar and direct. A preliminary test matrix has been formulated. A third set of ASTM samples will be prepared at the University of Utah for the Phase I and Phase II coals. This time the INAA counting time will be optimized for the elements in which we are interested, guided by the results from the first two samples. Seven samples will be generated.

The iodated charcoal which was used by MIT for vapor phase Hg collection was tested to see whether it collected other vapor phase metals. A second set of tests were performed at PSI using the entrained flow reactor (EFR). The result of the second test for Hg collection simply confirm that the sorbents collect 100% of the vapor phase Hg, and that they can be used at 105 C to prevent condensation. No other elements (e.g., As, Br, Cd, and Sb) were collected quantitatively in Test 1.

The University of Arizona's pilot-scale downflow laboratory combustion furnace was used to test the partitioning of toxic metals in the baseline experiments for the Phase II North Dakota lignite and the Pittsburgh seam bituminous coal at baghouse inlet sampling conditions. In addition, baseline data were collected on combustion of the Phase I Kentucky Elkhorn/Hazard bituminous coal.

Emphasis at the University of Kentucky was placed on (1) collection of new Hg XAFS data for various sorbents, and (2) on collection of XAFS and other data for arsenic, sulfur, chromium and selenium in two baseline ash samples from the University of Arizona combustion unit. There is a clear distinction in the Hg XAFS spectra and data between the carbonaceous sorbents and the two $Ca(OH)_2$ sorbents, which were the only inorganic sorbents to give acceptable XAFS data. For these latter two samples, it is clear that the sorption of $HgCl_2$ involves the formation of a Hg-O bond. This suggests that mercuric chloride will undergo chemisorption when the conditions are right. Hg XAFS experiments were also conducted on various fractions of fly-ash collected from the Cherokee power station, CO, by personnel at ADA Technologies, Inc. The data suggest that there is a specific fraction in the fly-ash carbon that is particularly effective for mercury sorption. The values of the Inflection Point Difference (IPD) from the second derivative of the XANES spectra would appear to reflect formation of Hg-Cl complexes, consistent with previous XAFS investigations of carbon-based sorbents

Revision was made to the matrix for the intial experiments on mercury-ash interactions to be conducted at EERC. The overall goal of this effort is to collect data which will allow us to model the interactions of mercury and fly ash (specifically, adsorption of Hg^0 and Hg^{+2} and oxidation of Hg^0) in the air heater and particulate control device of a coal-fired power plant. Ash

samples from the Phase II coals were collected at the University of Arizona down-fired combustor. Loss-on-ignition and surface area measurements were made on the ash samples.

The simple mass balance model for emissions of mercury from coal-fired power plants was revised to further test our current understanding of mercury transformations in flue gas. The predictions of mercury speciation, in terms of fraction as Hg^{+2} at the ESP inlet, agree well with measured values. The predictions are based primarily on the coal chlorine content and the LOI of the ash. Of these two factors, the coal chlorine content has the largest impact on mercury speciation. The model predicts the stack emissions very well. The prediction of speciation in the stack is not as good as the prediction of speciation at the ESP inlet, suggesting that the model has neglected some important transformations between the ESP inlet and the stack. Mercury transformations in the particulate control device (ESP) were not included in this model. The analysis shows that the behavior of mercury in the particulate control device has an impact on the speciation of mercury in the stack.

Improvements were made to the model for major element vaporization. The method for predicting vaporization of major elements predicts the total amount vaporized within a factor of two. Vaporization of alkali species is over-predicted, however. The assumption of combustion of the volatiles before char combustion provides better agreement between calculated and measured vaporization. The assumption of equilibrium between iron vapor and iron oxide in the ash gives better agreement between measured and predicted iron vaporization. Further work will be needed on the mechanisms for alkali vaporization. Improvements in the calculation of particle temperature and surface gas composition should improve the predictions.

SECTION 2

INTRODUCTION AND PROGRAM OVERVIEW

2. INTRODUCTION AND PROGRAM OVERVIEW

2.1 Introduction

Before electric utilities can plan or implement emissions minimization strategies for hazardous pollutants, they must have an accurate and site-specific means of predicting emissions in all effluent streams for the broad range of fuels and operating conditions commonly utilized. Development of a broadly applicable emissions model useful to utility planners first requires a sound understanding of the fundamental principles controlling the formation and partitioning of toxic species during coal combustion. PSI and its team members will achieve this objective through the development of an "Engineering Model" that accurately predicts the formation and partitioning of toxic species as a result of coal combustion. The "Toxics Partitioning Engineering Model" (ToPEM) will be applicable to all conditions including new fuels or blends, low-NO_x combustion systems, and new power systems being advanced by DOE in the Combustion 2000 program.

Based on a goal of developing and delivering this ToPEM model, a 5-year research program was proposed. This program is divided into a 2-year Phase I program and a 3-year Phase II program. The objective of the ongoing Phase II program is to develop an experimental and conceptual framework for the behavior of selected trace elements (arsenic, selenium, chromium, and mercury) in combustion systems and incorporate these concepts into a new engineering model. This Phase II objective will be achieved by a team of researchers from USGS, the Massachusetts Institute of Technology (MIT), the University of Arizona (UA), the University of Kentucky (UK), the University of Connecticut (UC), the University of Utah (UU), the University of North Dakota Energy & Environmental Research Center (EERC) and PSI. Model development and commercialization will be carried out by PSI.

2.2 Program Overview

Our general approach to the development of the ToPEM model is to break the process for toxic formation into sub-processes, each of which will be addressed by team members who are experts in the area. Ultimately, this will result in new sub-models which will be added to the existing Engineering Model for Ash Formation (EMAF) to create ToPEM. Table 2-1 describes the work breakdown structure for the Phase II program. Figure 2-1 illustrates the relationship between the elements of the Phase I work breakdown structure and the sub-processes. Each of the areas identified in the figure will be addressed in the Phase II program as described below.

Forms of Occurrence of Trace Elements in Coal

One of the most important questions to be answered in the program as a whole is whether the form of a particular element in the coal affects its form of emission at the end of the process. The answer to this question will determine the shape of the sub-models that must be developed in this program. Thus, a detailed understanding of the forms of individual trace elements in coal

Table 2-1. Task Breakdown

Technical Task	Team Member	Task (WBS) Number
Program management	PSI	1
Coal acquisition, characterization	PSI	2
Coal, ash trace element characterization	PSI	2
Coal (and ash) characterization -- forms of occurrence	UK, USGS	3, 4
Coal, ash trace element characterization and mercury capture and analysis	MIT	5.2
Mechanistic study: dilute bench scale combustion tests plus equilibrium, kinetic modeling	UU	5.1
Large scale tests at 100,000 Btu/h facility	UA	6
Mechanistic study of kinetic rates for gas-phase reactions	UC	10
Mercury-fly ash interactions at bench scale	EERC	11
Fundamental Engineering Model development	PSI	9.1
Inorganic emissions: literature survey and model validation	UC	9.2

provides a foundation for much of the rest of the program. Key issues that will be addressed in Phase II are the specific mineral associations of individual elements and the relationship between trace metal form and "standard" coal analyses.

Because of the importance of elemental form (e.g., sulfate versus silicate mineral) on partitioning, it is critical that coals representing a broad range of elemental forms be examined in this program. In Task 2 we will select and acquire a total of three coals for study in this program. The coals chosen will represent a broad range of elemental forms of occurrence taken from the major coal ranks and commercial coal seams used for pulverized coal power generation in the US. Once selected, fresh coal samples will be acquired and distributed to team members. These samples will be subjected to ultimate, proximate, and ASTM ash analysis. Coal samples will be analyzed for trace element concentrations by Neutron Activation Analysis (NAA) at the MIT Nuclear Reactor Laboratory (Task 5.2).

Advanced analytical techniques such as Mössbauer spectroscopy and Computer-Controlled Scanning Electron Microscopy (CCSEM) will be used by UK (Task 3) to determine the major mineral species present in the program coals and the combustion generated ash. Whole coal samples and density segregated coal samples will be studied. This analysis will provide important insight on the minerals present in the coal, how they interact during the combustion process, and how this interaction may affect the partitioning of toxic elements.

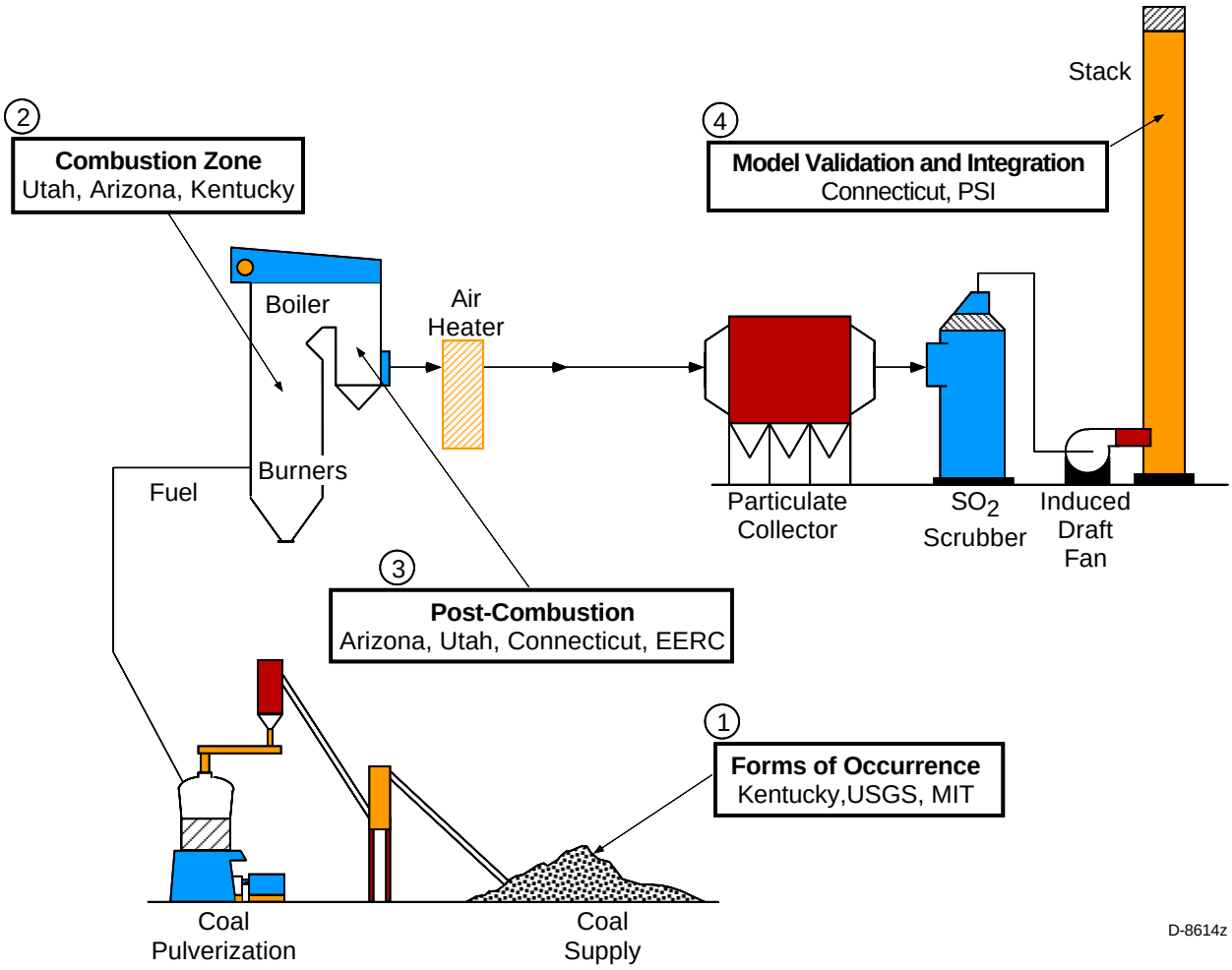

Figure 2-1. Phase II program organization.

Another important issue is the form-of-occurrence of the trace elements in the coal. In this task the mode of occurrence of As, Cr, and Se will be determined by combining XAFS and the Mössbauer/CCSEM derived data discussed above. Hg will also be evaluated where possible. Other less critical trace elements (Mn, Ni, Zn, Pb, U, etc.) may also be evaluated, especially if their abundance is unusually high in any of the program coals. In addition, the form-of-occurrence of Cl and S in coals and chars will be investigated.

As a complement to the XAFS analysis mentioned above, a unique protocol developed by USGS will be used in Task 4 to analyze selected raw coal, and size and density segregated coal, samples for trace element forms of occurrence. This protocol combines low temperature (< 200EC) ashing, chemical analysis, x-ray diffraction, coal segregation via flotation, ammonium acetate and selected acid leaching, electron microbeam measurements, and low and moderate temperature heating tests to determine the forms of elements in coal. Because of the unique combination of existing testing and analytical facilities available at USGS, the work will be conducted at USGS laboratories.

Combustion Zone Transformations

The effect of coal type and combustion conditions on the emission of the toxic trace elements will be investigated using the UU laminar-flow drop tube reactor (Task 5.1). The fundamental mechanisms of toxic species formation and partitioning will be determined from careful examination of the ash formed under a variety of combustion conditions. Measurements will be made of the partitioning of the trace elements in the three coals as a function of temperature and equivalence ratio. These measurements will provide the baseline data on the fraction vaporized. Individual size-segregated ash samples (collected with a cascade impactor) will then be analyzed by NAA for total composition and other analyses as needed, for example, Auger and STEM for surface composition, TEM and SEM for particle morphology, and possibly water washing and/or chemical leaching to determine the solubility of selected trace elements in the ash samples. Samples will also be submitted to UK for chemical species analysis by XAFS and other techniques.

Post-Combustion Transformations

The goal of this task is an increased understanding of the transformations of selected metals as the flue gases cool following the high temperature combustion zone. Bench scale experimentation will be carried out by several organizations as well as large scale combustion measurements. Advanced analytical methods will be used extensively to understand speciation of trace elements in the post-combustion flue gas.

At the UC (Task 10) experiments will focus on determination of trace vapor-ash particle reactions rates in post-combustion gases, including

- Identification of the rate controlling phenomena in the oxidation of arsenic under combustion conditions

- Relative rates of gas-phase reaction of elemental mercury with HCl and Cl_2 under combustion conditions

- Measurement of rates of heterogeneous conversion of HCl to Cl_2 in the presence of coal combustion products such as iron oxide, iron sulfate, and fly ash samples.

Interactions of mercury with ash and ash components at lower temperatures will be the focus of the effort at EERC in Task 11. A bench-scale sorbent evaluation system will be used to increase our understanding of the interactions between gas-phase mercury and coal ash. Experiments will explore the effects of temperature and the interactions between elemental mercury or mercuric chloride and fly ash samples generated under oxidizing conditions, the effect of mercury concentration on the interactions between elemental mercury and fly ash, and the effect of coal combustion conditions on the ash and ultimately on the interaction between mercury and ash.

On a larger scale in Task 6, UA will determine how both coal composition, detailed mineralogy and combustion conditions (including low NO_x conditions) govern the fate of toxic metals under practical time/temperature, self sustained, yet still aerodynamically well defined, pulverized coal combustion conditions. Program coals will be burned in the UA self-sustained combustor under premixed conditions. The baseline tests will employ the naturally occurring temperature profile for each coal at a stoichiometric ratio of 1.2. Samples will be withdrawn at several ports, representing a range of temperatures and residence times. Complete impactor samples will be collected and analyzed for each toxic metal (11 as listed in the CAAA plus U and Th) plus major elements. This will yield the particle size segregated toxic metal composition, which can be compared to data obtained from other tasks of this program. These data will then be examined to determine particle size dependence in order to infer possible mechanisms governing the fate of each metal.

Model Validation

UC will conduct a more in-depth review of the relevant field data on inorganic emissions (Task 9.2). In Phase II we will emphasize use of the field data to validate the models we will develop. The Phase II effort focuses on data from the following sources:

- EPRI PISCES
- DOE Program
- VTT (Finland)
- KEMA (Netherlands).

Important issues to be addressed when reviewing these data include mass balance closure, methods of analysis and sample collection, effect of APCD, effect of bulk coal ash chemistry, particle size distribution, and speciation of Hg.

Model Development

In Task 9.1, data obtained from subcontractor and PSI tasks will be combined to create a comprehensive model of the transformations of important inorganic species during combustion. This model, denoted the ToPEM, will be based on an existing model (the PSI Engineering Model for Ash Formation which predicts ash particle size and composition distributions – EMAF). Because the development of this model is strongly dependent on the mechanistic, equilibrium, and kinetic information being developed under the experimental tasks, ToPEM will incorporate information on the mechanisms controlling species behavior, equilibrium modeling where appropriate and kinetic modeling to mimic kinetic constraints on species behavior. During the later stages of the Phase II work, sufficient detailed information will be available to support specific modifications to EMAF in order to describe the combustion transformations of important inorganic trace elements. Based on the experimental studies, equilibrium modeling, and kinetic modeling, it will be clear which modifications are required. Once complete, the model will be validated using a combination of laboratory and field data. As part of the validation effort, coal and size fractionated ash samples collected from operating utility boilers will be provided by Dr. Esko Kauppinen of VTT, Finland. Once validated, the ToPEM will be

used to simulate the behavior of these and other coals under utility boiler conditions. The results from these simulations will then be compared to field data from PISCES obtained through EPRI participation in this program, DOE field sampling campaigns, and other relevant data in the literature. This validation procedure will ensure that the model developed as the result of the proposed research efforts accurately predicts the behavior of toxic metals species from a wide range of coals during the combustion process in any combustion system.

SECTION 3

RESULTS AND DISCUSSION

3. RESULTS AND DISCUSSION

3.1 Program Management (PSI)

An overview of the program was presented by J.Helble at Fortum in Finland. Fortum is part of a Finnish team working to develop a model of trace element emissions from fluidized bed boilers co-firing waste.

A program review meeting was held on 30 September 1999 at FETC-Pittsburgh. Team members presented work in progress. In addition, two guest speakers presented results obtained from fluidized bed combustion. Dr. Terttaliisa Lind from VTT in Finland presented the results of a study on the distribution of trace elements in the ash from a fluidized bed burning wood waste. Mr. Petri Kouvo from Fortum presented data on the distribution of trace elements from a fluidized bed burning mixtures of wood and waste.

The manuscripts for the special issue of Fuel Processing Technology were completed and sent to the publisher. Publication is tentatively scheduled for early in 2000. A manuscript based on the presentation of Sarofim at the Air Quality Conference (December 1998) was accepted for publication in Fuel Processing Technology. The title of the manuscript is "Emissions of Mercury, Trace Elements, and Fine Particles from Stationary Combustion Sources."

3.2 Coal Characterization (UK, USGS, MIT)

3.2.1 Trace Element Content of Coals

After discussions at UU, it was decided that the MIT INAA procedures needed to be changed from those used in Phase I in order to improve the quality of the analytical results. Two steps have been taken to reduce the analytical errors:

1. A second "longs" count will be used to reduce the statistical detection errors for several elements with long-lived activation products.

2. A newer set of NIST Standard Reference Materials are being used for Phase II which have either higher levels of the elements of interest or lower errors in their certified values.

Table 3-1 estimates the reduction in errors for individual elements that are expected, based on these changes. New INAA software makes it much easier to perform and record inter-standard comparisons for QA/QC purposes, and eliminates the need to enter data by hand, which will eliminate the possibility of errors in this step of the analyses.

Table 3-1. Projected Improved INAA Analyses of University of Utah Ash Samples

Element	Old Error	"New Error"	Comment
Mn	0.02		
V	0.04		
Al	0.04		
Fe	**0.05**	**0.02**	**longs 2**
La	0.06		
Sc	0.07	0.04	longs 2
Na	**0.07**	**0.02**	**new std. 1633b**
U	0.07		
Cr	**0.07**	**0.03**	**longs 2**
Co	0.07	0.03	longs 2
Ba	0.08		
Ce	0.08		
Sm	0.09		
Sb	0.09		
Th	0.09	0.05	longs 2
As	**0.10**	**0.02**	**new std. 1633b**
Sr	0.15		
Ti	0.15		
Zn	0.18	0.05	longs 2
Mg	**0.20**	**0.05**	**new std. 1633b**
Cl	0.24		sample limited
Mo	0.26	0.18	new std. 2710
Br	0.28		
K	**0.31**		**sample limited**
Hg	**0.32**		**sample limited**
Cd	0.67	0.30	new std. 2710
Se	**0.74**	**0.09**	**longs 2**

3.2.2 Forms of Occurrence of Trace Elements by Microprobe and Leaching Analyses

The USGS procedure is intended to determine quantitatively or semi-quantitatively the mode of occurrence of trace elements in coal. This is accomplished by an iterative selective leaching protocol, used in combination with a range of complementary techniques. In the leaching protocol, the amount of each element removed by four different reagents is compared to the concentration of that element in the whole coal to obtain the fraction of an element residing in a given coal component.

The sequence of leaching steps, and the intended results, are as follows: 1) exchangeable cations, and a fraction of the carbonate-hosted cations are removed by ammonium acetate; 2) cations primarily associated with carbonates and monosulfides such as galena, sphalerite and chalcopyrite are removed by hydrochloric acid; 3) silicate-associated cations are removed by hydrofluoric acid; and 4) elements associated with di-sulfides (pyrite and marcasite) are removed by nitric acid. Elements not leached by any of the four reagents may be present in the organic portions of the coal, or in insoluble phases such as zircon or titanium dioxides. Additionally, where mineral grains are completely encased by the organic matrix, these "shielded" grains may not be completely digested. As an internal check, leaching results are obtained for both the solid residues (by INAA) and leachates (by ICP-MS and ICP-AES). Element-specific methods are used for selenium (hydride generation) and mercury (see section on mercury). Quantitative results are obtained by interpreting the leaching data together with the results obtained by complementary techniques such as electron microprobe analysis.

The microprobe is especially useful for pyrite grains, as many of the elements of interest are present at concentration levels above the detection limit of about 100 ppm. Other essential components of the USGS procedure include semi-quantitative determination of mineralogy by X-ray diffraction (XRD) analysis of low temperature ash (LTA), and confirmation of mineralogy for operator-selected grains using a scanning electron microscope (SEM) equipped with an energy-dispersive X-ray analyser (EDX).

The USGS approach complements results obtained by X-ray absorption fine structure (XAFS) by our colleagues at the University of Kentucky. The USGS technique also provides data for elements such as Se and Hg, whose concentrations are commonly too low to obtain XAFS spectra, and for elements with atomic numbers beyond the routine XAFS atomic number range of about 20 to 42 (Ca to Mo). For elements that are common to the two approaches, such as As and Cr, comparison of results obtained by the USGS and by XAFS provides an important confirmation of our results.

Leaching Studies. Laboratory leaching procedures are conducted in duplicate in the coal chemistry lab at the USGS National Center in Reston. Leachates and solid residues are then sent to the Energy Program analytical labs in Denver for analysis. To date, the complete leaching procedure has been done (in duplicate) three times for the Ohio and North Dakota samples, and two times for the Wyodak sample. Repetition of the procedure was necessitated by problems with the nitric acid leaching step, resulting in incomplete digestion of pyrite, as outlined in Figure 3-1. In the first repeat (Ohio and North Dakota only), this incomplete pyrite digestion was

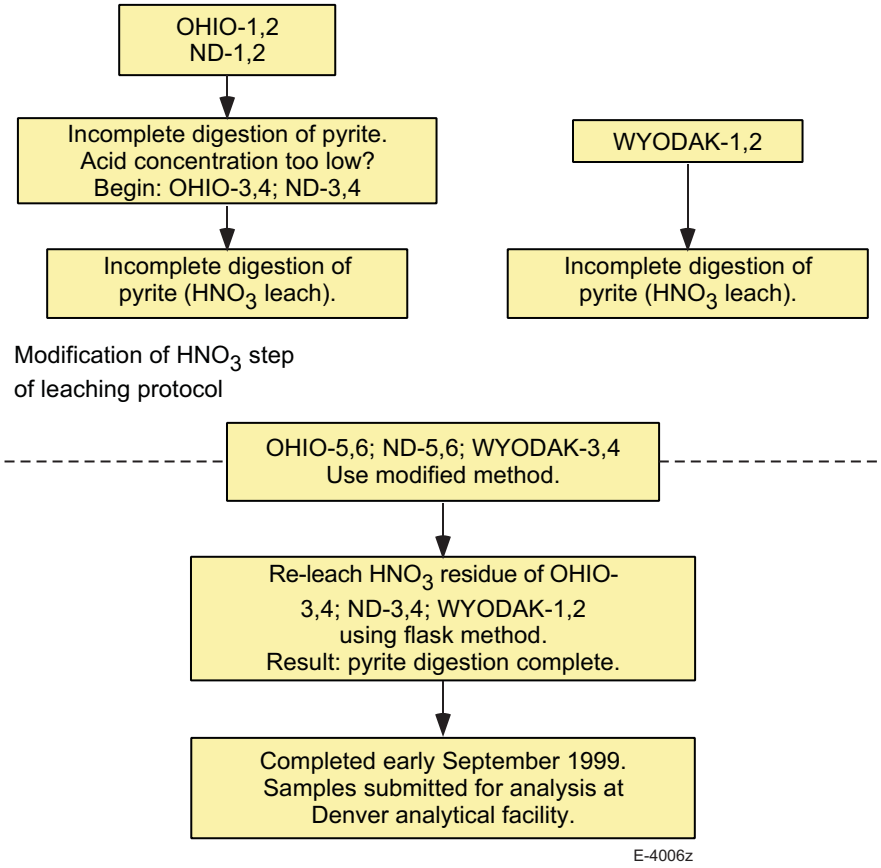

Figure 3-1. Leaching study timeline.

attributed to an error in the normality of the acid. After repeating the procedure with acid having the correct normality, we found that pyrite had still not been completely digested. As a result, a new procedure, modified from ASTM procedure D2492, Section 7.3.1 for determination of pyritic sulfur, was developed. The main difference is in the shape of the digestion vessel - the old procedure used a disposable centrifuge tube, whereas in the new procedure, a standard laboratory flask is used (Appendix 1). This "flask method" was used in the nitric acid step for a second repeat leaching of the Ohio and North Dakota samples, and a repeat leaching of the Wyodak coal. To further test the new method, solid residues from the incomplete HNO_3 leaching steps in the tube were re-leached using the flask method (Figure 3-1). Results for this re-leaching step confirm that 95 to 100% of the iron has been recovered for each of the three coals (see below). The first three steps of the procedure were unaffected by the problem with pyrite digestion in the last step. Therefore once all analyses are returned, we have six replicates for each of the first three steps of the procedure for the Ohio and North Dakota coals, and four replicates for the Wyodak coal for these steps of the procedure.

To date, analytical results have been returned for all but the last complete round of the four-step leaching procedure. Preliminary results are shown in Figure 3-2, consisting of complete analysis of leachates and solid residues for Ohio 1,2,3,4, North Dakota 1,2,3,4 and Wyodak 1,2 for the first three leaching steps, and INAA analysis only for the solid residues of the

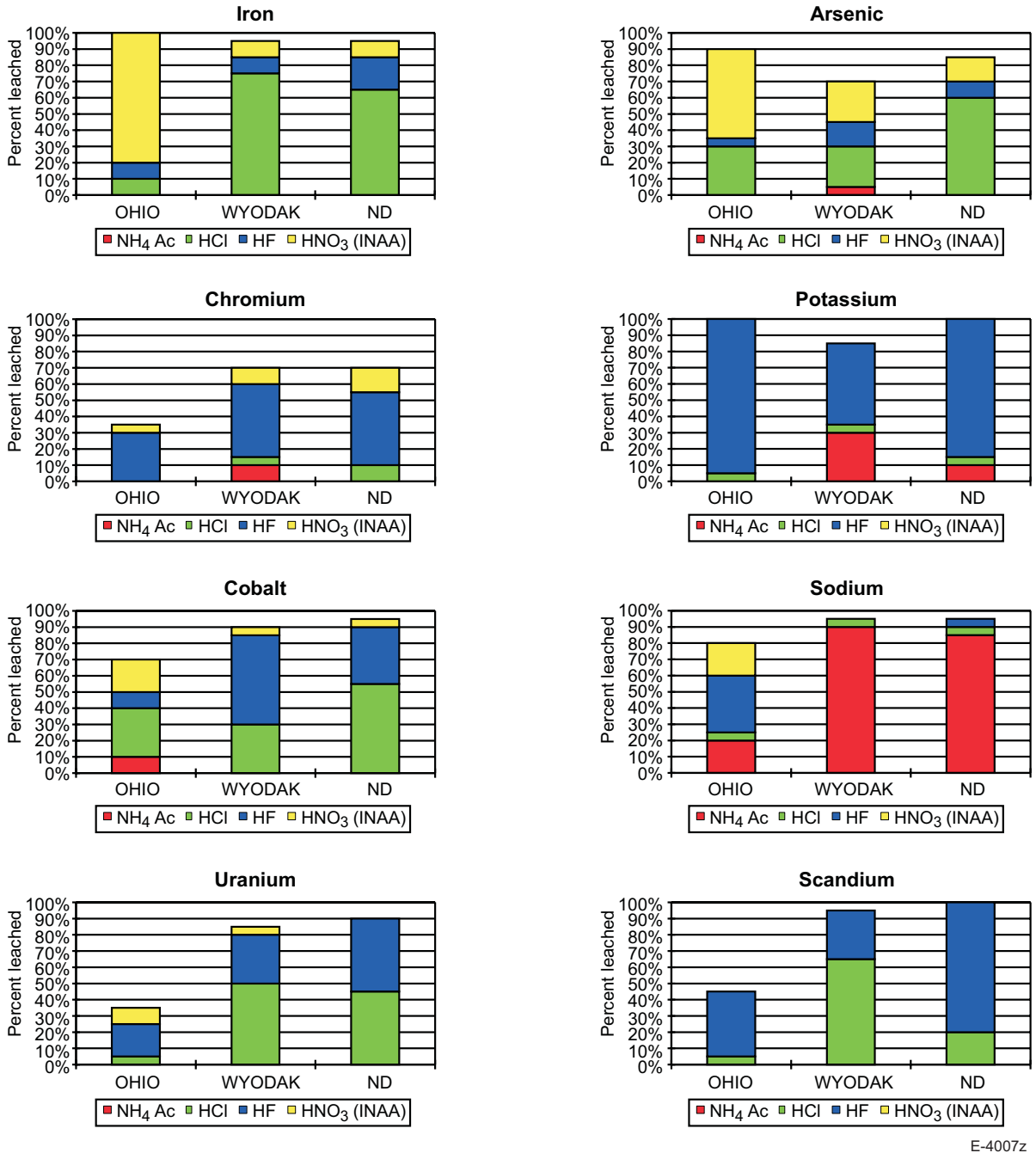

Figure 3-2. Preliminary leaching data.

HNO_3 re-leaching step (Figure 3-1). Note that these results lack leachate data for the re-leaching step, and all results from the final duplicate leachings, and therefore are subject to change in the final analysis.

For the Ohio 5/6/7 coal it is clear from the preliminary leaching data that iron and arsenic are strongly associated with pyrite, as in many bituminous coals, consistent with microprobe date for pyrite given in the last semi-annual report (Figure 3-2). A much smaller pyrite association is

indicated for Fe and As in the two low rank coals. These coals show a large HCl-leachable fraction we have previously interpreted as arsenate. For Cr, a significant HF-leachable fraction is shown for each of the coals, consistent with ion probe data for Cr in illite, reported in the section on microanalysis. However, each of the coals has significant (30-65%) unleached Cr, indicating an organic association for this fraction. For the other elements reported - potassium shows a strong silicate association- as it is a major component of illite/smectite. Sodium shows a significant ion-exchangeable component, especially in the low rank coals. Cobalt, uranium and scandium show mixed affinities that are dominated by organic, silicate, or HCl-leachable forms.

Mercury Analysis. Previously, we reported on development work for an alternate method of Hg analysis versus the Cold Vapor Atomic Absorption (CVAA) method used in Phase I of this program. Tests of the new method, cold vapor atomic fluorescence (CVAF) indicated that the minimum detection limit by this method was limited by a total analytical blank level in the 0.01 to 0.02 ppm (10 to 20 ppb) range, similar to the detection limit for CVAA. Although the CVAF blank-level problem is potentially resolvable, our analysts in Denver have halted development of this procedure in favor of a new direct analyzer for Hg that the USGS is in the process of acquiring. The new analyzer is compliant with EPA method 7473 and offers the following advantages: 1) sample digestion is unnecessary, thereby eliminating reagent blank-level problems; 2) sensitivity is similar to or better than levels we were hoping to achieve with CVAF; and 3) the new analyzer has a standard auto-sampler, allowing analysis of multiple samples in an automated mode. The new method will not be available until January, 2000 or some time thereafter. The old method (CVAA) will be used in the interim, or in cases where its detection limit is sufficient.

Microanalysis. Since early June, emphasis has been placed on microanalysis of clay minerals in project coals in preparation for use of the Stanford/USGS SHRIMP RG Ion Microprobe during August 1999. During the week of August 23, Allan Kolker traveled to Stanford University to conduct these analyses. The 2.6M instrument is the only SHRIMP facility in the U.S. with reversed geometry (RG). This instrument has the advantages of high sensitivity, and very high mass resolution, compared to smaller ion probes and the forward geometry (FG) SHRIMP. The purpose of Allan's visit was to evaluate the usefulness of the SHRIMP for project purposes, specifically to generate data on the contents of Cr and other metals of interest (Co, Ni, Mn, Cu, Zn, Ti, V, etc.) in clays (illite/smectites) in project coals. Preliminary results for Cr in the three Phase II coals and the Illinois #6 coal from Phase I are given in Figure 3-3. The SHRIMP-RG data confirm that Cr is present at concentrations of about 20 to 120 ppm, just below the electron microprobe detection limits (100 to 200 ppm), as suspected from Phase I microprobe work and previous studies of clay mineral separates [3]. Final SHRIMP-RG numbers for the illites will be given in a subsequent report, as we are still in the process of refining the data. Reconnaissance analysis of organic parts of the North Dakota sample show measurable Cr, as also indicated by preliminary XAFS work [4].

In preparation for use of the SHRIMP-RG suitable coarse (> 60 mesh) material was separated from project coals, and duplicate splits were made for preparation of polished grain mounts. One set of samples was sent to Stanford for preliminary tests of ionization of Cr in the illites. The other set of grains was retained for analysis and chemical mapping using the electron

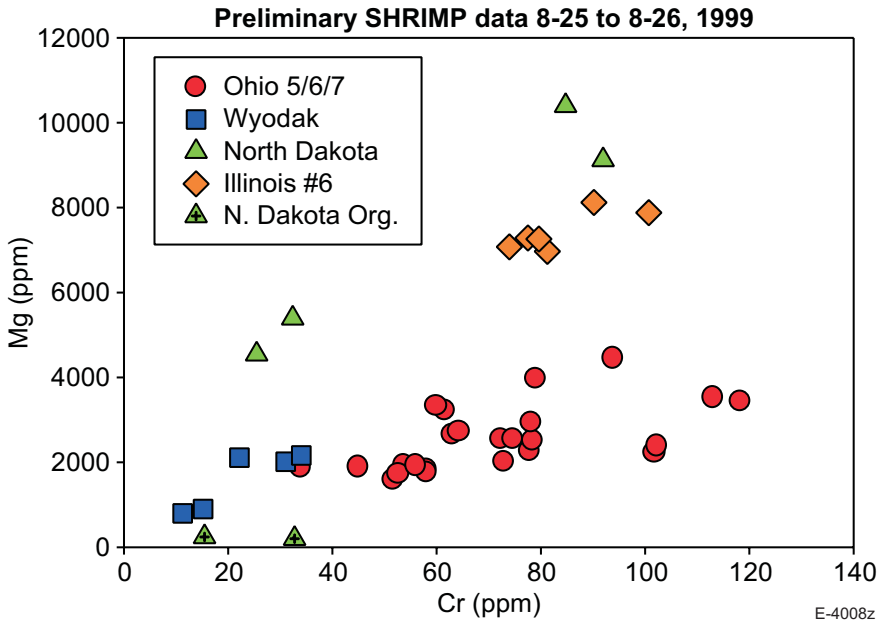

Figure 3-3. Preliminary SHRIMP data 8-25 to 8-26, 1999.

microprobe. These analyses were conducted in Reston prior to use of the SHRIMP-RG. Electron microprobe elemental maps and major element data were used as a guide for locating illite/smectite grains to analyze with the SHRIMP-RG. Additionally, because the SHRIMP-RG gives major, minor, and trace-element results simultaneously, these results were used together with corresponding electron microprobe data to minimize grain-overlap problems with adjacent minerals, typically quartz, pyrite, kaolinite, and calcite.

Analysis of the illite/smectites made use of the O^- ion source currently available at the SHRIMP-RG. Subsequent work on trace-metals in sulfides, and arsenic in fly ash, will likely utilize a new Cs^+ ion source, currently being tested. The Cs^+ ions are more energetic and are needed to ionize heavier elements such as Hg. Preliminary analysis of arsenic in doped-glass standards using the O^- ion source suggests that the ^{75}As peak is resolvable from organic interferences at the same mass, something we have been unable to do in reconnaissance studies using smaller ion probes. The Cs^+ ion source will be needed to obtain a sufficient count rate for As and Hg analysis.

SEM/LTA/XRD and Other Supporting Procedures. Low temperature ashing of the three project coal samples is complete, followed re-ashing of the North Dakota sample after leaching with ammonium acetate to remove the carboxyl-bound cations that may neutralize the oxygen plasma, and to prevent fixation of the organic sulfur as sulfate. These problems were outlined previously and have now been overcome. X-ray diffraction studies of the three project coals are underway. These results will provide semi-quantitative estimates of the modal proportions of minerals present in the coal, to be used in conjunction with the SEM data.

A large number of pellets have been prepared for routine SEM examination of residues after leaching, to insure that mineral matter, especially pyrite, is completely digested. Polished mounts of these residues are currently being examined.

To help integrate the leaching and XAFS portions of this project, XAFS splits have been taken for analysis from each of the leaching steps conducted, including rounds that were repeated due to problems outlined in the section on leaching results. During the recent program review meeting, we met with Drs. Huggins and Huffman to discuss their plans for upcoming analyses, and to prioritize the samples. We expect to provide the highest priority samples for their upcoming XAFS work at the end of October 1999.

3.3 Combustion Zone Transformations (UU, MIT)

3.3.1 Single Particle Combustion Studies

The past few months have been spent gathering supplies and modernizing the equipment at the University of Utah. A heating system has been built for the cascade impactor to ensure that high flow velocity can be maintained. There should be no slowing due to temperature drop. We have now received everything and the drop tube furnace is running smoothly. MIT's nuclear reactor is also working again.

We have started trial runs on the drop tube furnace to ensure that the gas analysis system is working properly and that the flow pattern within the furnace is laminar and direct. Mike Ames of MIT will be visiting the University of Utah soon to set up the vapor phase collection system, which uses activated carbon to absorb any metals that remain in the exhaust. While he is here, we will run the first set of experiments.

We will be working with the following three coals: Ohio (5/6/7), Wyodak, and ND Lignite. All experiments will be conducted at 1650 K. For each coal, the tests will be conducted using the gas compositions shown in Table 3-2.

Table 3-2. Preliminary Test Matrix for Single Particle Combustion Studies

% O_2	% N_2	% O_2	% CO_2
0	100	0	100
20	80	20	80
50	50	50	50
100	0		

Nitrogen provides an inert atmosphere for the reactions. The CO_2 atmosphere is selected to determine its effect on suppressing the vaporization of the refractory oxides because of the reverse reaction in $MO + CO = M + CO_2$. The furnace is designed to quickly burn the particles and rapidly cool the products, stopping the reactions in the combustion zone.

The vertical arrangement of the drop tube furnace ensures that all combustion products will be available for analysis, with no loss in the reactor. Particles will be size segregated through a cascade impactor with each stage lined with Durapore Millipore filters that have been greased with Apiezon H and dried. The grease will ensure adhesion and prevent particles from bouncing from other stages and allow for a more accurate separation of sizes. The impactor will be maintained at 120 C to prevent condensation of water and H_2SO_4. The impactor will separate the large residual ash from the submicron particles that are formed from vaporization and recondensation. The two size classes will be grouped and sent for INAA. Each stage of a few samples will be analyzed separately to determine the variation within the submicron ash and within the residual ash. Samples will also be sent to a local lab for complementary analysis because some metals may not be detected by INAA. The activated charcoal will collect any remaining metals and will also be analyzed by INAA to quantify the amount of metal that remains in the vapor phase.

The results of the fundamental models are being incorporated in simulations of practical boilers in a collaborative program with a parallel DOE PRDA on low NO_x and unburned carbon in ash (DE-AC22-95PC95103).

3.3.2 Metal Release with Volatiles

A third set of ASTM samples will be prepared for our seven coals. This time the INAA counting time will be optimized for the elements in which we are interested, guided by the results from the first two samples. Seven samples will be generated.

There is concern that the ASTM tests might be biased by the secondary pyrolysis reactions that the volatiles released low in the crucible can undergo as they pass through the heated char higher in the crucible. This secondary pyrolysis will result in some deposition of metals in the volatiles on their passage through the bed. We were not in agreement on how to best evaluate this effect. The heated grid experiments that were designed to study the pyrolysis of coals provide an example of how the problem can be overcome. We need to design a system that will work. One possibility is to use a screen mounted on a support that can be inserted in the pyrolysis furnace so that the sample can be heated in the same fashion as the ASTM sample with the difference being that the volatiles are allowed to escape freely without undergoing secondary pyrolysis. We need triple studies for one coal.

We have only the results on the volatile yield at ASTM temperatures. We need to determine if the temperature at which the volatile metals are released are similar to those at which the volatiles as a whole are released. The temperatures to be studied are those at which the total ASTM volatile release is 25, 50, and 75% of those obtained under the standard ASTM test. A lignite and a bituminous coal will be studied.

3.3.3 Gas-Phase Sampling of Metal Vapors

The iodated charcoal which used for vapor phase Hg collection (Figure 3-4) was tested to see whether it collected other vapor phase metals. The tests were performed at PSI using the

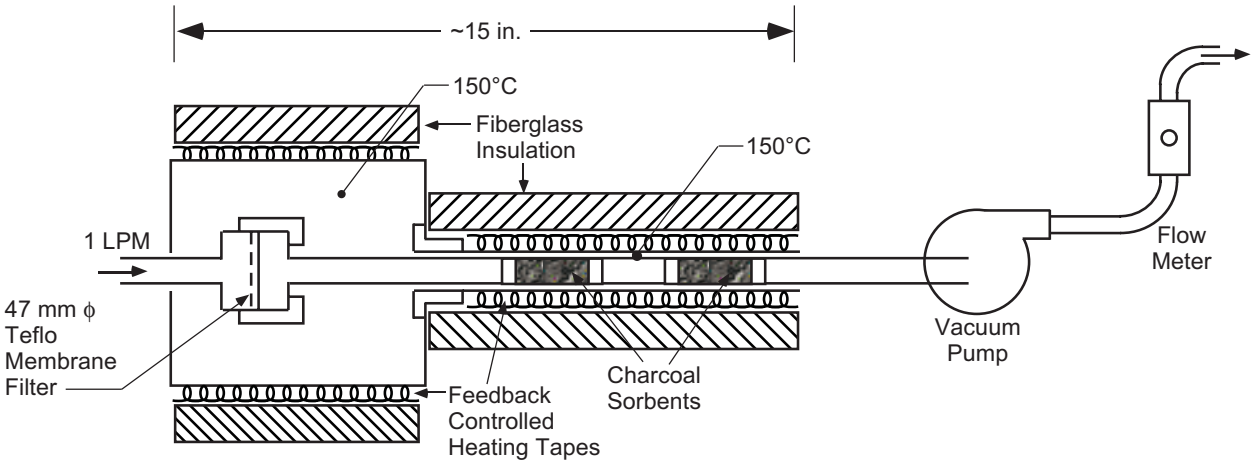

Figure 3-4. MIT vapor-phase metals sampling train.

entrained flow reactor (EFR). The Pittsburgh coal from Phase I was burned at 1500 C at rates of 1.2 and 1.34 grams per minute, a stochiometric ratio of 1.2, and a total gas flow of 12.5 and 14.2 liters per minute. The collection efficiency of the sorbent was checked by running two tubes in series. The flow rate through the sorbent tubes was 1 liter per minute.

The sorbents were run at a temperature of about 30 C for 2, 10 and 50 min (Test 1), and at 105 C for 30 and 60 min (Test 2) with and without a heated (150 C) prefilter. The charcoal in the front sorbent collected 100% of the vapor phase Hg (Figure 3-5) and Se (Figure 3-6, Test 1 only). The amounts collected increased linearly with the test duration. The result of the second test for Hg collection simply confirm that the sorbents collect 100% of the vapor phase Hg, and that they can be used at 105 C to prevent condensation. No other elements (e.g., As, Br, Cd, and Sb) were collected quantitatively in Test 1.

3.4 Post-Combustion Transformations (UA, UC, UU, UK)

3.4.1 Large Scale Integrated Combustion Studies

Wyodak Baseline Experiments. Note that Table 3-6 in the April through June 1999 quarterly report was in error. The sampling temperature values listed in this table are all degrees Celsius not degrees Kelvin as indicated. Appendix A provides the corrected information with temperature in degrees Kelvin.

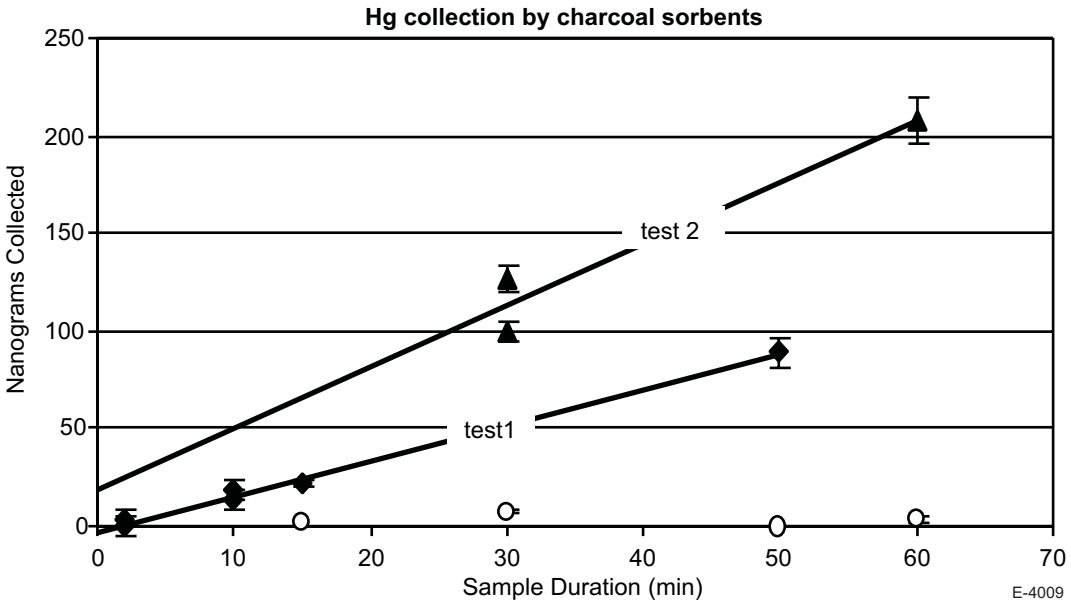

Figure 3-5. Mercury collected by charcoal sorbent from EFR combustion gas (front sorbents: filled data points; back sorbents: open data points).

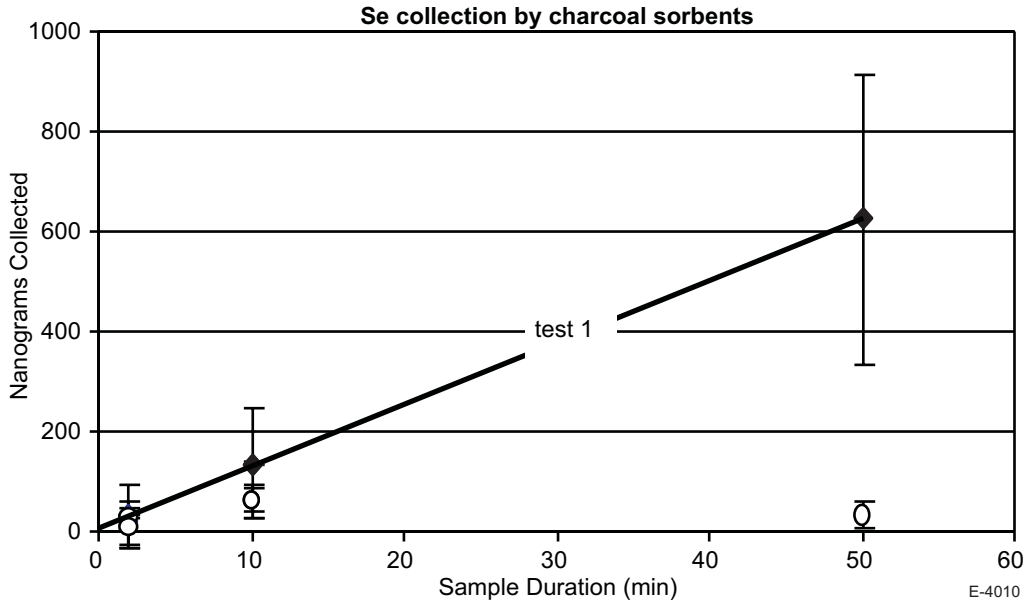

Figure 3-6. Selenium collected by charcoal sorbent from EFR combustion gas (front sorbents: filled data points; back sorbents: open data points).

North Dakota Lignite Baseline Experiments. The University of Arizona's pilot-scale downflow laboratory combustion furnace was used to test the partitioning of toxic metals in the baseline experiments for the Phase II North Dakota lignite. The objectives of these experiments were:

- To obtain toxic metal partitioning data under test conditions which simulate the time/temperature combustion and post-combustion conditions of commercial scale utility boilers at 20% excess oxygen.

- To investigate the differences in toxic metal partitioning from samples collected immediately after char burnout compared to samples collected near the furnace exit and to samples collected at the entrance to the baghouse.

A detailed description of the furnace and sampling systems is given in the Phase I Final Report. A Berner low pressure impactor (BLPI) was used for particulate sample collection for all of the experiments performed.

A total of 15 sets of particulate samples was collected during six test runs. All experiments were performed at a coal feed rate of 2.2 kg/hour. Due to the lower energy content of this lignite compared to other Phase I and Phase II coals, combustion gases experienced a longer residence time in the furnace. We chose to sample particulate at the same locations as those sampled during the Ohio and Wyodak baseline tests. Five sets of particulate samples were collected from Port 4 of the furnace, which is located immediately after the end of the combustion zone (around 1.9 seconds of residence time after the burner). Five sets of particulate samples were collected from Port 14 which is located near the bottom of the furnace (around 9.4 seconds of residence time after the burner) and represents a snapshot of the flue gas in the post combustion zone. These samples sets were typically taken immediately after one of the sample sets from Port 4 so that matched sample sets could be selected for analysis. Five sample sets were taken from the inlet to the baghouse and represent ESP inlet sampling conditions. The baghouse samples are taken after partial segregation of large particles in an ash trap and a small particle trap.

We found that a single collection test, performed without the BLPI inlet cyclone, could be used to collect all 11 size-segregated samples from the BLPI due to a smaller mean particle size for the North Dakota fly ash compared to the mean particle size for the bituminous coals previously tested under this program. The sample sets and test runs are summarized in Table 3-3. Table 3-4 shows the sampling conditions for the most important sample sets. Figure 3-7 shows the typical steady-state temperature profile from these tests.

Table 3-3. A Summary of the Phase II North Dakota Lignite Baseline Test Runs

Test Run #	Date	Coal Feed Rate	Sample Set #	Sampling Times	Sample Port Used
99ND-1	07/16/99	2.2 kg/hr	none[1]		
99ND-2	07/17/99	2.2 kg/hr	none	none	
99ND-3	07/24/99	2.2 kg/hr	99ND-1	4 min	4
			99ND-2	3 min	4
			99ND-3	4 min 30 sec	14
			99ND-4	3 min 30 sec	14
			99ND-5	5 min 30 sec	BG[2]
			99ND-6	4 min 30 sec	BG
99ND-4	7/25/99	2.2 kg/hr	99ND-7	3 min 30 sec	4
			99ND-8	3 min 30 sec	4
			99ND-9	4 min	14
			99ND-10	4 min	14
			99ND-11	6 min 21 sec	BG
			99ND-12	6 min	BG
99ND-5	7/26/99	2.2 kg/hr	none[3]	none	
99ND-6	7/31/99	2.2 kg/hr	99ND-13	3 min 30 sec	4
			99ND-14	4 min	14
			99ND-15	6 min	BG

[1]Complete temperature and gas profiles were obtained using this run
[2]BG-Baghouse inlet sample port
[3]Complete temperature and gas profiles obtained; blank sample running natural gas obtained

Table 3-4. Summary of Phase II North Dakota Lignite Experimental Sampling Conditions

SAMPLE SET # (Port Sampled)	TOTAL COMBUSTION GAS RATE (slpm)	SAMPLING RATE (slpm)	SAMPLING TEMP (°K at port where sample was taken)	PORT 4 O_2 CONC (%)	PORT 4 CO_2 CONC (%)	PORT 14 O_2 CONC (%)	PORT 14 CO_2 CONC (%)	PORT BG* O_2 CONC (%)	PORT BG CO_2 CONC (%)
99ND-1 (4)	174	0.59	1268	3.3	15.0				
99ND-2 (4)	174	0.59	1268	3.3	15.0				
99ND-3 (14)	202	0.69	916	3.3	15.0	5.7	13.7		
99ND-4 (14)	202	0.69	916	3.3	15.0	5.7	13.7		
99ND-5 (BG)	202[#]	0.69[+]	405	3.3	15.0	5.7	13.7	10.8	8.7
99ND-6 (BG)	202	0.69	405	3.3	15.0	5.7	13.7	10.8	8.7
99ND-7 (4)	172	0.59	1274	3.2	15.4				
99ND-8 (4)	172	0.59	1274	3.2	15.4				
99ND-9 (14)	218	0.74	884	3.2	15.4	6.9	12.3		
99ND-10 (14)	218	0.74	884	3.2	15.4	6.9	12.3		
99ND-11 (BG)	218	0.74	398	3.2	15.4	6.9	12.3	12.5	6.1
99ND-12 (BG)	218	0.74	398	3.2	15.4	6.9	12.3	12.5	6.1
99ND-13 (4)	174	0.59	1146	3.4	---[1]				
99ND-14 (14)	220	0.75	735	3.4	---	7.0	---		
99ND-15 (BG)	220	0.75	409	3.4	---	7.0	---	11.0	---

*BG = baghouse inlet sampling port

[#] Combustion rate for BG samples are assumed to equal rate at Port 14

[+] BG sampling rate is set equal to Port 14 rate; this is not an isokinetic sample

[1] CO_2 analyzer out of service during these sample sets

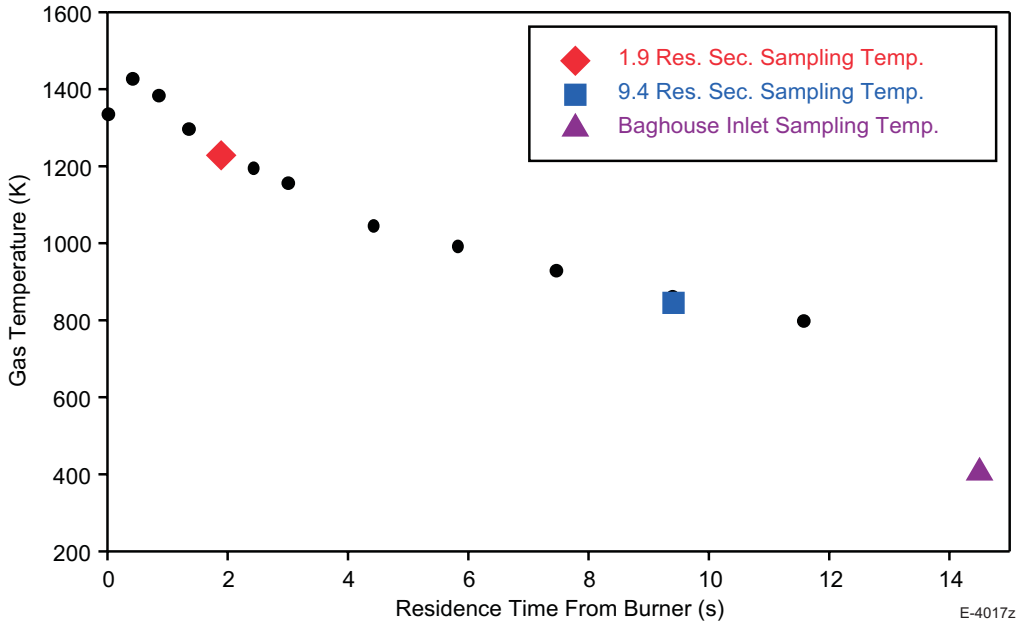

Figure 3-7. Typical self-evolving temperature profile for North Dakota Lignite Combustion in the University of Arizona Downflow Combustor.

Particle Size Distribution

Using the size-segregated ash weights collected in the BLPI in each test, particle size distributions (PSDs) were determined. Typical fly ash PSDs, developed following the method described by Markowski and Ensor,[5] are shown in Figure 3-8. Figures 3-9 through 3-11 show PSDs for individual sample sets at each of the three sampling locations. These figures provide insight into the variability in the PSDs shown in Figure 3-8. At all three sample locations, a typical BLPI PSD is observed which defines three distinct regions. A vapor phase region with a maximum around 0.08 microns, a submicron fume region having a maximum around 0.6 microns, and a supermicron, bulk fly ash region.

It should be noted that the large-size particle distribution for the baghouse sample is very similar to those from the 1.9 and 9.4 seconds residence time samples even though there are two particle traps for large particle collection prior to this sample location. A much smaller percentage of particles were collected in the particle traps upstream of the baghouse sample location compared to the bituminous coals previously studied.

Elemental Analysis

Two representative sample sets from the 1.9 seconds residence time sample location (sample runs 7 and 8), two representative sample sets from the 9.4 seconds residence time sample location (sample runs 9 and 10) and three representative sample sets from the hot-side of the particulate collection device (sample runs 5, 11, and 12) were selected for analysis of size-segregated particle metal content at the University of Arizona by AA/GFAA.

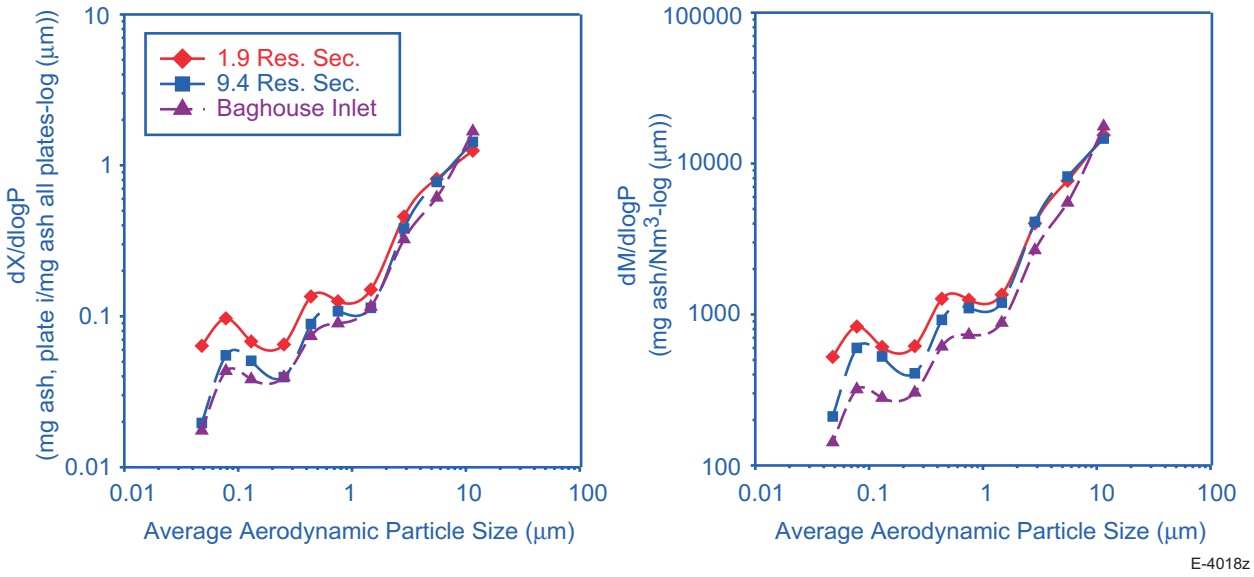

(a) (b)

Figure 3-8. Typical particle size distributions for North Dakota fly ash at various residence times (a) presented as a normalized mass fraction distribution, and (b) presented as a gas concentration distribution.

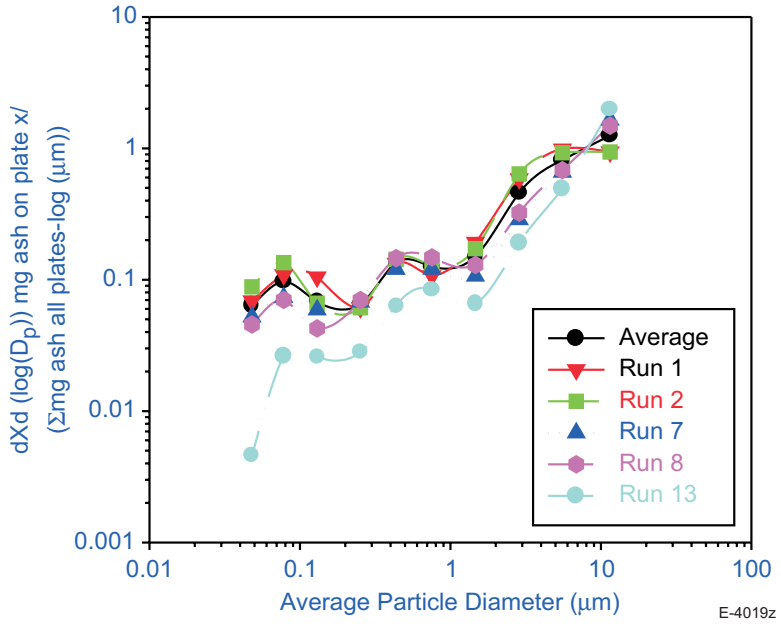

Figure 3-9. Particle size distribution data at 1.9 residence seconds for North Dakota fly ash.

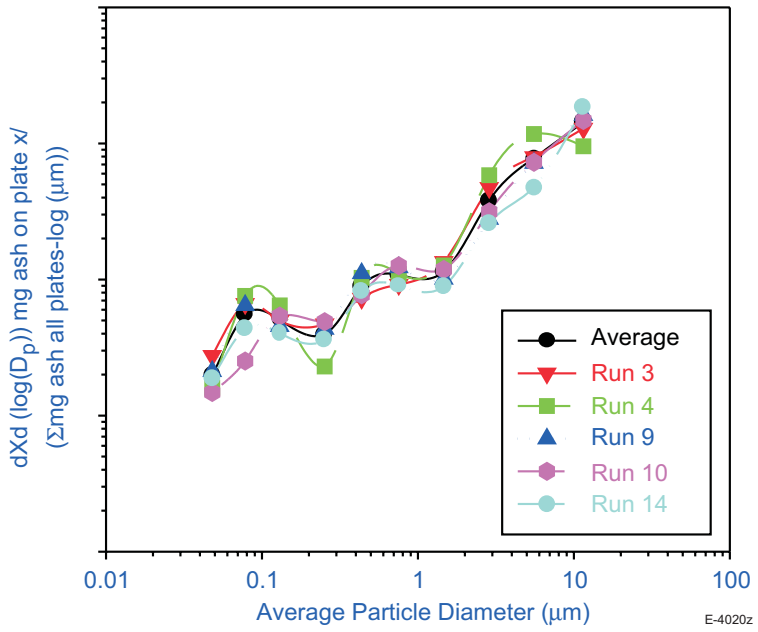

Figure 3-10. Particle size distribution data at 9.4 residence seconds for North Dakota fly ash.

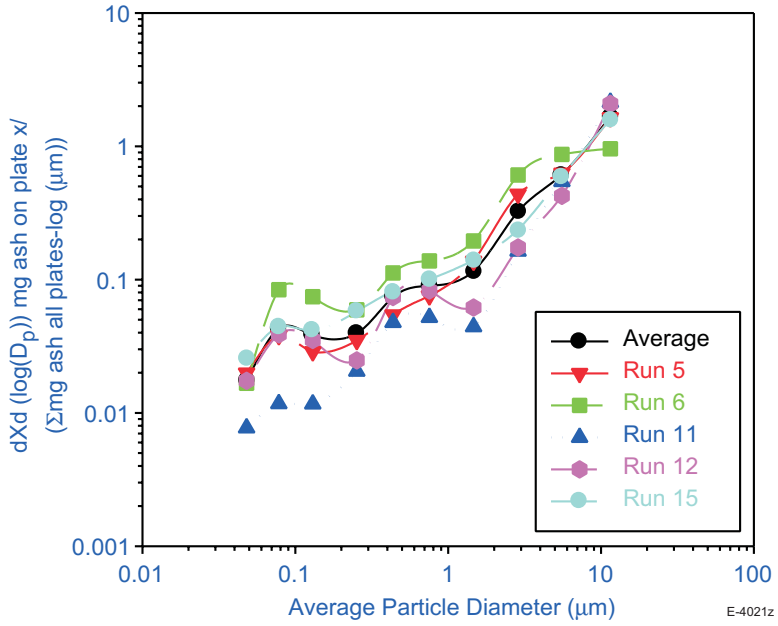

Figure 3-11. Particle size distribution data for samples from the Inlet Baghouse Port for North Dakota fly ash.

Tables 3-5 through 3-7 summarize preliminary trace element analytical results at each sampling location analyzed by GFAA. Analytical results for major species will be reported in the next quarterly report.

Table 3-5. Preliminary Size-Segregated Trace Element Concentration Data
North Dakota Lignite Baseline Combustion at 1.9 Residence Second Conditions

Impactor Stage		**1**	**2**	**3**	**4**	**5**	**6**	**7**	**8**	**9**	**10**	**11**
Cut-off	Diameter (microns)	0.0324	0.0636	0.0926	0.168	0.337	0.535	0.973	1.96	3.77	7.33	15.7
Element	**Analytical Method**					**(ppmw)**						
As	GFAA	587	363	241	147	151	164	142	147	109	45	101
Se	GFAA	83	54	29	nd	nd	20	28	14	9	1	nd[1]
Co	GFAA	nd	nd	nd	52	79	98	101	132	140	51	126
Sb	GFAA	800	1658	186	2254	616	56	13	8	46	253	40
Cr	GFAA	1689	2966	1981	1464	921	782	678	283	160	79	593

[1]nd - below detection limit

Table 3-6. Preliminary Size-Segregated Trace Element Concentration Data
North Dakota Lignite Baseline Combustion at 9.4 Residence Second Conditions

Impactor Stage		**1**	**2**	**3**	**4**	**5**	**6**	**7**	**8**	**9**	**10**	**11**
Cut-off	Diameter (microns)	0.0324	0.0636	0.0926	0.168	0.337	0.535	0.973	1.96	3.77	7.33	15.7
Element	**Analytical Method**					**(ppmw)**						
As	GFAA	415	360	274	237	281	231	200	194	148	65	105
Se	GFAA	nd[1]	153	60	nd	nd	21	25	9	4	2	nd
Co	GFAA	nd	nd	nd	66	76	94	85	107	98	66	87
Sb	GFAA	2064	73	23	12	1084	14	308	49	9	9	64
Cr	GFAA	3088	4579	1584	1431	1340	753	773	295	132	30	458

[1]nd - below detection limit

Table 3-7. Preliminary Size-Segregated Trace Element Concentration Data
North Dakota Lignite Baseline Combustion at Baghouse Inlet Conditions

Impactor Stage		**1**	**2**	**3**	**4**	**5**	**6**	**7**	**8**	**9**	**10**	**11**
Cut-off	Diameter (microns)	0.0324	0.0636	0.0926	0.168	0.337	0.535	0.973	1.96	3.77	7.33	15.7
Element	**Analytical Method**					**(ppmw)**						
As	GFAA	151	146	269	186	181	186	195	154	148	43	100
Se	GFAA	nd[1]	nd	nd	28	21	22	23	7	3	2	nd
Co	GFAA	nd	nd	nd	53	67	74	94	106	60	43	78
Sb	GFAA	5117	3506	1173	31	48	19	193	11	22	19	59
Cr	GFAA	3039	3336	2386	1335	1115	753	546	116	81	1	127

[1]nd - below detection limit

The typical concentration values from Tables 3-5 through 3-7 were used to generate individual element distribution profiles[5] for some of the more important trace elements (As - Figure 3-12, Se - Figure 3-13, Co - Figure 3-14, Sb - Figure 3-15, Cr - Figure 3-16).

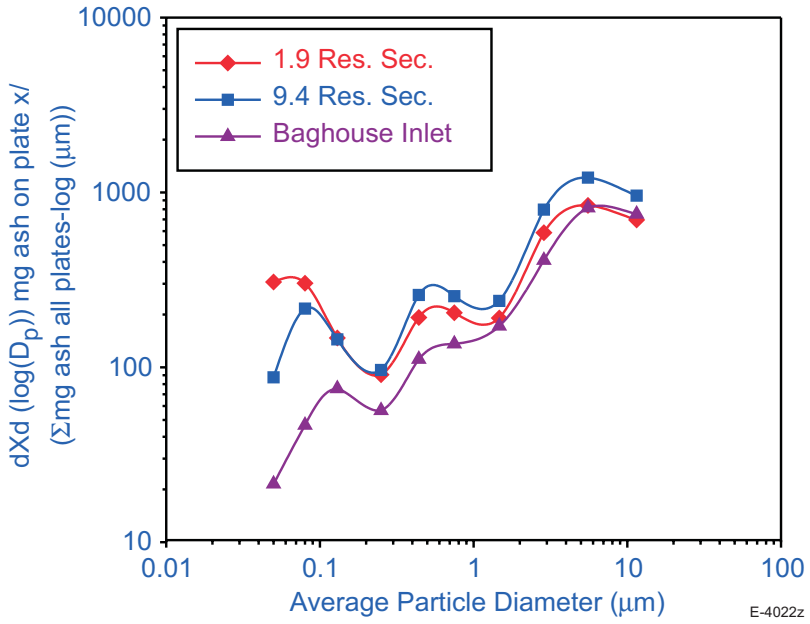

Figure 3-12. Typical arsenic distribution in North Dakota lignite baseline fly ash.

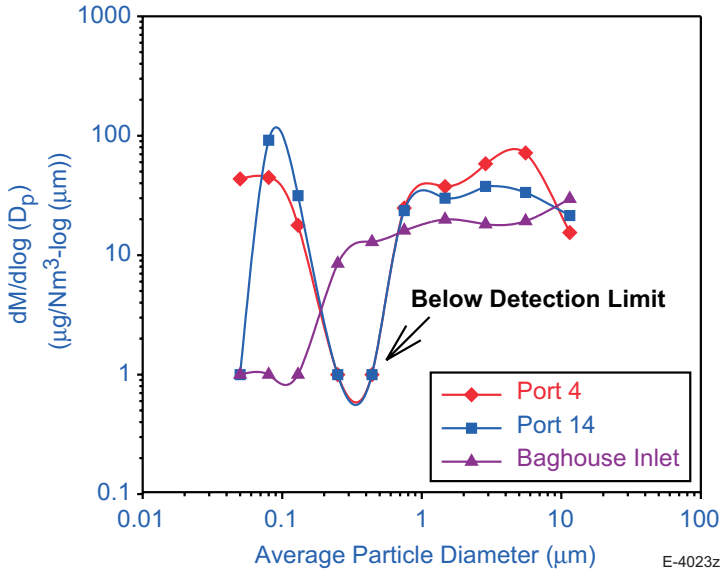

Figure 3-13. Typical selenium distribution in North Dakota baseline fly ash (Note: 1.0 dM/dlog(D_p) values represent samples with selenium concentrations below the detection limit).

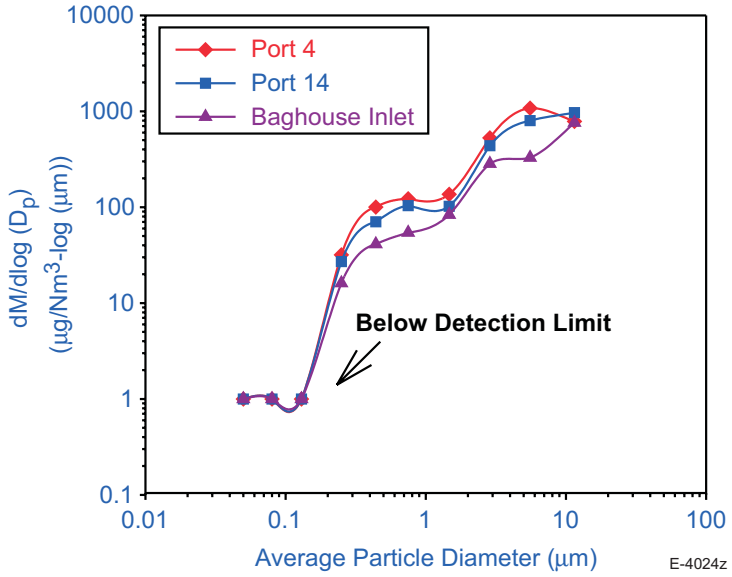

Figure 3-14. Typical cobalt distribution in North Dakota baseline fly ash (Note: 1.0 dM/dlog(D_p) values represent samples with cobalt concentrations below the detection limit).

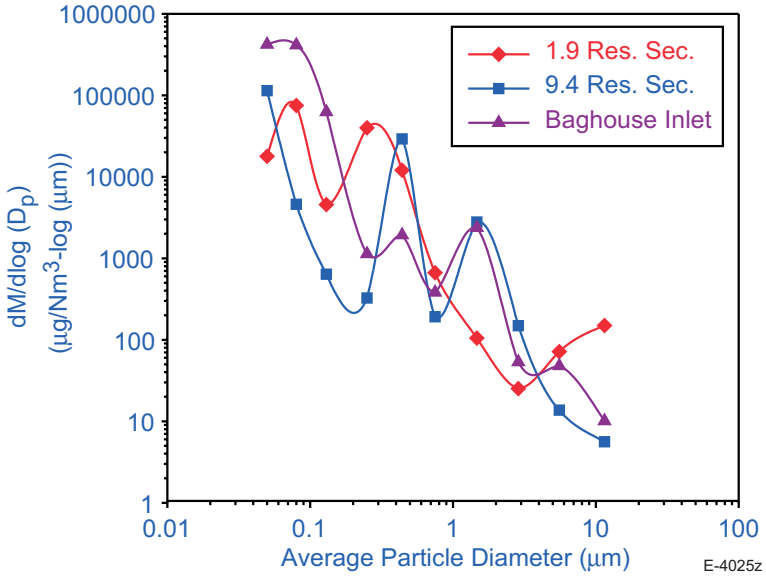

Figure 3-15. Typical antimony distribution in North Dakota lignite baseline fly ash.

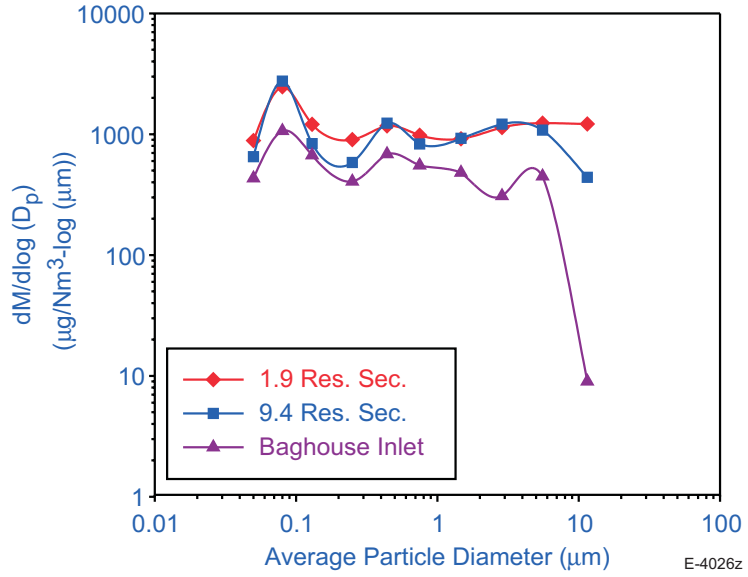

Figure 3-16. Typical chromium distribution in North Dakota lignite baseline fly ash.

Submicron Region

In order to compare the results at each sampling location, the PSDs can be normalized by calculating an enrichment factor, $E_{f,x}$, defined as the ratio of the ash mass collected at residence time x_m on a given plate to the average ash mass collected over the entire impactor.[6] Enrichment factors for the total fly ash, As, Se, Co, Sb, and Cr at all three sample conditions are listed in Table 3-8. This normalization removes the effect of sample condition upon the mass concentrations.

Comparing $E_{fa,x}$ at 9.4 residence seconds to $E_{fa,x}$ at 1.9 residence seconds ($\Delta E_{f,\ 9.4\text{-}1.9}$) provides insight into partitioning behavior in the post-combustion zone. This comparison is shown in Figures 3-17 through 3-21 for As, Se, Co, Sb, and Cr, respectively. For comparison purposes, the $\Delta E_{f,\ \text{Port 14-Port 4}}$ values for the corresponding samples from Pittsburgh seam, Illinois #6, Ohio 5/6/7, and Wyodak blend coal fly ash experiments are also included. A discussion of these $\Delta E_{f,}$ results are described in the April through June 1999 quarterly report.

The slightly positive North Dakota lignite submicron (0.1 to 1 micron range) $\Delta E_{f,\ 9.4\text{-}1.9}$ values in Figure 3-17 suggest that heterogeneous transformation of arsenic from the vapor phase to the surface of submicron particles is occurring in the post-combustion zone.

$\Delta E_{f,\ 9.4\text{-}1.9}$ values for North Dakota selenium cannot be calculated for two of the submicron impactor stages because the Se concentration was below the detection limit. The remaining value is slightly positive.

The North Dakota cobalt $\Delta E_{f,\ 9.4\text{-}1.9}$ values shown in Figure 3-19 in the submicron region for the North Dakota lignite are nearly zero. Therefore, no conclusions can be drawn about submicron partitioning mechanisms using this figure.

Table 3-8. Enrichment Factors ($E_{f,x}$) for North Dakota Lignite Fly Ash at 1.9 Residence Seconds, 9.4 Residence Seconds, and Baghouse Inlet Sampling Conditions

	Aerodynamic 50% Particle Cutoff Diameter (microns)										
	0.03	**0.06**	**0.09**	**0.17**	**0.34**	**0.54**	**0.98**	**1.98**	**3.77**	**7.33**	**15.7**
1.9 Residence Seconds											
Total fly ash	0.16	0.14	0.16	0.19	0.26	0.34	0.43	1.18	2.30	5.29	0.54
Arsenic	5.94	3.68	2.44	1.49	1.53	1.66	1.43	1.49	1.11	0.46	1.02
Selenium	10.39	6.73	3.66	*		2.49	3.47	1.82	1.17	0.13	
Cobalt				0.62	0.94	1.17	1.20	1.57	1.67	0.61	1.50
Antimony	3.54	7.33	0.82	9.97	2.72	0.25	0.06	0.04	0.20	1.12	0.18
Chromium	5.26	9.24	6.17	4.56	2.87	2.44	2.11	0.88	0.50	0.25	1.85
9.4 Residence Seconds											
Total fly ash	0.07	0.10	0.14	0.13	0.20	0.30	0.39	1.23	2.50	5.13	0.80
Arsenic	3.34	2.90	2.20	1.90	2.26	1.86	1.61	1.56	1.19	0.53	0.84
Selenium		23.96	9.36			3.36	3.93	1.44	0.64	0.25	
Cobalt				0.84	0.97	1.19	1.08	1.35	1.23	0.84	1.10
Antimony	34.13	1.21	0.37	0.20	17.93	0.24	5.10	0.82	0.15	0.15	1.06
Chromium	10.97	16.26	5.63	5.08	4.76	2.67	2.75	1.05	0.47	0.11	1.63
Baghouse Inlet Conditions											
Total fly ash	0.05	0.06	0.08	0.11	0.14	0.22	0.31	0.87	1.83	6.71	0.62
Arsenic	1.77	1.71	3.15	2.18	2.13	2.18	2.29	1.80	1.74	0.50	1.18
Selenium				7.47	5.63	5.87	6.03	1.82	0.94	0.45	
Cobalt				0.97	1.23	1.36	1.73	1.95	1.09	0.79	1.44
Antimony	66.67	45.68	15.28	0.41	0.62	0.25	2.52	0.15	0.29	0.25	0.77
Chromium	22.15	24.31	17.39	9.73	8.12	5.49	3.98	0.84	0.59	0.00	0.93

* Enrichment factors are not calculated when the elemental concentration is below the analytical detection limit.

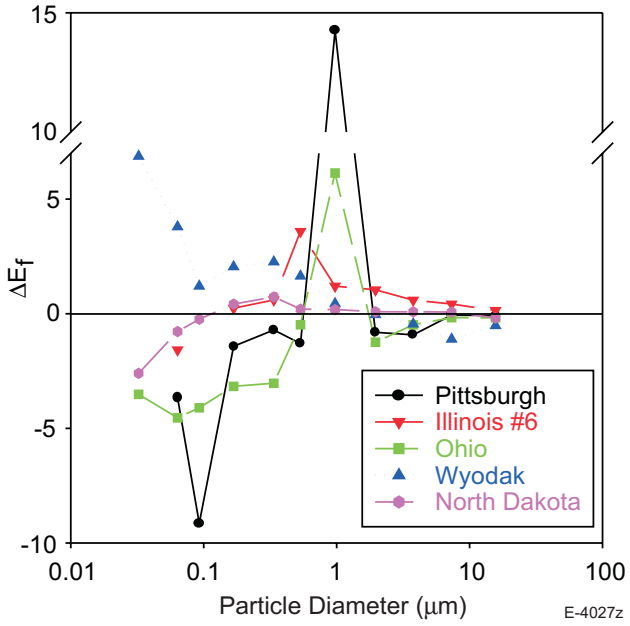

Figure 3-17. Arsenic differential enrichment factor comparison, ΔE_f ($E_{f,2.2}$ - $E_{f,0.5}$) for Pittsburgh, Illinois #6, and Ohio; ΔE_f ($E_{f,6.6}$ - $E_{f,1.4}$) for Wyodak; and ΔE_f ($E_{f,9.4}$ - $E_{f,1.9}$) for North Dakota.

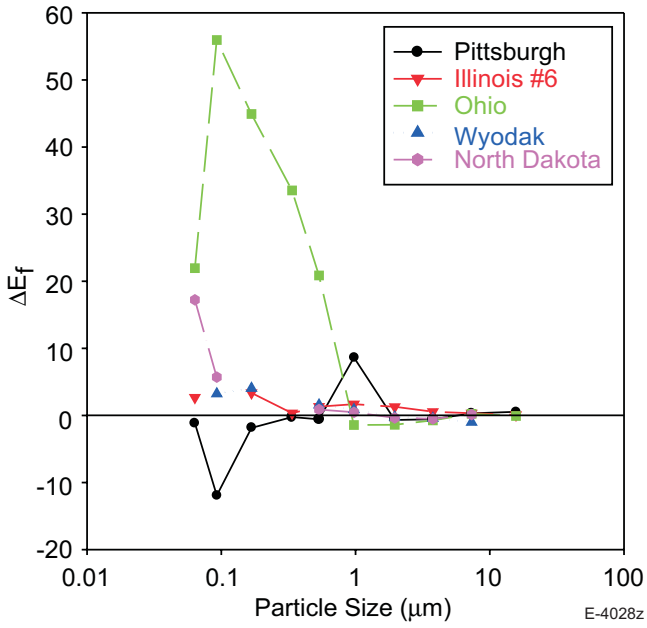

Figure 3-18. Selenium differential enrichment factor comparison, ΔE_f ($E_{f,2.2}$ - $E_{f,0.5}$) for Pittsburgh, Illinois #6, and Ohio; ΔE_f ($E_{f,6.6}$ - $E_{f,1.4}$) for Wyodak; and ΔE_f ($E_{f,9.4}$ - $E_{f,1.9}$) for North Dakota.

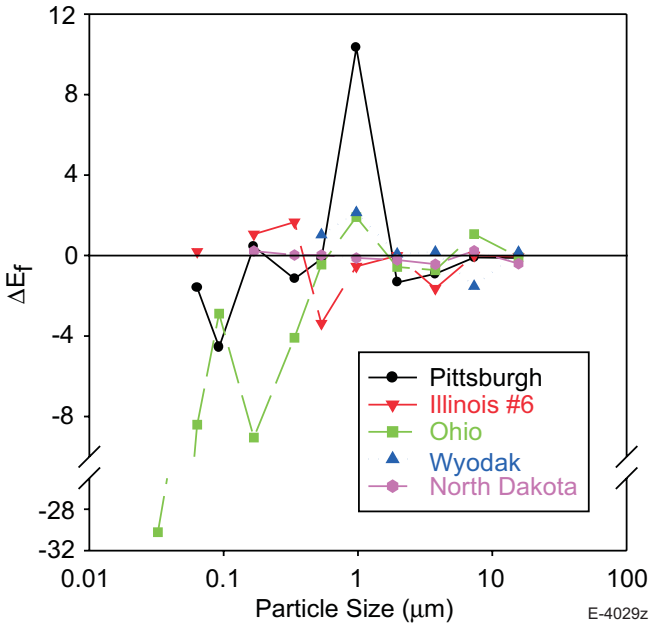

Figure 3-19. Cobalt differential enrichment factor comparison, ΔE_f ($E_{f,2.2}$ - $E_{f,0.5}$) for Pittsburgh, Illinois #6, and Ohio; ΔE_f ($E_{f,6.6}$ - $E_{f,1.4}$) for Wyodak; and ΔE_f ($E_{f,9.4}$ - $E_{f,1.9}$) for North Dakota.

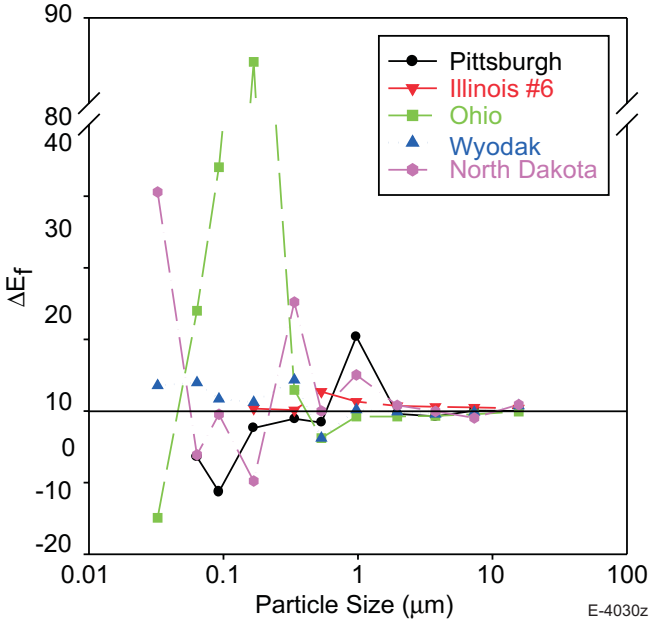

Figure 3-20. Antimony differential enrichment factor comparison, ΔE_f ($E_{f,2.2}$ - $E_{f,0.5}$) for Pittsburgh, Illinois #6, and Ohio; ΔE_f ($E_{f,6.6}$ - $E_{f,1.4}$) for Wyodak; and ΔE_f ($E_{f,9.4}$ - $E_{f,1.9}$) for North Dakota.

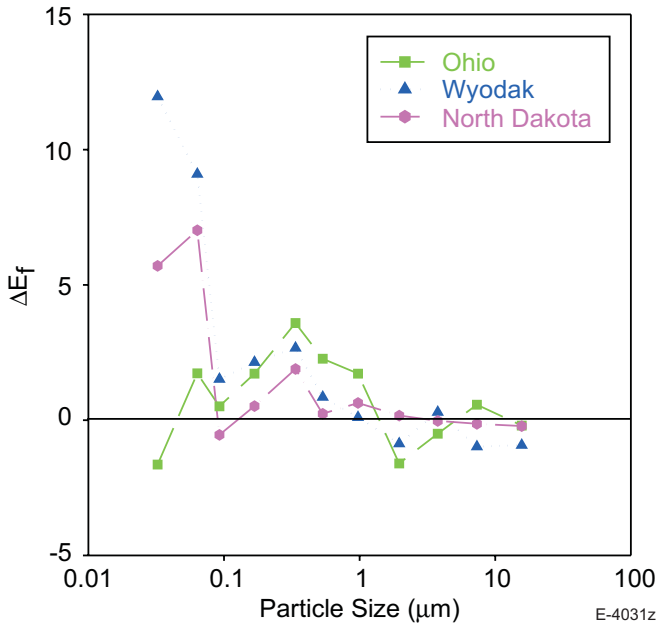

Figure 3-21. Chromium differential enrichment factor comparison, ΔE_f ($E_{f,2.2}$ - $E_{f,0.5}$) for Ohio; ΔE_f ($E_{f,6.6}$ - $E_{f,1.4}$) for Wyodak; and ΔE_f ($E_{f,9.4}$ - $E_{f,1.9}$) for North Dakota.

The North Dakota antimony $\Delta E_{f,\ 9.4\text{-}1.9}$ values in Figure 3-20 are inconclusive as well. Negative, positive, and near zero values were obtained in the submicron region.

Chromium results in Figure 3-21 are similar to those for arsenic. Volatilization and subsequent heterogeneous transformation to the surface of submicron particles appears to be an important transformation mechanism.

Supermicron Region

Log-log plots of the preliminary trace metal concentration versus particle size in the 9.4 residence second samples can provide some insight into heterogeneous partitioning mechanisms. A $1/d_p$ (particle diameter) dependence indicates that, in the continuum regime, exterior surface reaction or pore diffusion controlled surface reaction may be the dominant formation mechanism. $1/d_p^2$ dependence indicates that gas film transfer is the controlling rate process; which is true for condensation in the continuum regime or for infinitely fast surface reaction.[7] The results are shown in Figure 3-22 for As, Se, Co, Sb, and Cr from North Dakota fly ash sampled at 9.4 res. sec. A $1/d_p^2$ dependence is suggested for Se, Sb, and Cr. No particle size dependence is observed for Co. There appears to be a $1/d_p$ dependence for As. As with previous experimental results, the dependence correlation is most obvious in selenium. Note that impactor stage 11 (the inlet stage) results are not included in Figure 3-22. Due to the low mass loading collected, we believe the results to be inaccurate.

Pittsburgh Coal Baseline Experiments. The University of Arizona's pilot-scale downflow laboratory combustion furnace was used to test the partitioning of toxic metals in baseline experiments for the Pittsburgh seam bituminous coal at baghouse inlet sampling conditions.

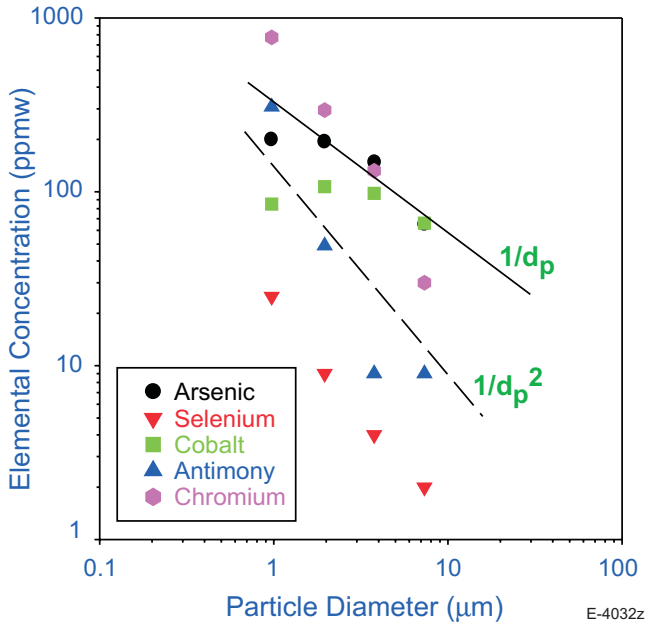

Figure 3-22. Particle size dependence of As, Se, Co, Sb, and Cr sampled at 9.4 residence seconds from combustion of North Dakota lignite.

Sample collection media for the BLPI consisted of polycarbonate membranes sprayed with a high purity grease. The membranes were dried in a vacuum dessicator for a minimum of 24 hours. One and a half milliliter PVC sample vials were used to contain the particulate-laden membranes. The vials were weighed with and without the particulate-laden membranes on a microbalance and stored in zipper locked sealed polyethylene bags. The dried sample collection media were also weighed on the microbalance just prior to loading into the BLPI. All microbalance weights were repeated. Two readings with a deviation of less than 0.00003 g were required before the weight data were accepted as accurate.

Particulate samples were collected during one test run. Both experiments were performed at a coal feed rate of 2.2 kg/hour. Two sample sets were taken from the inlet to the baghouse. The baghouse samples are taken after partial segregation of large particles in an ash trap and a small particle trap.

We found that a single collection test, performed without the BLPI inlet cyclone, could be used to collect both size-segregated samples from the BLPI. The sample sets are summarized in Table 3-9. Table 3-10 shows the sampling conditions for the sample sets. A typical steady-state temperature profile for a 2.2 kg/hour feed rate of Pittsburgh seam coal in the Univ. of Arizona downflow combustor is provided in the Phase I final report.

Table 3-9. A Summary of the Phase I Pittsburgh Seam Coal Baghouse Inlet Baseline Test Runs

Test Run #	Date	Coal Feed Rate	Sample Set #	Sampling Times	Sample Port Used
99P8-1	08/01/99	2.2 kg/hr	99P8-1[1]	20 min	BG[2]
			99P8-2	5 min 2 sec	BG
			99P8-3	5 min	BG

[1] This sample set rejected due to impactor overload
[2] BG - baghouse inlet sample port

Table 3-10. Summary of Phase I Pittsburgh Seam Coal Baghouse Inlet Experimental Sampling Conditions

SAMPLE SET # (Port Sampled)	TOTAL COMBUSTION GAS RATE (slpm)	SAMPLING RATE (slpm)	SAMPLING TEMP. (°K at port where sample was taken)	PORT 4 O_2 CONC (%)	PORT 14 O_2 CONC (%)
99P8-1 (BG[1])	460	1.56	472	3.2	5.1
99P8-2 (BG)	460	1.56	472	3.2	5.1
99P8-3 (BG)	460	1.56	472	3.2	5.1

[1] BG - baghouse inlet port

Particle Size Distribution

Using the size-segregated ash weights collected in the BLPI in each test, the particle size distribution (PSD) determined[5] from the two sample sets is shown in Figure 3-23. It should be noted that the large-size particle distributions for these baghouse inlet samples are artificially depressed because some of the large-size particles drop out of the gas phase prior to this sample collection point.

Elemental Analysis

Both sample sets were selected for analysis of size-segregated particle metal content at the University of Arizona by AA/GFAA. These results will be presented in the next quarterly report.

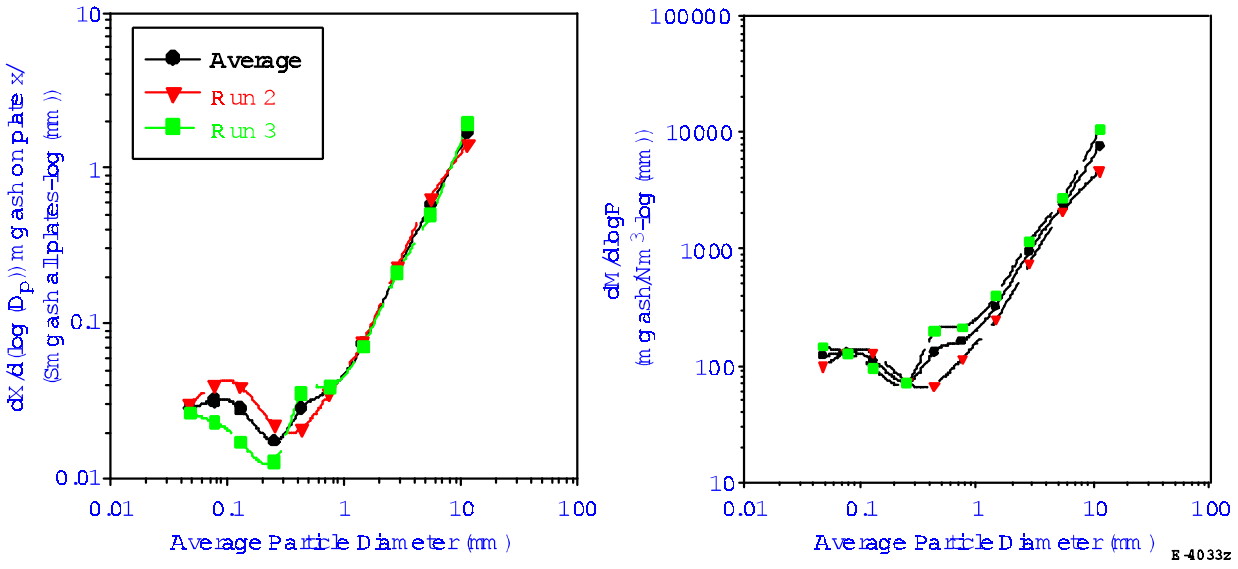

(a) (b)

Figure 3-23. Typical particle size distributions for Pittsburgh Seam coal fly ash at the baghouse inlet sampling port (a) presented as a normalized mass fraction distribution and (b) presented as a gas concentration distribution.

Elkhorn/Hazard Baseline Experiments. The University of Arizona's pilot-scale downflow laboratory combustion furnace was used to test the partitioning of toxic metals in the baseline experiments for the Phase I Kentucky Elkhorn/Hazard bituminous coal. The objectives of these experiments were:

- To obtain toxic metal partitioning data under test conditions which simulate the time/temperature combustion and post-combustion conditions of commercial scale utility boilers at 20% excess oxygen.

- To investigate the differences in toxic metal partitioning from samples collected immediately after char burnout compared to samples collected near the furnace exit and to samples collected at the entrance to the baghouse.

A detailed description of the furnace and sampling systems is given in the Phase I Final Report. A Berner low pressure impactor (BLPI) was used for particulate sample collection for all of the experiments performed.

Sample collection media for the BLPI consisted of polycarbonate membranes sprayed with a high purity grease. The membranes were dried in a vacuum dessicator for a minimum of 24 hours. One and a half milliliter PVC sample vials were used to contain the particulate-laden membranes. The vials were weighed with and without the particulate-laden membranes on a microbalance and stored in zipper locked sealed polyethylene bags. The dried sample collection media were also weighed on the microbalance just prior to loading into the BLPI. All

microbalance weights were repeated. Two readings with a deviation of less than 0.00003 g were required before the weight data were accepted as accurate.

A total of 15 sets of particulate samples was collected during six test runs. All experiments were performed at a coal feed rate of 2.2 kg/hour. We chose to sample particulate at the same locations as those sampled during the Ohio and Wyodak baseline tests. Five sets of particulate samples were collected from Port 4 of the furnace, which is located immediately after the end of the combustion zone (around 0.7 seconds residence time from the burner). Five sets of particulate samples were collected from Port 14 which is located near the bottom of the furnace (around 2.9 seconds residence time from the burner) and represents a snapshot of the flue gas in the post-combustion zone. These samples sets were typically taken immediately after one of the sample sets from Port 4 so that matched sample sets could be selected for analysis. Five sample sets were taken from the inlet to the baghouse and represent ESP inlet sampling conditions. The baghouse samples are taken after partial segregation of large particles in an ash trap and a small particle trap.

In order to obtain a complete PSD, collection tests were performed both with and without the BLPI inlet cyclone. A description of how the two sets of data are combined in provided in the Phase I Final Report. The sample sets and test runs are summarized in Table 3-11. Table 3-12 shows the sampling conditions for the most important sample sets. Figure 3-24 shows the typical steady-state temperature profile from these tests. A comparison of the typical steady-state temperature profiles for all six program coals is shown in Figure 3-25.

Particle Size Distribution

Using the size-segregated ash weights collected in the BLPI in each test, particle size distributions (PSDs) were determined. Typical fly ash PSDs, developed following the method described by Markowski and Ensor,[5] are shown in Figure 3-26. Figures 3-27 through 3-29 show PSDs for individual sample sets at each of the three sampling locations. These figures provide insight into the variability in the PSDs shown in Figure 3-26. At all three sample locations, a typical BLPI PSD is observed which defines three distinct regions: a vapor phase region with a maximum around 0.08 microns, a submicron fume region having a maximum around 0.4 microns, and a supermicron, bulk fly ash region. It should be noted that the large-size particle distribution for the baghouse sample is artificially depressed because some of the large-size particles drop out of the gas phase prior to this sample collection point. Therefore, the mass fraction distribution for the baghouse inlet location displayed in Figure 3-26a is not directly comparable to the other two distributions in this figure.

A mass fraction particle size distribution comparison for samples taken at Port 14 for all six program coals is shown in Figure 3-30.

Table 3-11. A Summary of the Phase I Kentucky Elkhorn/Hazard Coal Baseline Test Runs

Test Run #	Date	Coal Feed Rate	Sample Set #	Sampling Times	Sample Port Used
99KY-1	08/11/99	2.2 kg/hr	none[1]	none	
99KY-2	08/12/99	2.2 kg/hr	99KY-1	2 min	4
			99KY-1c	12 min 9 sec	4
			99KY-2	2 min	14
			99KY-2c	15 min 2 sec	14
			99KY-3	20 min	BG[2]
			99KY-6	20 min 1 sec	BG
99KY-3	8/13/99	2.2 kg/hr	99KY-4	2 min 31 sec	4
			99KY-4c	16 min 1 sec	4
			99KY-5	2 min 39 sec	4
			99KY-5c	16 min	4
			99KY-7	2 min 31 sec	14
			99KY-7c	16 min	14
			99KY-8	3 min 30 sec	14
			99KY-8c	25 min	14
99KY-4	8/18/99	2.2 kg/hr	99KY-10	3 min 30 sec	4
			99KY-10c	25 min	4
			99KY-11	3 min 30 sec	4
			99KY-11c	25 min	4
			99KY-13	3 min 30 sec	14
			99KY-13c	25 min 1 sec	14
			99KY-14	3 min 32 sec	14
			99KY-14c	25 min 1 sec	14
99KY-5	8/19/99	2.2 kg/hr	99KY-9	25 min	BG
			99KY-12	16 min	BG
			99KY-15	16 min	BG

[1]Complete temperature and gas profiles were obtained using this run
[2]BG-Baghouse inlet sample port

Table 3-12. Summary of Phase I Kentucky Elkhorn/Hazard Coal Experimental Sampling Conditions

SAMPLE SET # (Port Sampled)	TOTAL COMBUSTION GAS RATE (slpm)	SAMPLING RATE (slpm)	SAMPLING TEMP (°K at port where sample was taken)	PORT 4 O_2 CONC (%)	PORT 4 CO_2 CONC (%)	PORT 14 O_2 CONC (%)	PORT 14 CO_2 CONC (%)	PORT BG* O_2 CONC (%)	PORT BG CO_2 CONC (%)
99KY-1/1c (4)	401	1.36	1500	3.4	15.2				
99KY-2/2c (14)	410	1.39	1176	3.3	15.2	3.7	15.1		
99KY-3/6 (BG)	410*	1.39+	470	3.3	15.2	3.7	15.1	5.5	13.4
99KY-4/4c (4)	401	1.36	1530	3.4	15.6				
99KY-5/5c (4)	401	1.36	1522	3.2	15.6				
99KY-7/7c (14)	417	1.42	1182	3.3	15.6	4.1	15.0		
99KY-8/8c (14)	417	1.42	1189	3.3	15.6	4.0	15.1		
99KY-10/10c (4)	401	1.36	1458	3.4	15.4				
99KY-11/11c (4)	401	1.36	1444	3.4	15.4				
99KY-13/13c (14)	424	1.44	1102	3.4	15.4	4.3	14.5		
99KY-14/14c (14)	424	1.44	1102	3.4	15.4	4.3	14.5		
99KY-9/12/15 (BG)	424	1.44	495	3.4	15.4	4.4	14.4	5.3	13.7

*BG = baghouse inlet sampling port

Combustion rate for BG samples are assumed to equal rate at Port 14

+ BG sampling rate is set equal to Port 14 rate; this is not an isokinetic sample

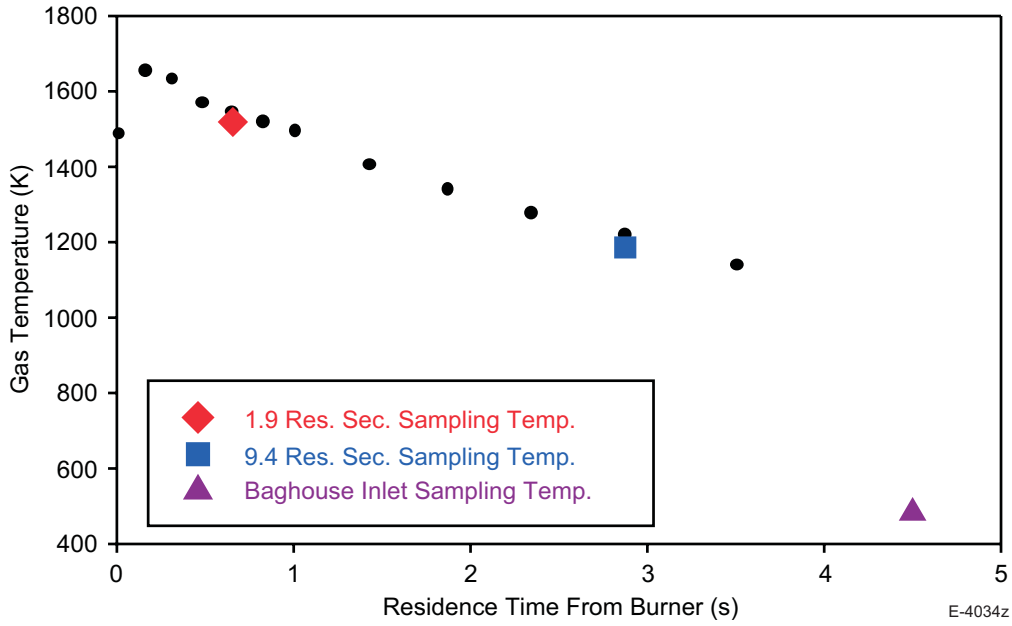

Figure 3-24. Typical self-evolving temperature profile for Kentucky Elkhorn Hazard Coal Combustion in the University of Arizona Downflow Combustor.

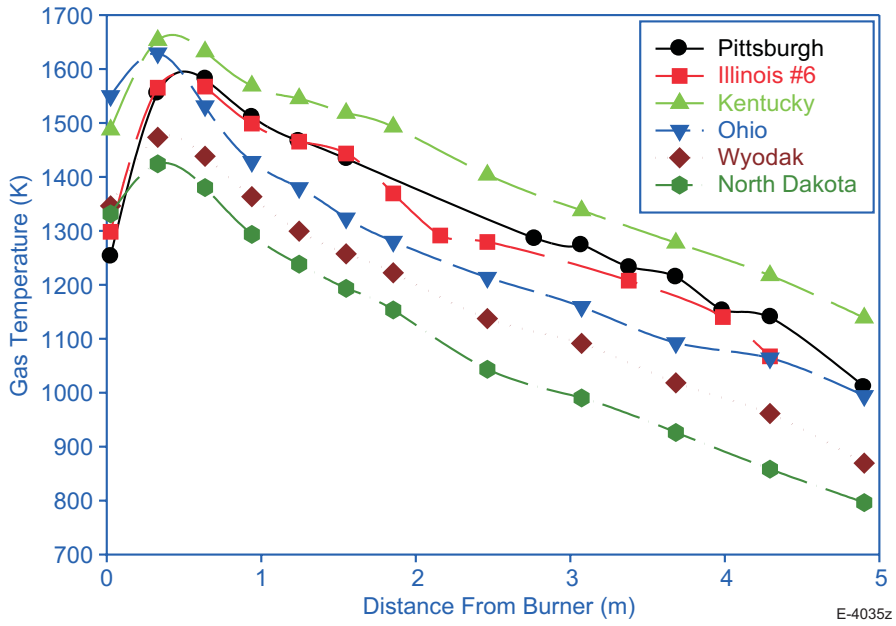

Figure 3-25. Typical self-evolving temperature profile for all program coals in the University of Arizona Downflow Combustor.

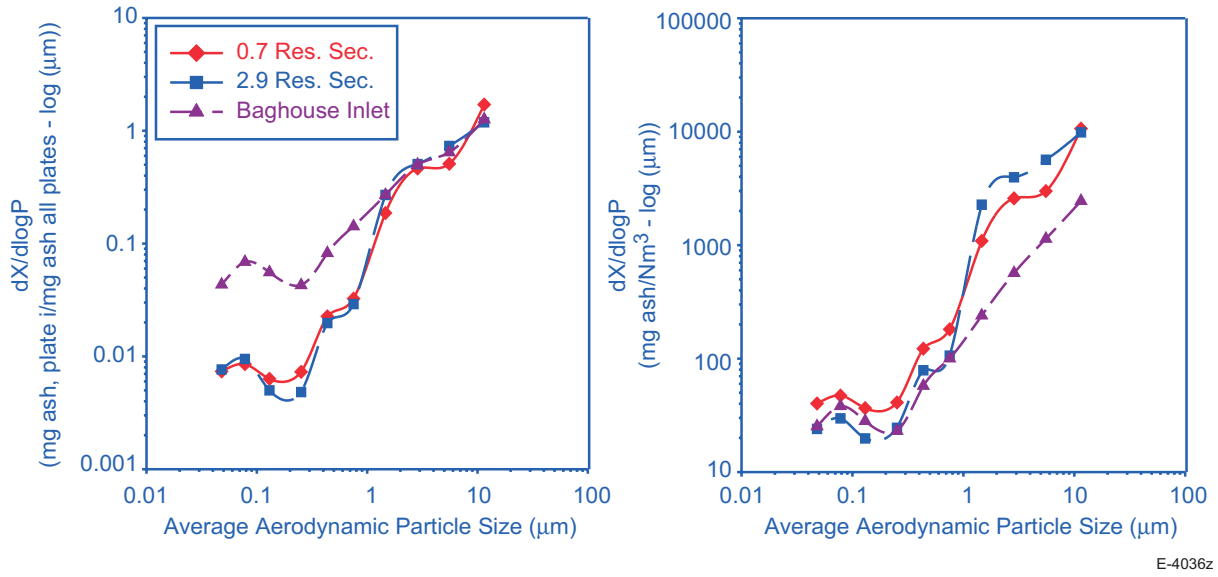

(a) (b)

Figure 3-26. Typical particle size distributions for Kentucky fly ash at various residence times (a) presented as a normalized mass fraction distribution, and (b) presented as a gas concentration distribution.

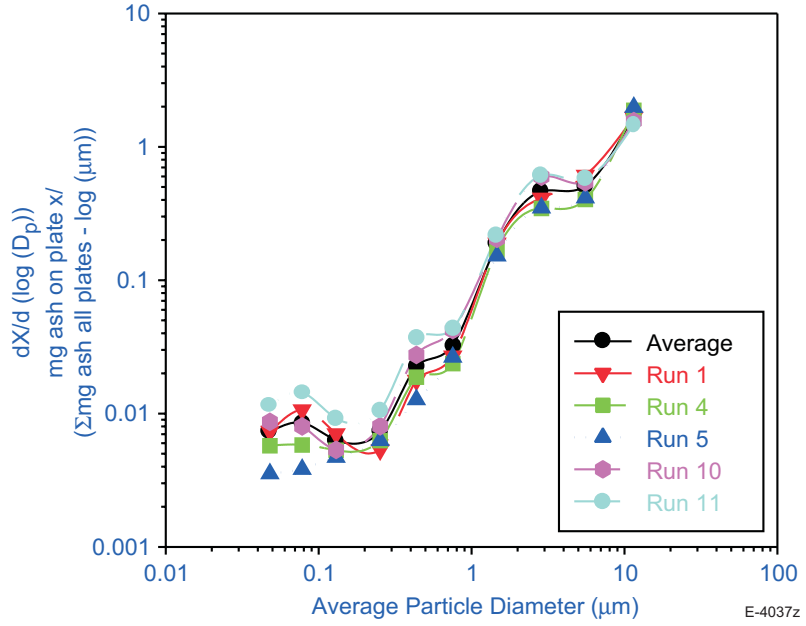

Figure 3-27. Particle size distribution data at 0.9 residence seconds for Kentucky fly ash.

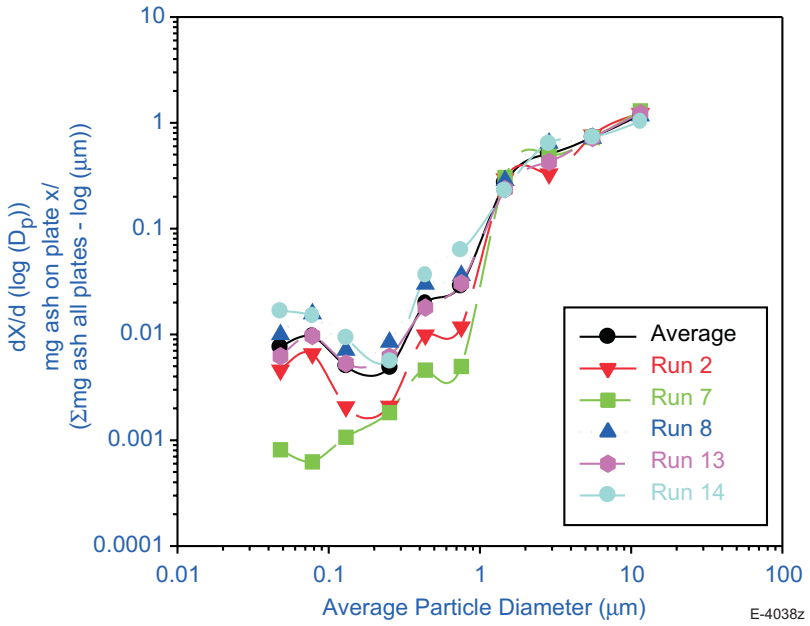

Figure 3-28. Particle size distribution data at 2.9 residence seconds for Kentucky fly ash.

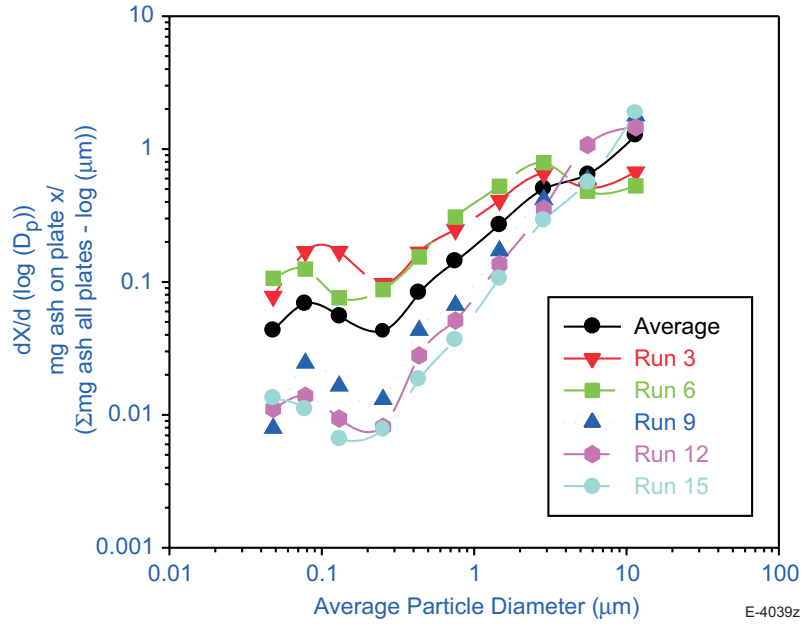

Figure 3-29. Particle size distribution data at the baghouse inlet port for Kentucky fly ash.

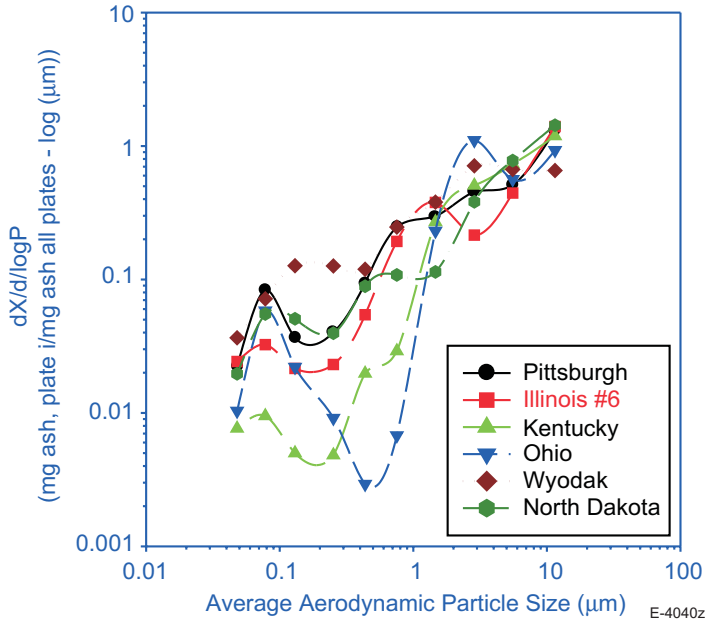

Figure 3-30. Particle size distributions at Port 14 for all program coals under baseline conditions.

Elemental Analysis

Two representative sample sets from the 1.9 seconds residence time sample location (sample sets 10 and 11), two representative sample sets from the 9.4 seconds residence time sample location (sample sets 13 and 14) and three representative sample sets from the hot-side of the particulate collection device (sample sets 9, 12, and 15) were selected for analysis of size-segregated particle metal content at the University of Arizona by AA/GFAA. The results will be presented in the next quarterly report.

3.4.2 Measurement of Post-Combustion Chlorine Speciation

EPA Method 26 will be used to measure chlorine speciation in coal combustion flue gas from the University of Utah's U-furnace. The test matrix to determine the usefulness of EPA Method 26 will be as described in Table 3-13. If Method 26 cannot distinguish HCl from Cl_2 in the presence of SO_2, we are prepared to try another collection system that uses KI to distinguish between the chlorine products.

3.4.3 XAFS Study of Mercury in Ash and Sorbents

During July, we conducted synchrotron XAFS runs from July 13th to 19th at the Stanford Synchrotron Radiation Laboratory (SSRL), Stanford, CA (beam-line IV-3: Cr-Hg) and from July 28th to August 1st at the National Synchrotron Light Source (NSLS), Brookhaven National Laboratory, NY (beam-line X-19A: S-Fe; beam-line X-18B: Cr-Hg).

Table 3-13. Test Matrix for Gas-Phase Chlorine Speciation Measurements

	Chlorine Gas	Hydrochloric Acid	Sulfur Dioxide
Test1	2 ppm		
Test 2		65 ppm	
Test 3	2 ppm	65 ppm	
Test 4	2 ppm		2000 ppm
Test 5		65 ppm	2000 ppm
Test 6	2 ppm	65 ppm	2000 ppm
Test 7	2 ppm		100 ppm
Test 8		65 ppm	100 ppm
Test 9	2 ppm	65 ppm	100 ppm

We obtained Hg XAFS data for 10 of 11 Hg sorbents from Dr. Behrooz Ghorishi (ARCADIS Geraghty and Miller, Inc.), for three new mercury standards (HgSe, $HgNO_3$, and aqueous $Hg(NO_3)_2$), and for the Cherokee station fly-ash samples (samples courtesy of ADA Technologies, Inc.; J. Albiston and J. Smith) and fractions prepared by triboelectrostatic separation. Analysis of the mercury XANES data has already commenced and a brief summary of findings to date will be given in this report.

Hg Sorbent Samples from Ghorishi and Gullett, EPA. The samples received from Dr. Ghorishi consisted of six carbonaceous sorbents and five inorganic sorbents. The XAFS data collected at SSRL have been analyzed and the normalized XANES and 1st derivative spectra are shown in Figure 3-31. Various parametric data derived from the XAFS data are summarized in Table 3-14, which also provides a brief description of the samples. There is a clear distinction in the Hg XAFS spectra and data between the carbonaceous sorbents and the two $Ca(OH)_2$ sorbents, which were the only inorganic sorbents to give acceptable XAFS data. For these latter two samples, it is clear that the sorption of $HgCl_2$ involves the formation of a Hg-O bond as the inflection point difference (IPD) for both samples was in excess of 10.0 eV. In addition, the RSF distance for one of the samples was significantly shorter and the RSF peak-heights for both lime-based samples were significantly less than those observed for the carbonaceous sorbents. Both the shortened RSF distance and the smaller RSF height are compatible with Hg-O bonding in contrast to the Hg-S or Hg-Cl bonding present in the carbonaceous samples. The following sorption reaction is suggested for the lime-based sorbents:

$$Ca(OH)_2 + HgCl_2 \rightarrow CaCl_2 + Hg(OH)_2$$

This reaction indicates that mercuric chloride will undergo chemisorption when the conditions are right.

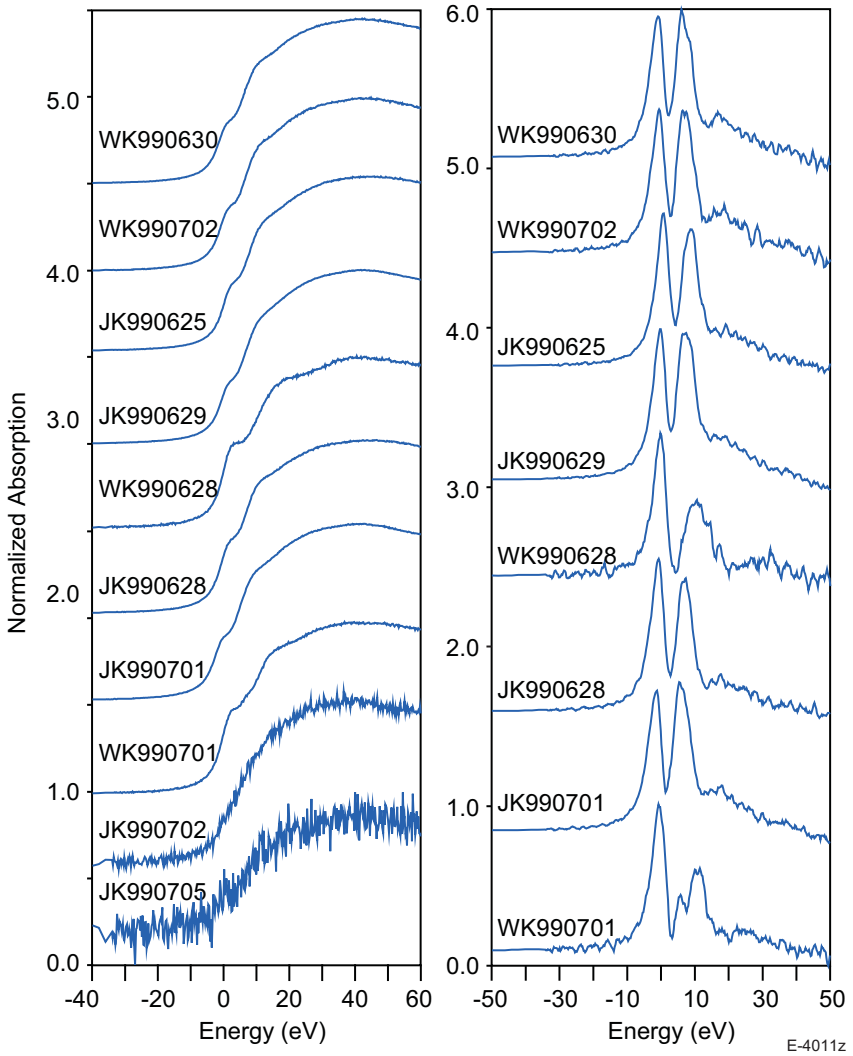

Figure 3-31. Hg XANES and 1st derivative spectra for sorbent samples from Drs. Ghorishi and Gullett, EPA RTP. Note that there are no derivative spectra presented for the bottom twoXANES spectra because of their poor signal/noise ratios.

The bottom derivative spectrum from lime-based sorbent (WK990701) suggests the possibility of a mixture of sorbent reactions as the dual peaked nature of the peak at high energy might arise from a combination of minor Hg-S and major Hg-O bonding. This would imply that the presence of SO_2 in the vapor phase can result in the formation of Hg-S bonds. Note that the other lime-based sample (WK990628) was not exposed to SO_2 in the vapor phase and shows no development of any interior peak. Finally, it should be noted that the six carbonaceous sorbents were prepared from two different treated carbon materials (FGD-C and PC-100 type carbons) and subjected to the same three sorption experiments. As summarized in Table 3-14 and also in Figure 3-32, the FGD-C derived sorbents always gave a higher IPD value that the PC-100 derived sorbents. The significance of this observation is not clear at this time, but implies that the Cl/S ratio on the carbon surface is systematically different for the two types of carbon based on previous observations of the importance of both chlorine and sulfur for mercury sorption on chars as discussed in the Quarterly Report covering August 1997 to June 1998.

Table 3-14. XAFS Systematics for Mercury Adsorbed on Various Sorbents from Ghorishi and Gullett

Sample	Conditions Sorbent/Gas Species/T °C	Step-Height	RSF Distance Å	RSF Height	Peak Height Ratio	IPD, eV
WK990630	FGD-C/$HgCl_2$/140	0.72	1.93	347	0.9	8.0
WK990702	PC-100/$HgCl_2$/140	0.71	1.94	360	1.0	7.5
JK990625	FGD-C/Hg, HCl/60	0.68	1.90	290	1.2	8.2
JK990629	PC-100/Hg,HCl/60	0.68	1.94	356	1.0	7.2
WK990628	$Ca(OH)_2$/$HgCl_2$/60	0.53	1.70	199	2.0	10.7
JK990628	FGD-C/Hg,HCl+SO_2/60	0.71	1.93	317	1.2	7.5
JK990701	PC-100/Hg,HCl+SO_2/60	0.72	1.93	394	0.9	7.2
WK990701	$Ca(OH)_2$/$HgCl_2$,SO_2/60	0.60	1.93	210	4.0 2.0	6.3 11.5
JK990702	Gypsum/Hg,HCl/60	0.22	---	---	---	---
JK990703	Gypsum/Hg, HCl+SO_2/60	n.d.				
JK990705	Fe_2O_3-Al_2O_3-SiO_2/Hg, O_2+CO_2+NO_2/100	0.05	---	---	---	---

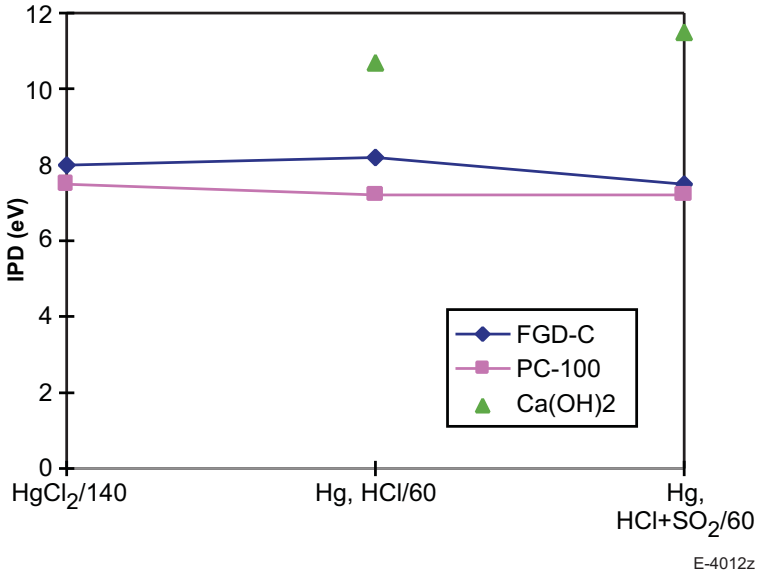

Figure 3-32. Plot of IPD values for different carbon-based sorbents and two lime-based sorbents for comparable experiments.

Samples Prepared from Cherokee Station Fly-Ash. Hg XAFS experiments were also conducted on various fractions of fly-ash collected from the Cherokee power station, CO, by personnel at ADA Technologies, Inc. This Cherokee fly-ash sample, derived from a western U.S. subbituminous coal, had been found to be especially effective for the adsorption of vapor-phase mercury. The sample we received from ADA Technologies had been exposed to a Hg-containing simulated flue gas. Ash-rich and ash-poor fractions were then prepared from this Hg-enriched sample by dry, triboelectrostatic (TES) separation, which was performed for us by Dr. James K. Neathery at the Center for Applied Energy Research (CAER) at the University of Kentucky. Data on the ash and Hg contents of the different fractions, reported in the previous quarterly report (April to June 1999), are summarized here again in Table 3-15 for convenience. As reported previously, the data suggest that there is a specific fraction in the fly-ash carbon that is particularly effective for mercury sorption.

Table 3-15. Analytical Data for Triboelectrostatic Separation on ADA Cherokee Fly-Ash Sample

Sample (fraction)	Wt %	Carbon Content (wt %)	Mercury Content (ppm)
Bulk sample	100	8.2	158
+'ve fraction	49.9	3.6	81
Middle fraction	38.9	6.4	87
-'ve fraction	11.3	13.8	745

Mercury XAFS data were collected for the fly-ash and fractions prepared by TES separation. The mercury XANES and derivative spectra for the fractions are shown in Figure 3-33. While the spectra themselves appear to show little difference, the derivative spectra show some subtle variations and this is reflected in the average IPD values determined for the samples (Table 3-16). However, the variation in the IPD parameter is not much larger than estimated experimental errors in the parameter. The values would appear to reflect formation of Hg-Cl complexes, consistent with previous XAFS investigations of carbon-based sorbents.[8,9] The subtle differences in the derivative spectra and the value of the IPD parameter may be indicative of secondary factors. For example, the higher value of the IPD parameter for the undifferentiated center fraction could be accounted for by a mixture of the Hg-Cl complex on the carbon and a Hg-O complex on the aluminosilicate fraction. In other studies we have seen values of the IPD in excess of 9.0 eV for zeolite and the lime-based sorbents discussed above in which the sorption complex must involve the formation of a Hg-O complex.

Project Coals and Ashes. In addition to the Hg data discussed above, some new XANES data were obtained for S and Se in project coals and for S and various metals in fly-ash samples obtained from the combustion unit at the University of Arizona. These data will be analyzed and reported in detail at a later date.

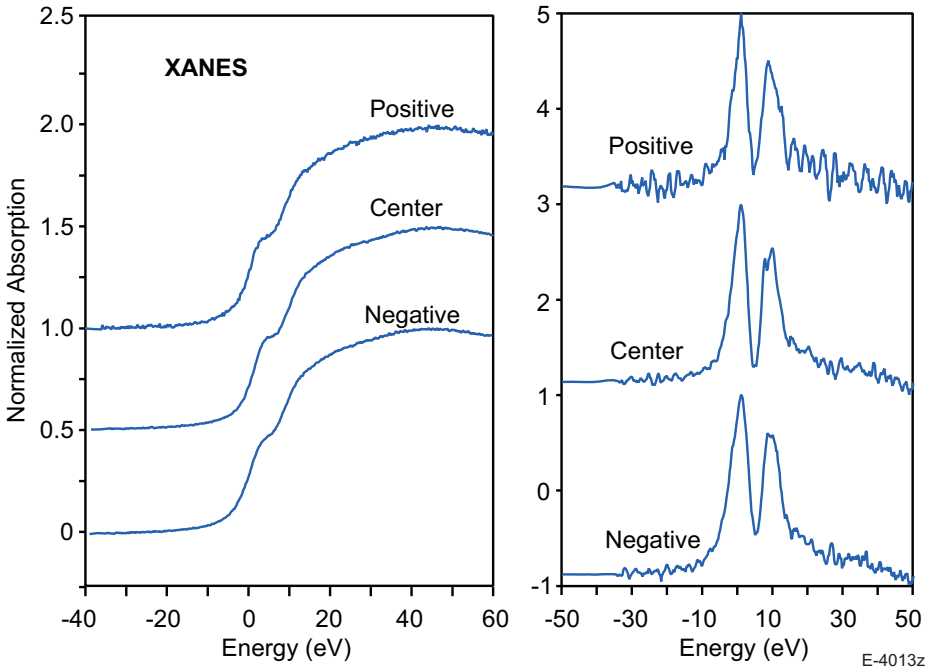

Figure 3-33. Mercury XANES (left) and derivative (right) spectra of fractions obtained from Cherokee fly ash by triboelectrostatic separation.

Table 3-16. IPD Values for Fractions of Cherokee Fly-Ash Separated by Triboelectrostatic Separation

Sample	Bulk Ash	Negative fn.	Center fn.	Positive Fn.
IPD Value, eV	8.5	8.2	8.7	7.8

3.4.4 Mercury-Ash Interactions in Fixed Bed Tests

A meeting was held between EERC (Dunham, Miller) and PSI (Senior) to map out the matrix for the intial experiments on mercury-ash interactions to be conducted at EERC. The overall goal of this effort is to collect data which will allow us to model the interactions of mercury and fly ash (specifically, adsorption of Hg^0 and Hg^{+2} and oxidation of Hg^0) in the air heater and particulate control device of a coal-fired power plant. A test matrix for these tests was included in the Phase II Statement of Work. However, in the time since this was written, much has changed on the mercury landscape. Therefore, we need to revisit the test matrix. General themes or guidelines for these experiments are as follows:

- Use fly ash from the Phase II program coals collected from the UA self-sustained combustor and from selected power plants. Note that we will need to verify that the UA ash is representative. This will be done by making a comparison of the CCSEM analysis from the ash collection system with that from a sample extracted from the gas.

- Characterize the fly ash and correlate with coal composition.

- As much as possible, use flue gas compositions corresponding to combustion of the parent coal at 20% excess air. That is, the effects of flue gas constituents will not be studied as there is ongoing work by EERC and others in this area.

- Look at the interactions of Hg^0 and Hg^{+2} separately to help understand mechanisms.

- Measure sorption and oxidation on-line in the EERC fixed bed reactor.

The ash samples will be from the Ohio bituminous blend, the Wyodak PRB coal, and the North Dakota lignite. Fly ash will be obtained from the baseline combustion conditions at UA. For the Ohio blend, fly ash will also be collected at lower excess air conditions in order to maximize unburned carbon. Temperature in the fixed bed will be either 250°F or 350°F in order to span the range of conditions expected in particulate control devices. The mercury concentration in the flue gas will be 15 $\mu g/m^3$ as either Hg^0 or Hg^{+2}. Other than mercury, the flue gas composition will generally be calculated on the basis of combustion of the coal at 20% excess air (see Appendix B). A reasonable value for NO_x will be chosen (300 ppm); NO_2 will be fixed at 7% of the total nitrogen oxides (20 ppm). A relatively large bed of ash (1 to 2 g) will be used for the experiments in order to see small effects. EERC will experiment with the bed size to optimize it.

Based on the discussion above, the preliminary initial test matrix is given in Table 3-17. Note that this does not include repeat measurements which will be made by EERC.

We discussed additional ash samples which might be analyzed, for example, samples from full scale power plants such as Coal Creek, Comanche, Cherokee or some of the high carbon CONSOL samples. The possibility was also raised that the carbon could be removed from the high carbon ash by low temperature ashing to look at the properties of an ash with and without carbon. We will discuss this further as we get into the experiments. We may also decide to skip some of the tests in Table 3-17 based on early results.

An important and unique aspect of this study is the ash characterization. Table 3-18 summarizes the measurements to be made on the ash both before and after the fixed bed experiments. There are two “after” measurements to be made, Hg content and XAFS. This will have to be coordinated between EERC and Kentucky to make sure that there is enough sample for both measurements.

Table 3-17. Test Matrix for Initial Mercury-Ash Interaction Experiments

Ash	Temperature, F	Mercury
Wyodak	250	Hg^0
Wyodak	350	Hg^0
North Dakota Lignite	250	Hg^0
North Dakota Lignite	350	Hg^0
Ohio Blend	250	Hg^0
Ohio Blend	350	Hg^0
Ohio Blend-High LOI	250	Hg^0
Ohio Blend-High LOI	350	Hg^0
Wyodak	250	$HgCl_2$
Wyodak	350	$HgCl_2$
North Dakota Lignite	250	$HgCl_2$
North Dakota Lignite	350	$HgCl_2$
Ohio Blend	250	$HgCl_2$
Ohio Blend	350	$HgCl_2$
Ohio Blend-High LOI	250	$HgCl_2$
Ohio Blend-High LOI	350	$HgCl_2$

Table 3-18. Ash Analyses Planned for Each Fly Ash Sample

Before/After Exposure (1)	Analysis	Responsibility
Before	Hg content	EERC
Before	CCSEM	Kentucky
Before	Mössbauer	Kentucky
Before	XAFS: Hg, Ca, S, Cl	Kentucky
Before	Surface area	PSI
Before	Loss on ignition	EERC
After	Hg content	EERC
After	XAFS: Hg, S, Cl	Kentucky
(1) Analysis of “before” samples will be on splits of ash sample, but “after” samples will be on 1 to 2 g filter samples.		

Samples of ash were received from the University of Arizona. These were collected in the bag collector during combustion of each of the three Phase II coals (Ohio blend, North Dakota lignite, and Wyodak) at 20% excess air. During these runs, the ash particle trap located upstream of the bag collector collected some ash (4% to 18% of the total ash collected). However, the ash in the particle collector appeared to have large pieces of unburned carbon and refractory. Therefore, this sample will not be used for fixed bed experiments.

Ash from the bag collector appeared brown to dark gray in color, indicating some degree of unburned carbon. For the Wyodak coal, it was suspected that this unburned carbon was very fine. During combustion of the Wyodak coal, ash samples were withdrawn from the gas phase and directed into a sampling system consisting of a cyclone pre-separator with a cutoff diameter of approximately 5 microns and an impactor. There was no large ash collected in the cyclone. Therefore, any carbon in the sample is in small particles, probably soot.

Table 3-19 gives the loss-on-ignition (LOI) values and the surface area of the ash samples from the bag collector. LOI was measured at EERC. Surface area measurements were made at PSI using a single-point BET method with N_2. The values of LOI for both the North Dakota lignite and the Wyodak are higher than observed by other researchers. The Wyodak ash, in particular, has a very high surface area. This, together with the absence of large ash particles in the extractive ash sample, suggests that this ash contains very fine soot instead of unburned char.

Table 3-19. Surface Area and LOI of Ash Samples from University of Arizona Bag Collector

Sample	Moisture (wt%)	LOI (wt% dry)	Surface Area, m^2/g
Ohio blend	0.64	6.79	1.52
North Dakota lignite	0.38	2.86	0.55
Wyodak	0.73	4.45	13.42

3.5 Model Development

3.5.1 Mercury Emissions Model

The simple mass balance model for emissions of mercury from coal-fired power plants was revised to further test our current understanding of mercury transformations in flue gas (Figure 3-34). The post-combustion region of the boiler was divided into three parts: 1) convective section to air heater (AH); 2) electrostatic precipitator (ESP); and 3) flue gas desulfurization unit (FGD). Concentrations of mercury species (gaseous and condensed) in each section were either calculated from equilibrium or plant parameters, or assigned based upon limited observations available from field data.[10,11] All of the mercury is assumed to start as gaseous elemental mercury (Hg^0). In the AH and ESP sections, elemental mercury could oxidize to Hg^{+2}, nominally the sum of HgO and $HgCl_2$. In addition, both Hg^0 and Hg^{+2} could be adsorbed

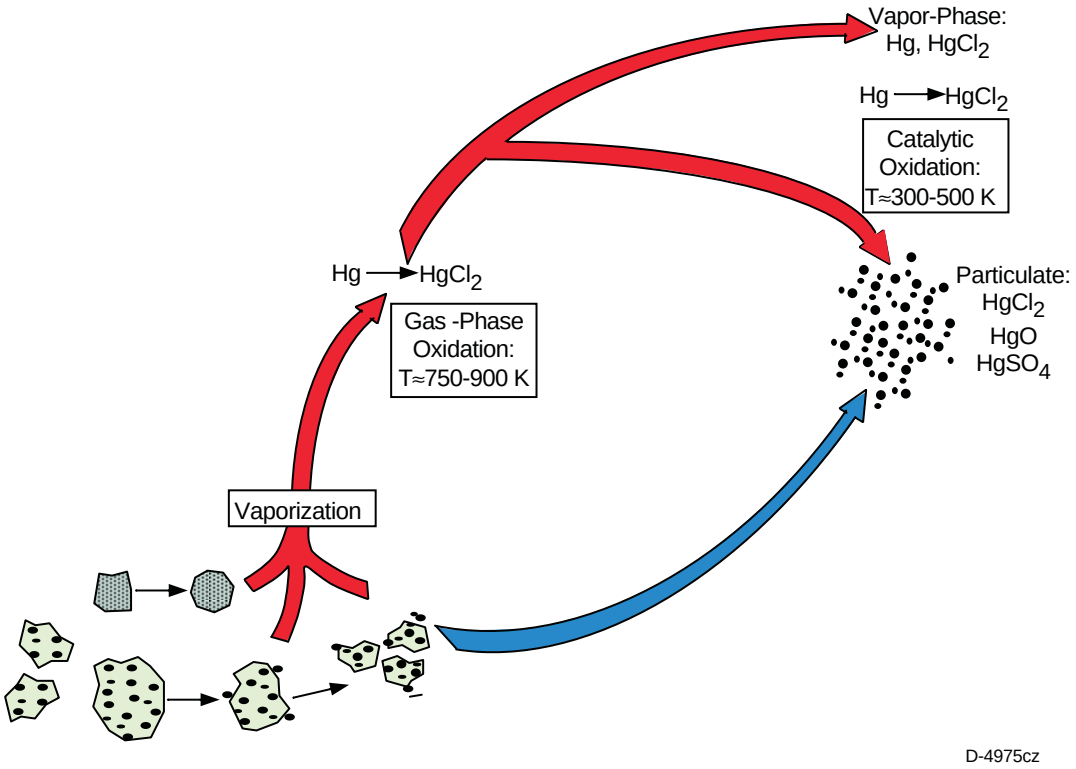

Figure 3-34. Proposed mercury transformations in coal-fired power plant flue gas.

on particulate matter in the AH and ESP sections, converting them to Hg_p. In the FGD section, both Hg^0 and Hg^{+2} could be absorbed into the scrubber solution. The model therefore predicts the speciation and emissions of mercury from the boiler based upon coal mercury content, equilibrium at elevated temperatures, assumed mercury partitioning coefficients in the various sections of the boiler, and particulate and SO_2 capture efficiencies as outlined in Table 3-20.

In deriving the parameters reported in Table 3-20, the following assumptions were made. The amount of oxidation that occurs in the AH section was calculated assuming that the chemical composition is frozen, equal to the equilibrium composition at 825 K. The results of equilibrium calculations at 20% excess air for a number of different coals were used to derive this correlation, shown in Figure 3-35. A range of chlorine contents, from 25 to 4500 ppm, were used in the calculation. At very low chlorine contents (< ~50 ppm), most of the oxidized mercury is HgO (Figure 3-36). Many western fuels fall into this low-chlorine category. The adsorption behavior of HgO on fly ash may be different from $HgCl_2$.

The oxidation of elemental mercury in the AH was assumed to proceed entirely via gas-phase reaction. Experimental evidence suggests that some fly ash can catalyze oxidation of elemental mercury. Iron oxide is thought to be responsible for this oxidation.[12] Subsequent versions of the model may thus need to include a contribution from catalytic oxidation by fly ash. In this case, the iron content of the coal (and perhaps mineralogy) would be needed as input data.

Table 3-20. Mercury Model Parameters

Parameter	Value	Notes
Fraction of Hg^0 oxidized in AH	**	Calculated from Equilibrium at 825 K (see Figure 3-35)
Fraction of Hg^0 adsorbed in AH	0%	Assumed
Fraction of Hg^{+2} adsorbed in AH	**	Function of LOI (see Figure 3-37)
Fraction of Hg^0 oxidized in ESP	0%	Assumed
Fraction of Hg^0 adsorbed in ESP	0%	Assumed
Fraction of Hg^{+2} adsorbed in ESP	0%	Asumed
Collection efficiency of ESP	**	Input from Plant Operation
Fraction of Hg^0 absorbed in FGD	0%	Assumed
Fraction of Hg^{+2} absorbed in FGD	**	Calculated from Figure 3-39 or limestone scrubber; 90.9% for Mg-lime scrubber; function of SO_2 removal for Chiyoda
Fraction of adsorbed Hg^{+2} oxidized to Hg^0 in FGD	**	Calculated from L/G (Figure 3-40)

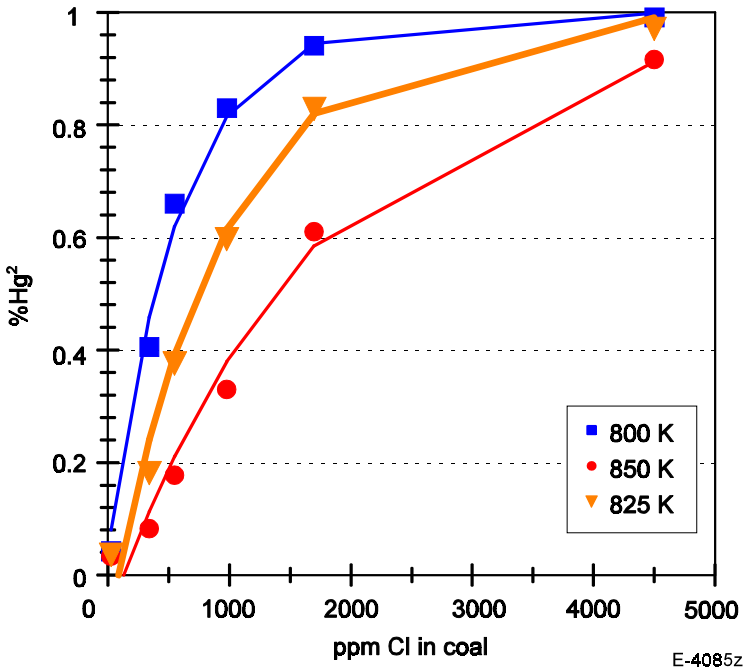

Figure 3-35. Fraction of elemental mercury oxidized under equilibrium conditions and 20% excess air, as a function of coal chlorine content.

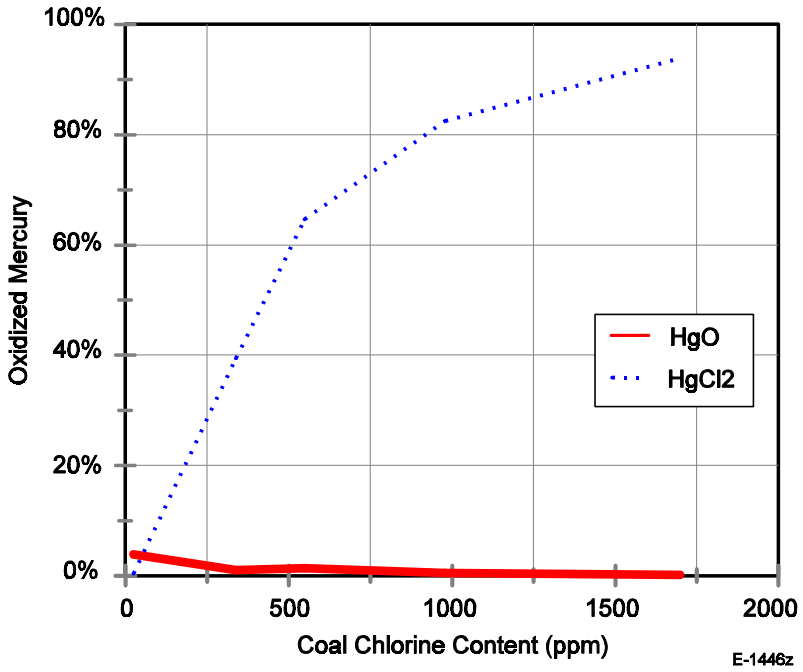

Figure 3-36. Relative amounts of HgO and $HgCl_2$ under equilibrium conditions at 20% excess air as a function of coal chlorine content and gas temperature.

A portion of the mercury may be adsorbed on the fly ash at the inlet to the particulate control device.[10,11,13,14] Combustion of bituminous coals can result in unburned carbon which has been suggested to adsorb mercury. Mercury has been found to concentrate in the carbon-rich fraction of fly ash.[15] Preliminary experimental work on adsorption of gaseous mercury on coal char[16] showed that $HgCl_2$ was adsorbed more efficiently than Hg^0, with two to fifty times more $HgCl_2$ adsorbed than Hg^0 under the same conditions, and the adsorption of the former was correlated with char surface area. This would also indicate that adsorption of $HgCl_2$ is a physical adsorption process. Adsorption of elemental mercury depended on the rank of the coal from which the char was derived. These results suggest that the nature of the unburned carbon, in terms of morphology and surface chemistry, strongly affects mercury adsorption.

At this time, it is not possible to generalize and conclude that high carbon in ash will always give high levels of particulate-bound mercury. However, in the case of similar coals, there may be a relationship as illustrated in Figure 3-37. The data shown in Figure 3-37 were taken either at full scale power plants[10] or at a large pilot scale unit.[13] The coals were from the Northern Appalachian or Illinois Basins. Based on the mercury measured in the ash, as sampled directly from the flue gas using the Ontario Hydro method, the amount of particulate phase mercury was normalized with respect to the sum of the particulate phase and gaseous oxidized mercury. For these coals, there is a relationship between carbon content of ash (as measured by loss-on-ignition) and mercury content. Data will have to be obtained from a wider range of bituminous coals in order to generalize this relationship.

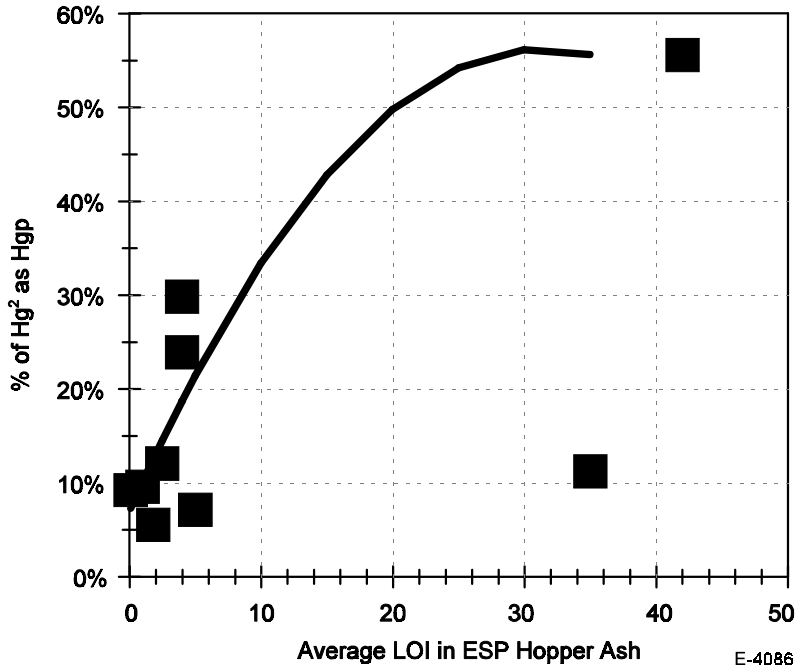

Figure 3-37. Mercury in particulate phase at ESP inlet as a function of carbon content (LOI) of ESP hopper ash (References 10,13).

Western sub-bituminous coals produce fly ash which is very high in calcium. In some cases, ash from these coals has been observed to adsorb large amounts of mercury in the particulate collection device.[16] Calcium silicate sorbents also adsorb mercury chloride.[17] However, western coals are generally low in chlorine and produce very little mercury chloride. Some component of the ash from these coals appears to adsorb elemental mercury. At this time, the mechanism by which elemental mercury is removed by the ash from western sub-bituminous ash is not known.

Of the coal-fired utility plants in the U.S., 159 out of 1035 have wet FGD systems for control of SO_2. Using 1996 data,[18] this represents 23% of the total capacity (70 GW out of 299). Recent sampling campaigns on full scale utility boilers[10,11] and a large pilot scale unit[13] have provided data on the speciation of mercury before and after the FGD. Scrubbers have been observed to efficiently remove oxidized mercury, but not elemental mercury.

Based on a detailed study of the behavior of mercury in a pilot scale wet scrubber,[13] the adsorption of oxidized mercury appears to be strongly correlated with the mass transfer in the scrubber. The liquid-to-gas ratio (L/G) was a good indicator for the amount of Hg^{+2} removed by the scrubber. The composition of the scrubber liquid and design of the scrubber are also important in determining the removal of Hg^{+2}. Figure 3-38 shows the removal of Hg^{+2} across the scrubber as a function of L/G for five full scale scrubbers burning eastern bituminous coal.[10] Two scrubbers used a magnesium-enhanced lime system and three used limestone. There are clear differences between the limestone and magnesium-enhanced limestone scrubbers. For the former, the L/G ratio had an effect on removal of Hg^{+2}, while a clear effect of L/G ratio was not

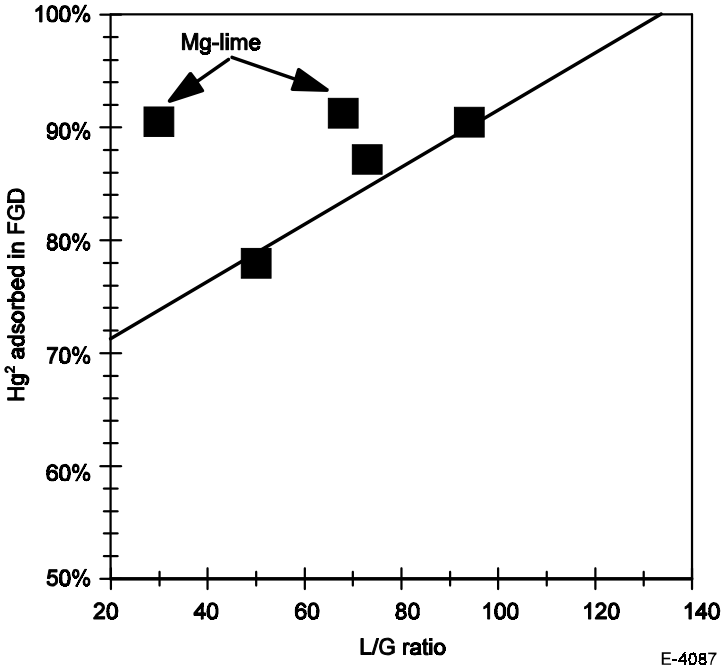

Figure 3-38. Fraction of oxidized mercury adsorbed in scrubber for limestone scrubbers and Mg-lime scubbers (Reference 10).

evident for the magnesium-enhanced lime system. Thus, the nature of the scrubbing solution must be known in order to model mercury removal.

Pilot scale data have been taken on the effect of scrubber slurry pH on mercury removal in limestone scrubbers. These are shown in Figure 3-39 together with full scale data on limestone scrubbers. These figures suggest that the type of scrubber and the L/G ratio are the two key variables for modeling adsorption of Hg^{+2} across FGDs. Under some conditions, limestone scrubbers have been observed to reduce adsorbed mercury back to Hg^0 giving rise to higher concentrations of elemental mercury at the outlet than at the inlet. Assuming that no Hg^0 is adsorbed by the scrubber, the amount of adsorbed Hg^{+2} that is reduced can be calculated from the ratio of the increase in elemental mercury to the decrease in Hg^{+2} across the scrubber. Based on very limited data, this also appears to be related to the L/G ratio in the scrubber, as shown in Figure 3-40.

Recent DoE-sponsored field studies have been conducted to measure mercury speciation and mercury mass balances on coal-fired power plants using the Ontario Hydro method for gaseous mercury sampling. These data provide the best set for testing the model. In one study, four power plants were sampled[10] which all burned Eastern bituminous coal. The plants all had wet scrubbers and ESP's. In another study, a power plant burning a Western lignite was sampled.[11] This plant also had a wet scrubber and an ESP. Table 3-21 summarizes the coal and boiler information for these cases.

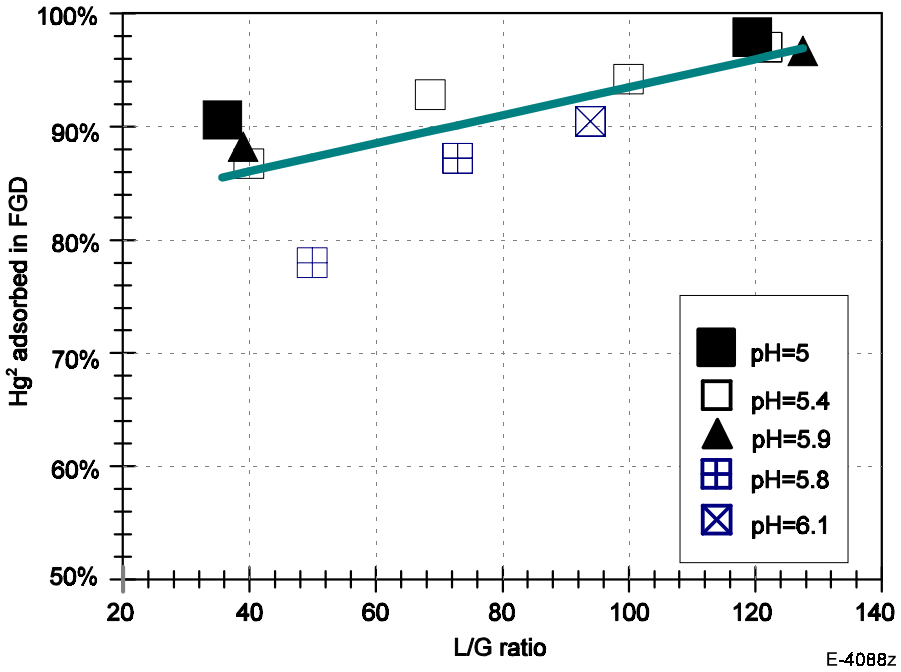

Figure 3-39. Fraction of oxidized mercury adsorbed in limestone scubbers as a function of L/G ratio (References 10,13).

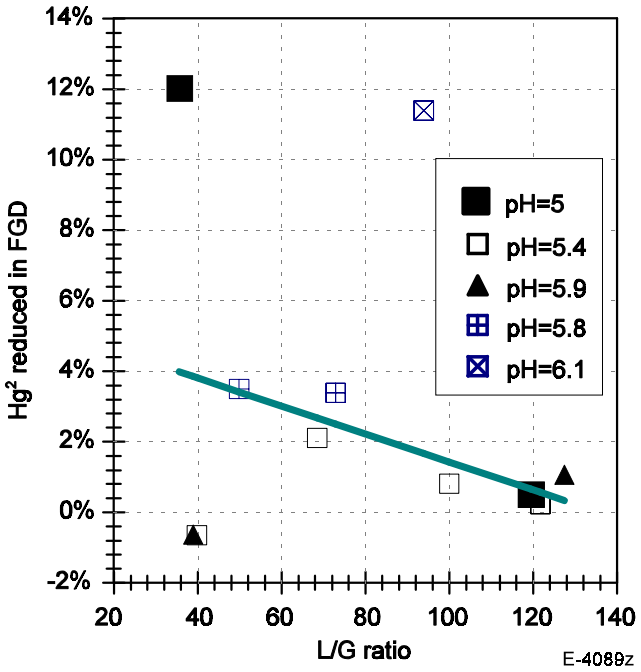

Figure 3-40. Increase in elemental mercury across limestone scubbers as a function of L/G ratio (References 10,13).

Table 3-21. Coal and Boiler Parameters from DoE Field Sampling (References 10,11)
(Composition Values Reported on Dry Basis)

Quantity	Plant 1	Plant 2	Plant 3	Plant 4	Plant 5	Plant 6
Boiler design	PC	PC	PC	PC	PC	PC
Particulate control	ESP	ESP	ESP	ESP	ESP	ESP
SO_2 control	Mg-lime	limestone	limestone	Mg-lime	Chiyoda	limestone
Coal rank	bituminous	bituminous	lignite	bituminous	bituminous	bituminous
Heating value, Btu/lb	13,130	12,737	10,135	12,332	12,731	12.753
Coal flow, lb/hour	197,600	139,230	540,670	1,052,540	29,670	316,575
Chlorine content, ppm	1,100	1,600	59	1,300	2,300	1,400
Mercury content, ppm	0.124	0.086	0.098	0.19	0.090	0.080
ESP collection efficiency	99.5	99.5	99.5	99.5	99.5	99.5
ESP ash LOI, %	4%	1%	0%	0.1%	43%	4%
FGD efficiency for SO_2	97%	82%	90%	96%	87%	96%
Scrubber L/G	68	94	100 *(est)*	30		50

The predictions of mercury speciation, in terms of fraction as Hg^{+2} at the ESP inlet are compared against measured values in Figure 3-41. The predictions are based primarily on the coal chlorine content and the LOI of the ash. Of these two factors, the coal chlorine content has the largest impact on mercury speciation. The impact of LOI is based on the correlation in Figure 3-37 for a number of similar bituminous coals (including the full scale data). However, the impact of coal chlorine content is based solely on the kinetic argument for gas-phase oxidation and not on any correlations with data. The agreement between measured and predicted speciation at the ESP inlet is very good ($r^2 = 0.95$).

Figures 3-42 and 3-43 show a comparison of the measured and calculated values for mercury speciation (denoted by the fraction of mercury as Hg^{+2}) and total mercury emissions from the stack, respectively. The model predicts the stack emissions very well (r^2=0.94). The prediction of speciation in the stack is not as good ($r^2 = 0.59$); this is poorer than the prediction of speciation at the ESP inlet, suggesting that the model has neglected some important transformations between the ESP inlet and the stack. Mercury transformations in the particulate control

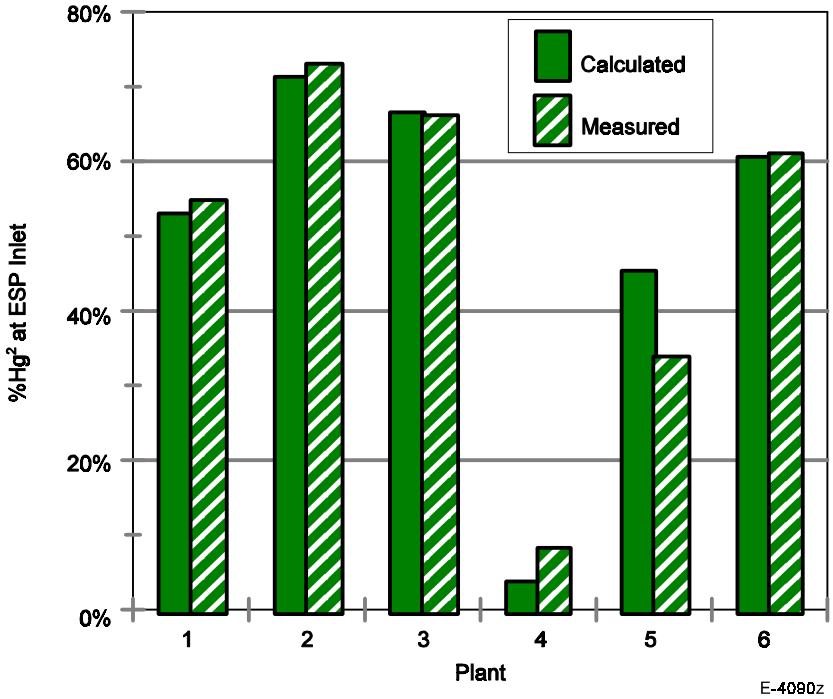

Figure 3-41. Comparison of predicted and measured mercury speciation at the ESP inlet. Data from References 10 and 11.

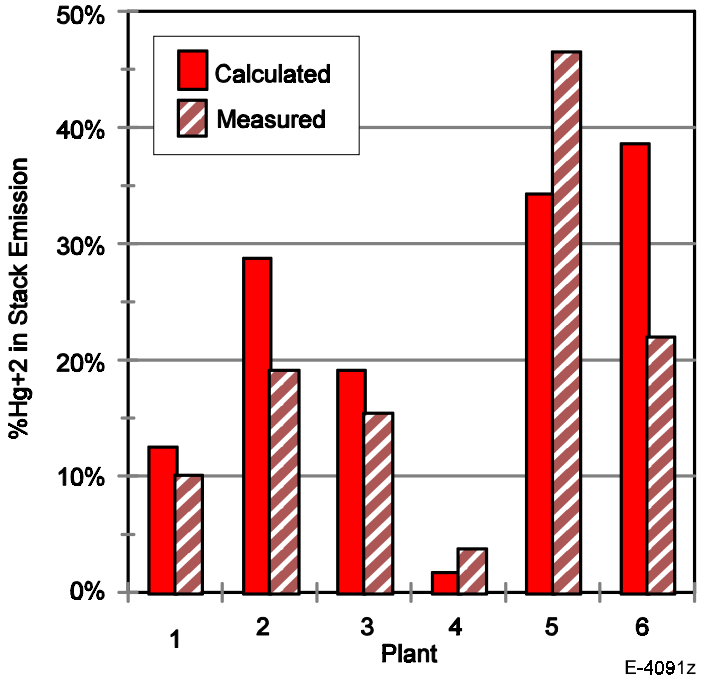

Figure 3-42. Mercury speciation in stack of coal-fired power plants: comparison of measurements (References 10,11) and predictions.

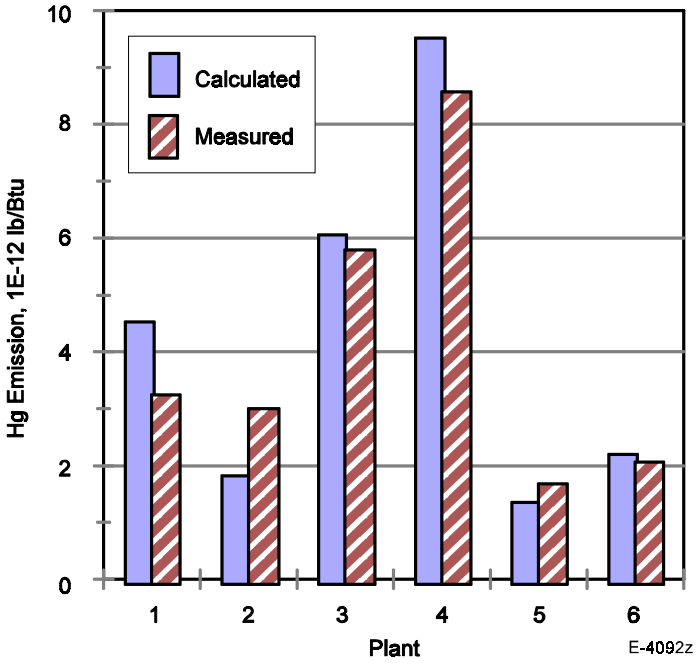

Figure 3-43. Mercury emissions in stack of coal-fired power plants: comparison of measurements (References 10,11) and predictions.

device (ESP) were not included in this model. The analysis shows that the behavior of mercury in the particulate control device has an impact on the speciation of mercury in the stack. Further research is indicated on the specific transformations of mercury in ESPs and fabric filters.

3.5.2 Model of Major Element Vaporization

The purpose of this work is to improve the major metal vaporization model that was recently incorporated into the EMAF program to produce the ToPEM program.

Vaporization Model. Previous work on vaporization of inorganic elements during *single particle* combustion in a Drop Tube Furnace was done by Quann et al.,[19] Quann and Sarofim,[20] and Mims et al.[21] This work was both experimental and theoretical. The effects of coal rank, particle size, particle temperature and oxygen concentration were examined experimentally. Also, a theoretical analysis of vaporization from included, excluded and atomically dispersed minerals was accomplished. This theoretical analysis indicates that the element vaporization depends on one or more of the following parameters: coal rank, coal type, bulk O_2 and CO_2 concentrations, particle size and composition of inherent ash. Results of this effort for Si, Ca and Mg were in very good agreement with the experiments.

For the case where we have vaporization from both internal inclusions and exposed inclusion on the char surface (See Figure 3-44), Mims gives for the fractional vaporization rate of a metal:

$$\frac{f_v}{t_b} = \frac{9\pi\theta c}{r_i^2 C_o \rho_p}\left[\frac{r_i D_e x_i^{\,e}}{2r_o(3\theta)^{1/2}} + \frac{D_m x_i^{\,es}}{5}\right] \qquad (3\text{-}1)$$

where,

f_v	=	fraction of metal that vaporizes
t_b	=	burnout time
C_o	=	metal concentration in coal
θ	=	volume ratio of inclusions in coal
r_i	=	inclusion radius
r_0	=	char radius
D_e	=	effective diffusivity
D_m	=	metal diffusivity
$x_i^{\,e}$	=	equilibrium mole fraction metal at internal inclusion surface
$x_i^{\,es}$	=	equilibrium mole fraction metal at surface of exposed inclusion
ρ_p	=	density of the char particle
c	=	molar concentration coefficient.

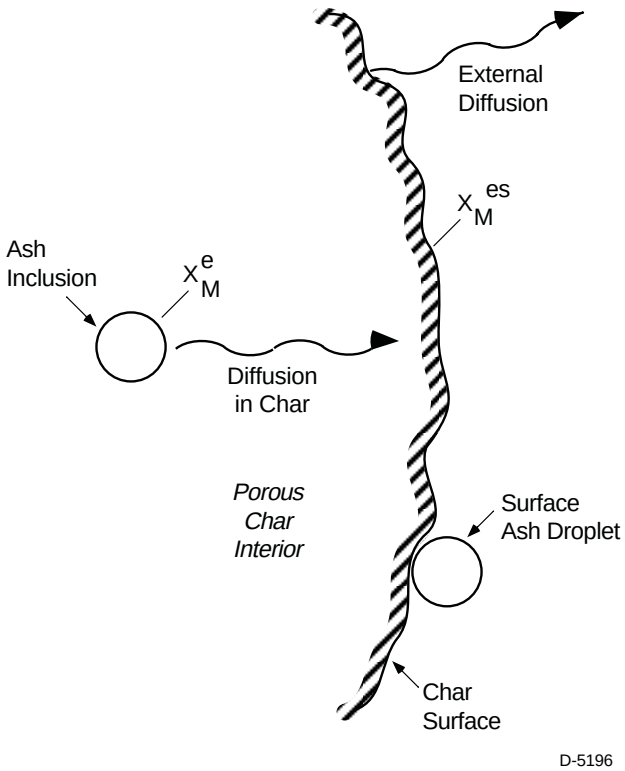

Figure 3-44. Schematic of vaporization and transport with porous char particle.

In the limiting case of vaporization from the external or excluded particles, have $D_e << D_m$. Therefore Eq. (3-1) becomes:

$$\frac{f_v}{t_b} = \frac{9\pi\theta c}{r_i^2 C_o \rho_p}\left[\frac{D_m x_i^{es}}{5}\right] \tag{3-2}$$

In the limiting case of vaporization from discrete inclusions, we have $D_e >> D_m$. Therefore Eq. (3-1) becomes:

$$\frac{f_v}{t_b} = \frac{9\pi\theta c}{r_i\, C_o \rho_p}\left[\frac{D_e x_i^e}{2r_o(3\theta)^{1/2}}\right] \tag{3-3}$$

For vaporization from organically associated minerals, which are in the form of fine inclusions, we assume $r_i << r_o$ then:

$$\frac{f_v}{t_b} = \frac{4c\, D_m\, x_i^e}{r_o^2 C_o} \tag{3-4}$$

Instead of calculating the fractional vaporization rate directly from Eqs. (3-1) through (3-4), we utilize as reference two sets of past experimental data for fractional vaporization rate. One set of these data was obtained for a bituminous coal and the other set for a low rank coal. Both were obtained at reference combustion conditions, which were 20% oxygen and gas temperature of 1750 K. These data correspond to *single particle* combustion experiments conducted by Quann and Sarofim.[19,20] To calculate metal vaporization of a different coal, we adjust the reference vaporization data for the combustion conditions and the properties of the coal in question.

Experimental results show that vaporization of most metals depends on the metal concentration in coals.[19,20] Exceptions are Mg and Fe, the vaporization of which was found to be independent of concentration. Dependence of metal vaporization on concentration is also predicted from the theoretical analysis presented in References 19 through 21 and expressed with Eq. (3-1). The following formula was derived for discrete mineral particles:

$$\frac{f_v}{t_b} = \left(\frac{f_v}{t_b}\right)_r \left(\frac{x_i^e}{x_{ir}^e}\right)\left(\frac{r_{or}}{r_o}\right)\left(\frac{C_{or}}{C_o}\right) \tag{3-5}$$

The following formula was derived for organically bound elements:

$$\frac{f_v}{t_b} = \left(\frac{f_v}{t_b}\right)_r \left(\frac{x_i^{es}}{x_{ir}^{es}}\right) \left(\frac{r_o}{r_{or}}\right)^2 \left(\frac{C_{or}}{C_o}\right) \tag{3-6}$$

The following formula was derived for excluded minerals:

$$\frac{f_v}{t} = \left(\frac{f_v}{t_b}\right)_r \left(\frac{r_o}{r_{or}}\right)^2 \left(\frac{C_{or}}{C_o}\right) \tag{3-7}$$

Variable *t* in Eq. (3-7) is the residence time of the excluded particles in the boiler. This is different than the burnout time of coal particles and usually at least twice as long.

In diffusion-controlled combustion, which is usually the case of coal particle combustion in pc-fired boilers, there is a simple relationship between the burnout time, t_b, the initial coal particle radius, r_o, and the oxygen volume fraction, x_{o_2}. This relationship has the following form:

$$t_b \propto \left(\frac{r_o^{\,2}}{\ln(1+x_{O_2})}\right) \tag{3-8}$$

If we substitute Eq. (3-8) to Eqs. (3-5) to (3-7) we get an expression for the *fraction* of the metal that vaporizes for discrete, organically bound and excluded minerals.

For discrete mineral particles:

$$f_v = \left(\frac{f_v}{t_b}\right)_r \left(\frac{x_i^e}{x_{ir}^e}\right) \left(\frac{\ln(1+x_{O_2 r})}{\ln(1+x_{O_2})}\right) \left(\frac{r_o}{r_{or}}\right) \left(\frac{C_{or}}{C_o}\right) t_{b,r} \tag{3-9}$$

For organically bound elements:

$$f_v = \left(\frac{f_v}{t_b}\right)_r \left(\frac{x_i^{es}}{x_{ir}^{es}}\right) \left(\frac{\ln(1+x_{O_2 r})}{\ln(1+x_{O_2})}\right) \left(\frac{C_{or}}{C_o}\right) t_{b,r} \tag{3-10}$$

The following formula was derived for excluded minerals:

$$f_v = \left(\frac{f_v}{t_b}\right)_r \left(\frac{r_o}{r_{or}}\right)^2 \left(\frac{C_{or}}{C_o}\right) t_{b,r} \qquad (3\text{-}11)$$

A series of calculations were performed and described in the Quarterly Report for July to September 1998, in which the concentration term for a specific metal in Eqs. (3-9) through (3-11) was either considered or omitted. Generally better results were obtained when the concentration of Mg and Fe was not considered, which is consistent with Quann's experimental results. However it appears that the vaporization of a particular metal is not a unique function of the concentration of this metal in the coal, but also depends on the type and rank of the coal.

In this section we will investigate the effect of bulk CO_2 on vaporization of major metals. Quann has shown experimentally[19] that presence of CO_2 in the exhaust gases depresses vaporization, as long as oxygen concentration is held constant. By performing his experiments at constant oxygen concentration environment, Quann was able to isolate the effect of burnout times and char temperatures, which remained constant, from the effect of CO_2 concentration in the combustion gases. Results of these experiments revealed that CO_2 decreases vaporization of all metals, but the effect is more pronounced on two atomically dispersed metals, Ca and Mg.

The above experimental results are consistent with the proposed mechanism for metal vaporization. The vaporization mechanism involves reduction of solid metal oxides with CO and production of metal vapors in reduced form, along with CO_2 (as discussed in detail below). This mechanism predicts that the presence of CO_2 decreases metal vaporization, as long as O_2 concentration stays constant.

However, in a pulverized coal flame, O_2 concentration decreases as the volatiles burn and form CO_2. Char combustion is generally thought to begin after the volatiles have burned. Lower oxygen in the bulk gas during char combustion affects both combustion times and char temperatures. These in turn affect metal vaporization, as does the presence of CO_2 in the bulk gas. The net result of lower O_2 in the bulk gas and the presence of CO_2 during char combustion should be the combined effect of longer combustion times, lower combustion temperatures and change in the molar fraction of metal vapors due to presence of CO_2.

Initially we will summarize our previous approach, which assumes that there is no bulk CO_2. This is a reasonable assumption for single particle combustion, but it may not be so for combustion of coal particles in a flame which is the case in industrial combustors. Subsequently we will present another approach, which more correctly assumes that there is bulk CO_2 due to combustion of other coal particles.

We assume that there is equilibrium among the metal oxide in the char, a reduced form of the metal oxide, CO and CO_2. For example, for SiO_2 we have:

$$SiO_{2(s)} + CO \rightarrow SiO_{(g)} + CO_2 \tag{3-12}$$

The equilibrium constant can be expressed in terms of partial pressures of gaseous species in the following way:

$$K_{eq} = \frac{p_{SiO} \cdot p_{CO_2}}{\alpha_{SiO_2} \cdot p_{CO}} \tag{3-13}$$

where α_{SiO_2} is the activity coefficient and p are the partial pressures of the various species on the surface of the mineral particle. For simplicity we assume that the partial pressures of the gaseous species are equal to those at the char surface.

The equilibrium constant, K_{eq}, for the above chemical equation is a function of temperature and, over a limited range of temperatures, may be expressed by the following relationship:

$$K_{eq} = \exp\left(A - \frac{B \cdot 10^4}{T_p} \right) \tag{3-14}$$

where T_p is the temperature of the burning char. We assume that combustion is controlled by gas phase diffusion, which is true for most industrial combustors. Oxygen reacts with the coal particle and forms CO at the surface of the particle. There is no CO_2 at the surface of the char as a result of combustion. The partial pressure of CO on the char surface is a function of the oxygen bulk concentration, p_{O2b}, and is given by the equation:

$$p_{CO} = \frac{2 \cdot p_{O_{2b}}}{1 + p_{O_{2b}}} \tag{3-15}$$

For single particle combustion under diffusion-limited conditions, the char temperature is a function of bulk oxygen concentration and gas temperature, and is given by the equation:

$$T_p = T_g + 2000 \cdot p_{O_{2b}} \tag{3-16}$$

If we assume that there is no bulk CO_2, the partial pressure of CO_2 on the surface, p_{CO_2}, is equal to the partial pressure of vaporized oxide, p_{SiO}. Under this assumption, the partial pressure of the vaporized oxide is given by the equation:

$$P_{SiO} = \left(K_{eq} \cdot \alpha_{SiO_2} \frac{2 \cdot p_{O_{2b}}}{1 + p_{O_{2b}}} \right)^{1/2} \tag{3-17}$$

The following equation can be used to calculate the ratio of the molar fractions of vaporized metals, which correspond to the coal in question and the reference coal:

$$\frac{P_{SiO}}{(P_{SiO})_r} = \frac{x_i^{es}}{x_{ir}^{es}} = \frac{\left(K_{eq} \frac{2 \cdot p_{O_{2b}}}{1 + p_{O_{2b}}} \right)^{1/2}}{\left(K_{eq} \frac{2 \cdot p_{O_{2b}}}{1 + p_{O_{2b}}} \right)_r^{1/2}} \tag{3-18}$$

The fractional vaporization rates were calculated using Eq. (3-18) in conjunction with Eqs. (3-9) to (3-11). Results were presented in the quarterly report for July to September 1998.

At any instant of time in a boiler environment, coal particles are at different stages of combustion and burn interactively with other particles close by. In this case, there may be CO_2 in the bulk gas, resulting from the volatile and char combustion of particles. When bulk CO_2 is present, Eqs. (3-13) to (3-16) still hold. However, the concentration of the vaporized oxide is not equal to CO_2 concentration, as was the case without bulk CO_2 present. When bulk CO_2 is present, we have:

$$P_{SiO} = \frac{K_{eq}}{p_{CO_{2b}}} \cdot \alpha_{SiO_2} \frac{2 \cdot p_{O_{2b}}}{1 + p_{O_{2b}}} \tag{3-19}$$

If we neglect the effect of the activity coefficient, the ratio of the molar fractions of the coal in question and the reference coal is:

$$\frac{P_{SiO}}{(P_{SiO})_r} = \frac{x_i^{es}}{x_{ir}^{es}} = \frac{\left(\frac{2 \cdot p_{O_{2b}}}{1 + p_{O_{2b}}} \right) \left(\frac{K_{eq}}{P_{CO\,2b}} \right)}{\left(K_{eq} \frac{2 \cdot p_{O_{2b}}}{1 + p_{O_{2b}}} \right)_r^{1/2}} \tag{3-20}$$

Table 3-22 lists the equilibrium equations we initially used to calculate vaporization of Na, K, Fe, Si, Al, Mg and

Ca, and the values of the equilibrium constants in the range of 1500 to 2500 K. Recently, we changed the equations that describe Al vaporization to be consistent with thermodynamically favored species: the reduced species in Al vaporization was considered to be

Table 3-22. Vaporization Equilibrium Equations and Equilibrium Coefficients – Equilibrium Constants at Temperature Char Temperature T Are Calculated from $\ln(kp)=A+B\cdot 10^4/T$

Vaporization Equation	New Coefficients		Old Coefficients	
	A	B	A	B
$Na_2O+CO=2Na+CO_2$	17.8966	-2.8487	17.7349	-2.8271
$K_2O+CO=2K+CO_2$	17.9507	-2.0891	19.185	-2.1940
$FeO+CO=Fe+CO_2$	11.4942	-4.2064	11.0258	-4.2495
$FeS+CO=Fe+COS$	10.9323	-5.1305	---	---
$SiO_2+CO=SiO+CO_2$	18.8256	-5.9700	18.6621	-5.9507
$Al_2O_3+CO=2AlO+CO_2$	---	---	38.2805	-16.7937
$Al_2O_3+2CO=Al_2O+CO_2$	24.0505	-11.3361	---	---
$MgO+CO=Mg+CO_2$	14.4976	-5.4094	11.8032	-4.5773
$CaO+CO=Ca+CO_2$	13.2182	-6.1507	10.1895	-5.1918

Al_2O instead of AlO. The vaporization of iron was also tested to see if the vapor pressure of iron in equilibrium with iron sulfide (from pyrite) would produce different results than that of equilibrium with iron oxide. The entire set of equilibrium constants was recalculated for the sake of consistency. As Table 3-22 shows, there are no major differences in the two sets of equilibrium constants.

To account for the presence of bulk CO_2, we will first estimate the bulk composition of the gaseous phase both after the complete combustion of volatiles and after the overall combustion. These calculations will provide us with bulk gas compositions that provide bounds for the vaporization calculations.

Following is the overall combustion equation for a stoichiometric ratio ϕ.

$$C_aH_bN_cO_dS_eCl_f + \frac{1}{2}\varphi\left(2a+\frac{b-f}{2}+2e-d\right)(O_2+3.78N_2) \rightarrow aCO_2+\frac{b-f}{2}H_2O+eSO_2+fHCl$$
$$+\frac{1-\varphi}{2}\left(2a+\frac{b-f}{2}+2e-d+\frac{c}{2}\right)O_2+\left[\frac{\varphi}{2}3.78\left(2a+\frac{b-f}{2}+2e-d\right)+\frac{c}{2}\right]N_2 \qquad (3\text{-}21)$$

Following is the combustion equation that describes the complete combustion of the volatiles:

$$C_x H_y N_z O_w + \frac{1}{2}\left(2x + \frac{y}{2} - w\right)(O_2 + 3.78N_2) \rightarrow xCO_2 + \frac{y}{2}H_2O + \frac{1}{2}\left[z + 3.78\left(2x + \frac{y}{2} - w\right)\right]N_2 \quad (3\text{-}22)$$

The chemical formula of the coal and the volatiles can be calculated from the ultimate and proximate analysis of coal. By subtracting this last equation from the overall combustion equation and assuming that the chlorine content in the coal is negligible, the combustion of char can be obtained from the following equation:

$$C_{X'}S_{Y'} + \frac{1}{2}\frac{X' + 2Y'}{X'}(A\,O_2 + B\,N_2 + C\,H_2O + D\,CO_2) \rightarrow X'\,CO + Y'SO_2 + \frac{1}{2}\frac{X' + 2Y'}{X'}(B\,N_2 + C\,H_2O + D\,CO_2) \quad (3\text{-}23)$$

The coefficients X', Y', A, B, C and D are calculated from Eqs. (3-21) and (3-22).

The compositions of the gas after the volatile combustion for the three coals burned in Phase I at stoichiometric ratio of 1.2 are given in Table 3-23. For the same coals and stoichiometric ratio, the compositions of the gas after complete combustion are shown in Table 3-24. Thus, CO_2 bulk concentrations in a boiler may be very different than those in single particle combustion. It is possible that presence of bulk CO_2 affects the vaporization rate of metals, as can be inferred from Eqs. (3-8), (3-9) and (3-19) and suggested by experimental results.[19] However, it is important that we make a distinction between the bulk CO_2 and the CO_2 at the surface of inclusions. Before combustion starts there is no CO_2 inside the pores of a coal particle. During diffusion controlled combustion, CO_2 forms far away from the surface of the particle, which contributes to the bulk CO_2. Eventually CO_2 may diffuse though the pores of the coal particle. It is possible, however, that the time scales of combustion and CO_2 diffusion are equivalent, since gas diffusion controls both processes. If this is the case, bulk CO_2 may not influence much metal vaporization from inclusions, although it may still influence vaporization of atomically dispersed metals and vaporization of excluded minerals.

Vaporization Calculations-Single Particle. Vaporization calculations were carried out for three different coals that were used in Phase I of this program and we will compare the results with

experimental data. *Three* different cases of vaporization calculations were conducted, in which we examined the effect of bulk CO_2 concentration on metal vaporization. For two of these we examined how the vaporization equations and the equilibrium constants affect the vaporization calculations.

Table 3-23. Bulk Composition of Gas Phase after Volatile Combustion

Species	Elk.-Haz.	Illinois 6	Wyodak
CO_2 %	3.8	4.1	6.6
H_2O %	5.6	6.2	9.2
O_2 %	13.2	12.7	9.1
N_2 %	77.2	76.9	75.1

Table 3-24. Bulk Composition of Gas Phase after Overall Combustion

Species	Elk.-Haz.	Illinois 6	Wyodak
CO_2 %	14.2	13.7	13.1
H_2O %	5.2	6.1	8.9
O_2 %	3.3	3.2	2.9
N_2 %	77.1	76.6	75.1
SO_2 %	0.06	0.27	0.02

To isolate the effect of particle size, we assumed that the coal particles were of the same size and equal to that of the reference particles. In reality, the experimental data are from combustion of utility grind coal (i.e., polydisperse particle size). As discussed in the Quarterly Report for July to September 1998, this assumption does not affect the results from the calculations and therefore is not expected to affect conclusions drawn from this work. The three cases considered are as follows:

Case 1. Combustion of char and volatiles with 20% oxygen at 1750 K gas temperature. No CO_2 is present in the bulk combustion gas. The underlying assumption to this approach is that the coal particles are far from each other and burn individually as single particles.

Case 2. Combustion occurs in two discrete stages: (a) combustion of volatiles without metal vaporization and (b) char combustion where metal vaporization takes place. The oxygen content during char combustion is the initial oxygen concentration minus the oxygen consumed during volatile combustion. The oxygen and CO_2 concentration are shown in Table 3-23.

Case 3. Combustion occurs in two discrete phases as described in Case 2. This time, the oxygen

content during char combustion is the initial oxygen concentration minus the oxygen consumed during the overall combustion (volatiles plus char). This case applies to poorly mixed pockets in the boiler with high particle concentration. The oxygen and CO_2 concentration are shown in Table 3-24.

In each of these cases, the char temperature was calculated from Eq. (3-16), assuming 20% O_2 for the first case and, depending on the coal, 9 to 14% O_2 for the second case and 2 to 4% O_2 for the third. The burnout times were calculated from Eq. (3-8), making use of the experimental data for the reference coal particles. Table 3-25 shows the burnout temperatures and combustion times of coal particles having the size of the reference particles, which is 50 µm for bituminous coals and 60 µm for low rank coals. The combustion conditions correspond to Cases 1 through 3. The char temperatures and burnout times predicted under these conditions vary substantially.

Table 3-25. Indicative Burnout Times and Char Temperatures at Three Combustion Atmospheres

	Single Particles 20% O_2		After Volatile Combustion Approx. 12% O_2		After Overall Combustion Approx. 3% O_2	
	Burnout Time (ms)	Char Temp. (K)	Burnout Time (ms)	Char Temp. (K)	Burnout Time (ms)	Char Temp. (K)
Bituminous Coals	20	2150	30	2000	92	1830
Low Rank Coals	7.4	2170	16	1930	48	1800

The choice of the equilibrium reactions and the accuracy of the equilibrium constants affect the overall vaporization calculations. As explained earlier, the molar fraction ratio, $x_i/x_{i,r}$, is calculated from the equilibrium equations, as shown in Eqs. 3-18 and 3-20. Only when combustion occurs at the reference conditions, 20% O_2 and at 1750 K gas temperature, as in Case 1, is the molar fraction ratio, $x_i/x_{i,r}$, equal to 1. Therefore, this is the only case not affected by the choice of equilibrium constants. For each of the Cases 2 and 3, three sub-cases were considered, each one corresponding to a different set of equilibrium equations or equilibrium constants.

Sub-case a. The first sub-case involves the old values of equilibrium constants, as shown in Table 3-22.

Sub-case b. The second sub-case involves the new equilibrium constants, as shown in Table 3-22. However, it assumes that iron vaporization occurs through reduction of the iron oxide.

Sub-case c. The third sub-case is similar to the second, but it assumes that iron vaporization takes place through oxidation of pyrite (FeS).

Table 3-26 shows the partial pressure of vaporized metals calculated using various bulk gas compositions (Cases 1 through 3). The partial pressure of Na and K from these calculations are greater than 1. However, these partial pressures represent ideal solution behavior. It is well known that silicate melts (such as ash particles during combustion) are not ideal solutions. The

Table 3-26. Calculated Partial Pressure of Metals under Various Assumptions

	Case 1 Single Particle 20% O_2 0% CO_2	Case 2 Volatiles Combusted 12% O_2 4% CO_2	Case 3 Complete Combustion 3% O_2 14% CO_2
Na	1.04E+02	4.26E+01	9.06E+00
K	3.77E+03	1.95E+03	6.28E+02
Fe	3.13E-04	8.34E-05	8.48E-06
SiO	1.31E-04	2.00E-05	7.82E-07
Al_2O	3.52E-13	9.99E-15	2.11E-17
Mg	2.34E-05	4.27E-06	2.26E-07
Ca	2.07E-07	3.00E-08	1.06E-09

activity coefficient of alkali species in a silicate melt will be much less than one. In our approach, we normalize the vapor pressure relative to the reference condition with the implicit assumption that the activity coefficients are equal.

The partial pressures of individual metals calculated for combustion in 20% O_2 (Case 1) are higher than those calculated for the other cases. This is to be expected since Case 1 corresponds to the highest char temperature and also the bulk CO_2 concentration is assumed to be zero.

Metal vaporization calculations were performed for Cases 1 through 3 for three coals that were burned in Phase I of this program: (a) the bituminous Elkhorn-Hazard, (b) the bituminous Illinois 6 and (c) the sub-bituminous Wyodak. Figures 3-45 through 3-47 show the predicted values for ash vaporization, while Figures 3-48 through 3-50 show the predicted values for iron vaporization. The predicted values are compared to the measured values for ash and iron vaporization based on data taken in PSI's entrained flow reactor and reported in the Phase I Final Report.

All three cases predict more submicron ash than observed, from 5 to 75% more than the measured amount. This is largely due to the large amounts of sodium and potassium predicted to vaporize; in some cases, ten times the amount of alkali species are predicted to vaporized as compared to the measurements. Iron vaporization is overpredicted for the cases in which equilibrium with iron sulfide is assumed (Case 3). Predicted iron vaporization is greatly reduced at lower O_2 concentrations for the cases in which equilibrium with iron oxide is assumed (Cases 1 and 2). In spite of the fact that the lower bulk oxygen concentrations in Cases 2 and 3 reduce particle temperature and suppress vaporization, the longer burnout times of these cases allow about the same overall vaporization as Case 1.

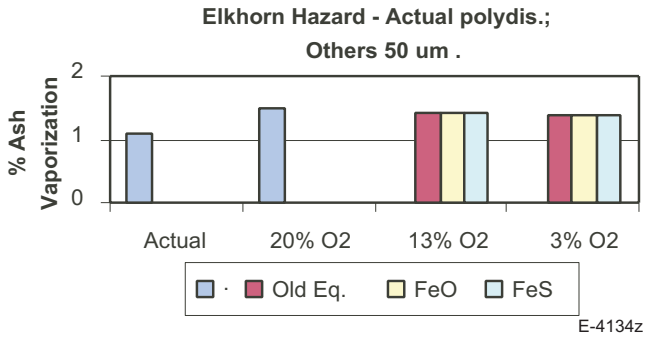

Figure 3-45. Ash vaporization for Elkhorn Hazard.

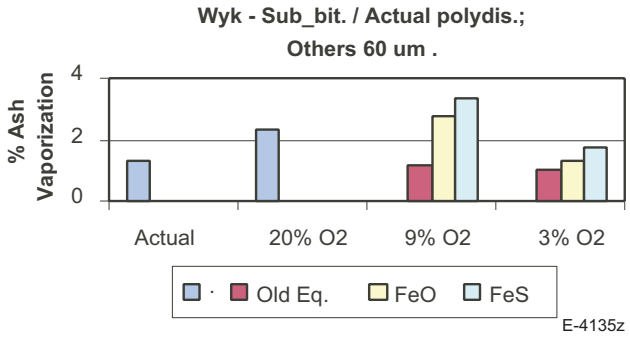

Figure 3-46. Ash vaporization for Wyodak.

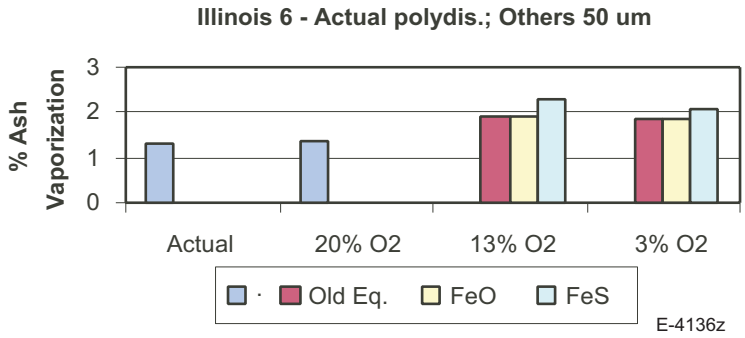

Figure 3-47. Ash vaporization for Illinois 6.

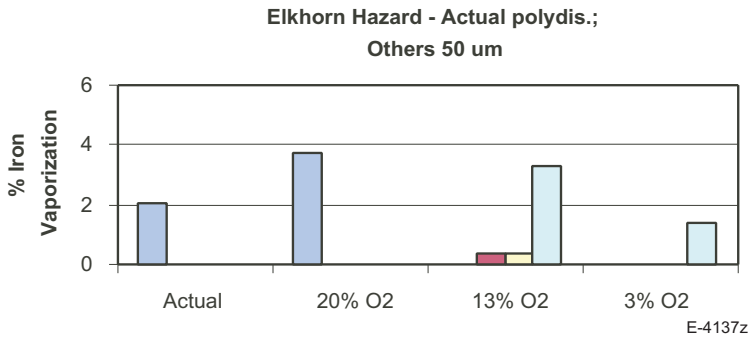

Figure 3-48. Iron vaporization for Elkhorn Hazard.

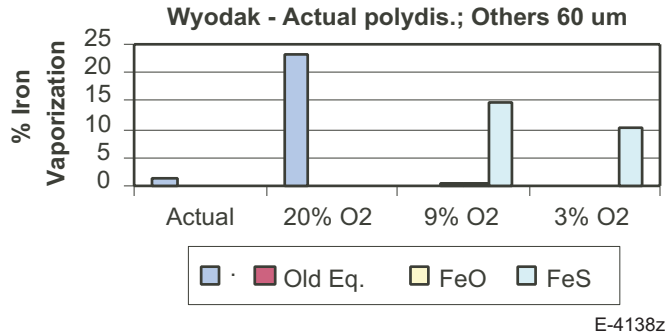

Figure 3-49. Iron vaporization for Wyodak.

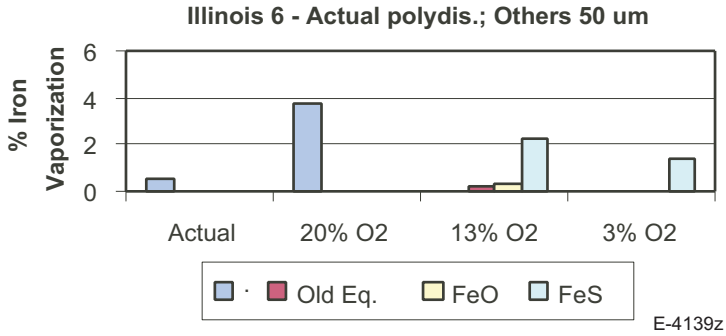

Figure 3-50. Iron vaporization for Illinois 6.

Vaporization Calculations-Particle Ensemble. ToPEM calculates the vaporization from an ensemble of initial coal particle sizes corresponding to the coal size distribution. The model described above has been added to ToPEM and the results are discussed here. Figures 3-51 and 3-52 show predicted ash compositions as a function of initial coal particle size for Elkhorn-Hazard, combustion in 20% O_2. The metal oxide concentrations do not add up to 100% since only five metals were considered here: Fe, Al, Si, Na and K. This coal is low in Ca and Mg. The predicted concentrations of these oxides from the 20 to 150 μm coal particles are close to the concentration of the oxides in the bulk ash.

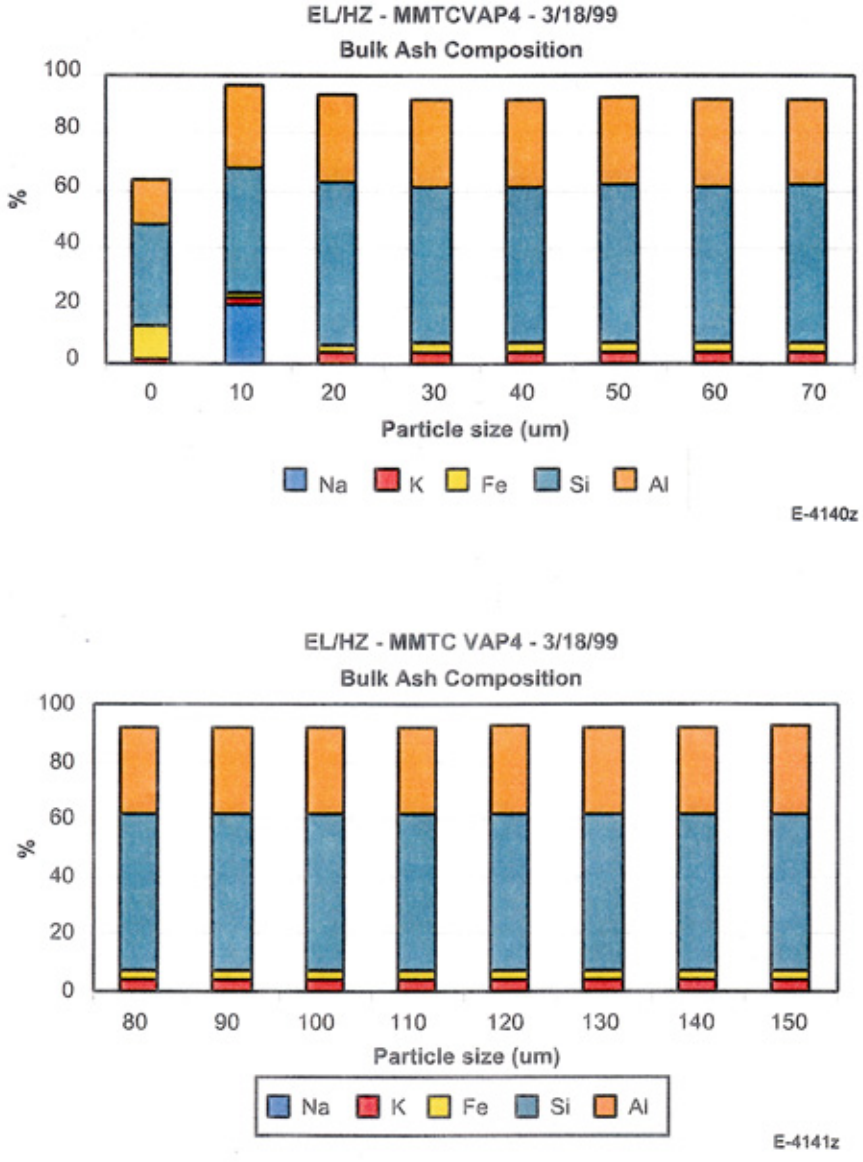

Figure 3-51. Residual ash composition from Mineral Matter Transformation (MMT) Model in ToPEM as a function of initial coal particle size for Elkhorn/Hazard coal.

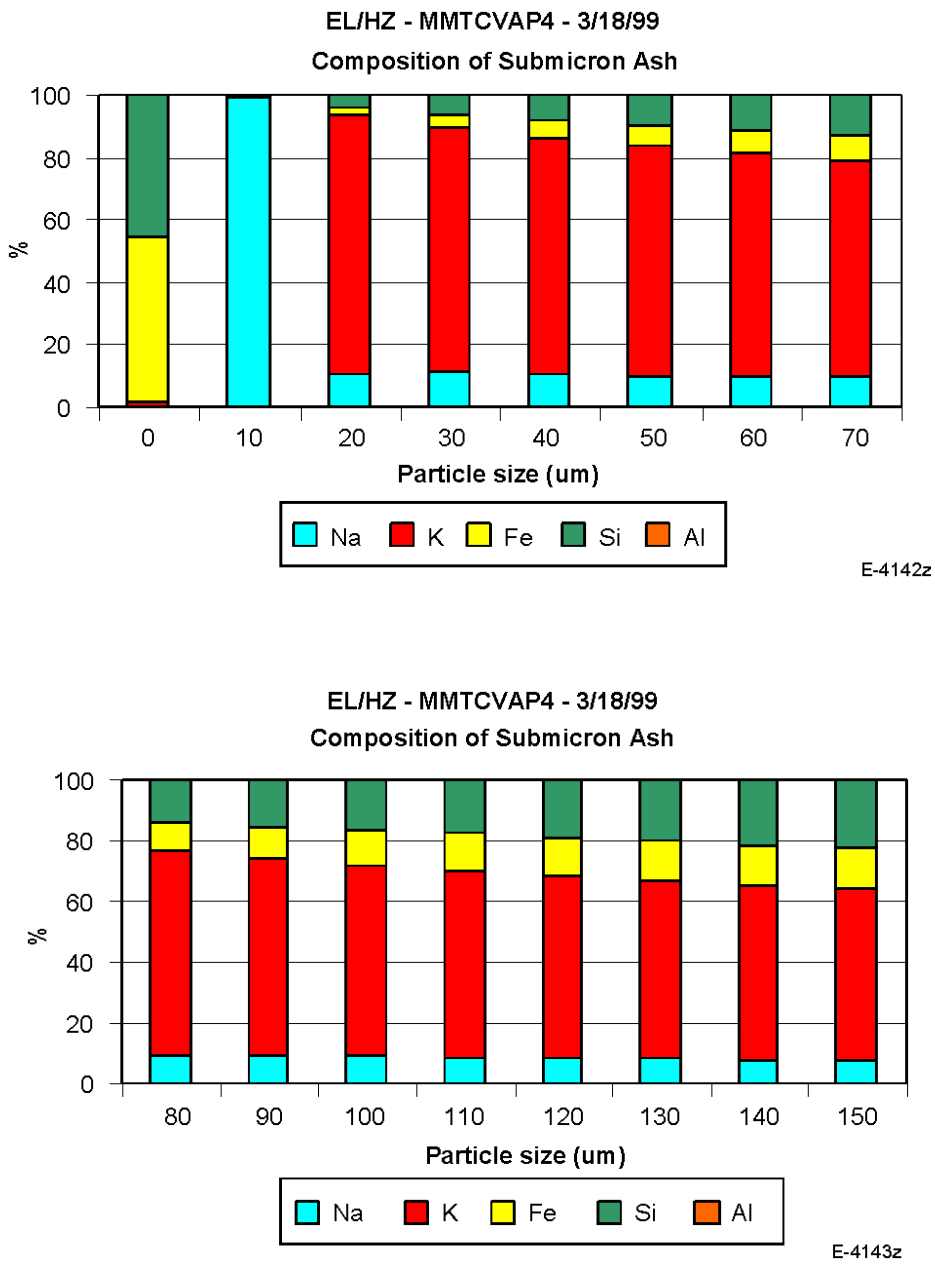

Figure 3-52. Submicron ash composition from Mineral Matter Transformation (MMT) Model in ToPEM as a function of initial coal particle size for Ekhorn/Hazard coal.

The residual ash composition corresponding to coal particles in the range of 20 to 150 µm is predicted to be essentially independent of the coal particle size, except for residual ash particles from the smallest coal particles. For the Elkhorn/Hazard coal, the minerals in these particles mostly consist of Si, Al, Fe and K. Very small amounts of Na are present. However, 10 µm coal particles contain substantial amounts of Na. The reason for this is that only very small mineral particles can fit in the 10 µm coal particles. ToPEM assumes that organically bound metals such as Na exist in very small particles with a diameter of 0.1 µm. These are

particles which fit in the small coal particles. The vaporized material is predicted to consist largely of potassium, with minor amounts of silicon, iron, and sodium.

Figures 3-53 and 3-54 summarize the overall major element vaporization and submicron ash composition for the ToPEM calculation of Elkhorn/Hazard coal. Approximately 30% of the sodium and 20% of the potassium are predicted to vaporize. Because of the relatively high potassium content of the bulk ash, the submicron ash is predicted to consist primarily of potassium oxide. Measurements from the EFR indicate that approximately 2% of the sodium and iron were found in the submicron mode. The ToPEM results match the measurements for iron, but not for sodium. Sodium vaporization was predicted to be over ten times higher than the measurement. Potassium was not measured in the EFR experimental data set. However, the amount of potassium seems high. This will have to be checked against data from the University of Arizona and the University of Utah, when experiments are complete.

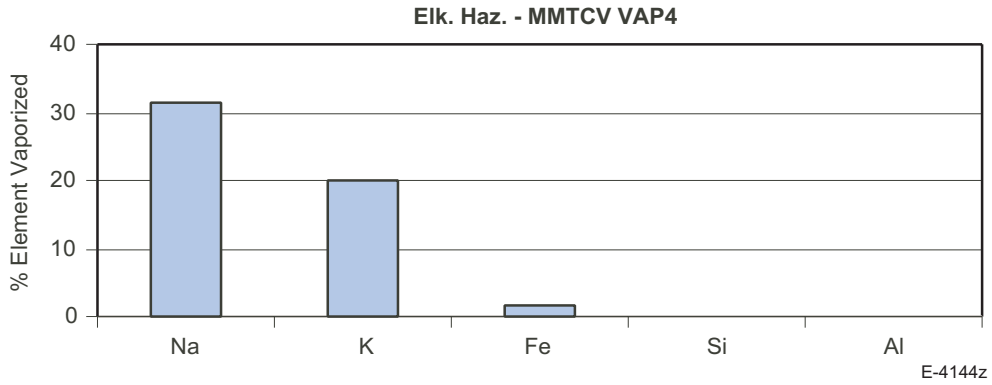

Figure 3-53. Total amount of major elements vaporized during combustion of Elkhorn/Hazard coal (as calculated by ToPEM).

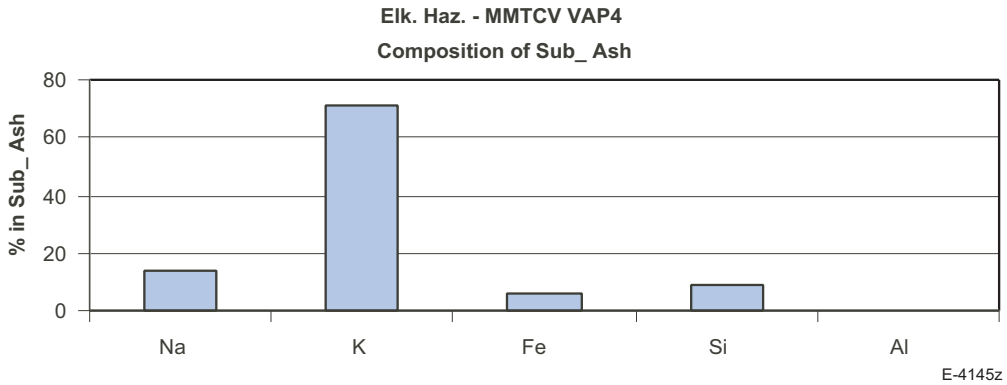

Figure 3-54. Composition of submicron ash from combustion of Elkhorn/Hazard coal (as calculated by ToPEM).

In summary, the method for predicting vaporization of major elements predicts the total amount vaporized within a factor of two. Vaporization of alkali species is over-predicted, however. The assumption of combustion of the volatiles before char combustion provides better agreement between calculated and measured vaporization. The assumption of equilibrium between iron vapor and iron oxide in the ash gives better agreement between measured and predicted iron vaporization.

Further work will be needed on the mechanisms for alkali vaporization. Improvements in the calculation of particle temperature and surface gas composition should improve the predictions.

SECTION 4

SUMMARY AND FUTURE PLANS

4. SUMMARY AND FUTURE PLANS

4.1 Summary

During this period the MIT INAA procedures were revised to improve the quality of the analytical results. Two steps have been taken to reduce the analytical errors. Estimates are included in this report on the reduction in errors of individual elements that are expected, based on these changes.

Incomplete pyrite extraction in the USGS leaching procedure has been noted previously. As a result, a new nitric acid leaching procedure, modified from ASTM procedure D2492, section 7.3.1 for determination of pyritic sulfur, was developed and validated. For the Ohio 5/6/7 coal it is clear from the preliminary leaching data that iron and arsenic are strongly associated with pyrite, as in many bituminous coals, consistent with microprobe date for pyrite. A much smaller pyrite association is indicated for Fe and As in the two low rank coals. These coals show a large HCl-leachable fraction we have previously interpreted as arsenate. For Cr, a significant HF-leachable fraction is shown for each of the coals, consistent with ion probe data for Cr in illite, reported in the section on microanalysis. However, each of the coals has significant (30 to 65%) unleached Cr, indicating an organic association for this fraction. For the other elements reported- potassium shows a strong silicate association- as it is a major component of illite/smectite. Sodium shows a significant ion-exchangeable component, especially in the low rank coals. Cobalt, uranium and scandium show mixed affinities that are dominated by organic, silicate, or HCl-leachable forms. USGS analysts in Denver have halted development of the cold vapor atomic fluorescence technique for mercury analysis procedure in favor of a new direct analyzer for Hg that the USGS is in the process of acquiring. Since early June, emphasis at USGS has been placed on microanalysis of clay minerals in project coals in preparation for use of the Stanford/USGS SHRIMP RG Ion Microprobe during August 1999. The SHRIMP- RG data confirm that Cr is present at concentrations of about 20 to 120 ppm, just below the electron microprobe detection limits (100 to 200 ppm), as suspected from Phase I microprobe work and previous studies of clay mineral separates.

The University of Utah has started trial runs on the drop tube furnace to ensure that the gas analysis system is working properly and that the flow pattern within the furnace is laminar and direct. A preliminary test matrix has been formulated. A third set of ASTM samples will be prepared at the University of Utah for the Phase I and Phase II coals. This time the INAA counting time will be optimized for the elements in which we are interested, guided by the results from the first two samples. Seven samples will be generated.

The iodated charcoal which was used by MIT for vapor phase Hg collection was tested to see whether it collected other vapor phase metals. A second set of tests were performed at PSI using the entrained flow reactor (EFR). The results of the second test for Hg collection simply confirm that the sorbents collect 100% of the vapor phase Hg, and that they can be used at 105^{o}C to prevent condensation. No other elements (e.g., As, Br, Cd, and Sb) were collected quantitatively in Test 1.

The University of Arizona's pilot-scale downflow laboratory combustion furnace was used to test the partitioning of toxic metals in the baseline experiments for the Phase II North Dakota lignite and the Phase I Pittsburgh seam bituminous coal at baghouse inlet sampling conditions. In addition, baseline data were collected on combustion of the Phase I Kentucky Elkhorn/Hazard bituminous coal.

Emphasis at the University of Kentucky was placed on (1) collection of new Hg XAFS data for various sorbents, and (2) on collection of XAFS and other data for arsenic, sulfur, chromium and selenium in two baseline ash samples from the University of Arizona combustion unit. There is a clear distinction in the Hg XAFS spectra and data between the carbonaceous sorbents and the two $Ca(OH)_2$ sorbents, which were the only inorganic sorbents to give acceptable XAFS data. For these latter two samples, it is clear that the sorption of $HgCl_2$ involves the formation of a Hg-O bond. This suggests that mercuric chloride will undergo chemisorption when the conditions are right. Hg XAFS experiments were also conducted on various fractions of fly-ash collected from the Cherokee power station, CO, by personnel at ADA Technologies, Inc. The data suggest that there is a specific fraction in the fly-ash carbon that is particularly effective for mercury sorption. The values of the Inflection Point Difference (IPD) from the second derivative of the XANES spectra would appear to reflect formation of Hg-Cl complexes, consistent with previous XAFS investigations of carbon-based sorbents

Revision was made to the matrix for the intial experiments on mercury-ash interactions to be conducted at EERC. The overall goal of this effort is to collect data which will allow us to model the interactions of mercury and fly ash (specifically, adsorption of Hg^0 and Hg^{+2} and oxidation of Hg^0) in the air heater and particulate control device of a coal-fired power plant. Ash samples from the Phase II coals were collected at the University of Arizona down-fired combustor. Loss-on-ignition and surface area measurements were made on the ash samples.

The simple mass balance model for emissions of mercury from coal-fired power plants was revised to further test our current understanding of mercury transformations in flue gas. The predictions of mercury speciation, in terms of fraction as Hg^{+2} at the ESP inlet agree well with measured values. The predictions are based primarily on the coal chlorine content and the LOI of the ash. Of these two factors, the coal chlorine content has the largest impact on mercury speciation. The model predicts the stack emissions very well. The prediction of speciation in the stack is not as good as the prediction of speciation at the ESP inlet, suggesting that the model has neglected some important transformations between the ESP inlet and the stack. Mercury transformations in the particulate control device (ESP) were not included in this model. The analysis shows that the behavior of mercury in the particulate control device has an impact on the speciation of mercury in the stack.

Improvements were made to the model for major element vaporization. The method for predicting vaporization of major predicts the total amount vaporized within a factor of two. Vaporization of alkali species is over-predicted, however. The assumption of combustion of the volatiles before char combustion provides better agreement between calculated and measured vaporization. The assumption of equilibrium between iron vapor and iron oxide in the ash gives better agreement between measured and predicted iron vaporization. Further work will be

needed on the mechanisms for alkali vaporization. Improvements in the calculation of particle temperature and surface gas composition should improve the predictions.

4.2 Future Plans

Next quarter, analytical work will continue at USGS, Kentucky, and MIT. USGS will complete the leaching analysis and continue detailed analysis of trace elements in mineral grains. Coal mineralogy will also be completed. Kentucky will continue analysis of XAFS data in hand and obtain new XAFS data at Brookhaven. Work will continue on CCSEM analyses of coal and ash. MIT will continue with NAA analysis and assist other team members in making measurements of gas-phase mercury and other volatile metals.

The University of Utah will begin taking data from single particle combustion in the laminar drop tube reactor. Another round of devolatilization experiments will commence. Preliminary measurements of chlorine species in the gas phase will also take place. The University of Arizona will continue analysis of baseline impactor samples. Plans will be made for staged combustion experiments in 2000.

The University of Connecticut will begin taking data on gas-phase mercury reaction with the bench-scale burner system. Modeling of mercury kinetics will also continue. EERC will begin to collect data on mercury adsorption and oxidation over ash samples in the fixed bed reactor. Modeling work will continue at PSI.

SECTION 5

REFERENCES

5. REFERENCES

1. Bragg, L.J., Oman, J.K., Tewalt, S.L., Oman, C.L., Rega, N.H., Washington, P.M., and Finkelman, R.B., U.S. Geological Survey Coal Quality (COALQUAL) Database, V.2.0, U.S.Geological Survey Open File Report 97-134, CD-ROM.

2. Toole-O'Neil, B., Tewalt, S.J., Finkelman, R.B., and Akers, D.J., 1999, Mercury concentration in coal-unraveling the puzzle: Fuel, v.78, p. 47-54.

3. Palmer, C.A., and Lyons, P.C., 1996, Selected elements in major minerals from bituminous coal as determined by INAA: Implications for removing environmentally sensitve elements from coal: International Journal of Coal Geology, v. 32, p. 151-166.

4. Frank Huggins, University of Kentucky, 30 September 1999, personal communication.

5. Markowski, G.R. and D. S. Ensor, Proc. Of 70th Annual Meeting of the Air Pollution Control Assoc., Toronto, 20-24 June, 1977, Paper No. 77-35-5.

6. Haynes, B.S., Neville, M., Quann, R.J., and A.F. Sarofim, J. of Colloid and Interface Science, 87/1, May, 1982, pp. 266-279.

7. Linak, W.P and J.O.L. Wendt, Fuel Processing Technology, 39:173-198 (1994).

8 F. E. Huggins, G. P. Huffman, G. E. Dunham, and C. L. Senior, XAFS investigation of mercury sorption on three activated carbons. Energy & Fuels, 13(1), 114-121, (1999).

9. F. E. Huggins, N. Yap, and G. P. Huffman, XAFS investigation of mercury sorption on carbon-based and other sorbent materials. Jpn. J. Appl. Phys., 38 (Suppl. 1), 588-591, (1999).

10. DeVito, M.S and Rosenhoover, W.A., "Flue Gas Mercury and Speciation Studies at Coal-Fired Utilities Equipped with Wet Scrubbers," presented at 15th International Pittsburgh Coal Conference, Pittsburgh, PA, September 15-17, 1998.

11. Laudal, D.L., "Mercury Speciation Sampling at Cooperative and United Power Associations' Coal Creek Station," Final Report, Energy & Environmental Research Center, University of North Dakota, January 1999.

12. Ghorishi, S.B., "Fundamentals of Mercury Speciation and Control in Coal-Fired Boilers," EPA-600/R-98-014, February 1998.

13. Holmes, M.J., Redinger, K.E., Evans, A.P., and Nolan, P.S., "Control of Mercury in Conventional Flue Gas Emissions Control Systems," presented at the Fourth International Conference on Managing Hazardous Air Pollutants, Washington, D.C., November 12-14, 1997.

14. Sjostrom, S., Smith, J., Hunt, T., Chang, R., and Brown, T.D., "Demonstration of Dry Carbon-Based Sorbent Injection for Mercury Control in Utility ESPs and Baghouses," presented at the Air & Waste Management Association 90th Annual Meeting, Toronto, Ontario, Canada, June 8-13, 1997, paper 97-WA72A.07.

15. Li, Z. and Hwang, J.-Y., "Mercury Distribution in Fly Ash Components," presented at the Air &Waste Management Association 90th Annual Meeting, Toronto, Ontario, Canada, June 8-13, 1997, paper WP72B.05.

16. Wu, B., Peterson, T.W., Shadman, F., Senior, C.L., Morency, J.R., Huggins, F.E., and Huffman, G.P., "Interactions Between Vapor-Phase Mercury and Coal Char Under Simulated Utility Power Plant Flue Gas Conditions," *Fuel. Proc. Technol*., in press, 2000.

17. Ghorishi, S.B. and Sedman, C.B., "Low Concentration Mercury Sorption Mechanisms and Control by Calcium-Based Sorbents: Application to Coal-Fired Processes," *J.Air Waste Management Assoc.* **48**, 1191-1198 (1998).

18. Brown, T.D., Smith, D.N., Hargis, Jr., R.A., and O'Dowd, J., "Mercury Measurement and Control; What We Know, Have Learned, and Need to Further Investigate!" presented at the 92nd Annual Meeting of the Air & Waste Management Association, June 20-24, 1999, St. Louis, MO.

19. Quann, R.J., Sc.D. Thesis, Department of Chemical Engineering, MIT, Cambridge, MA (1982).

20. Quann, R.J. and Sarofim, A. F. , "Vaporization of Refractory Oxides During Purverized Coal Combustion". Nineteenth (International) Symposium on Combustion, The Combustion Institute, 1982, pp. 1429-1440.

21. Mims, C.A., Neville, M., Quann, R.J. and Sarofim, A.F. "Laboratory Studies of Trace Element Transformations During Coal Combustion". Presented at 87th AIChE Meeting, Boston, MA 1979.

APPENDIX A

Summary of Experimental Sampling Conditions for Wyodak Baseline Combustion

Table A-1. Summary of Experimental Sampling Conditions for Wyodak Baseline Combustion

SAMPLE SET # (Port Sampled)	TOTAL COMBUSTION GAS RATE (slpm)	SAMPLING RATE (slpm)	SAMPLING TEMP (°K at port where sample was taken)	PORT 4 O_2 CONC (%)	PORT 4 CO_2 CONC (%)	PORT 14 O_2 CONC (%)	PORT 14 CO_2 CONC (%)	PORT BG* O_2 CONC (%)	PORT BG CO_2 CONC (%)
99W-3 (4)	222	0.73	1331	3.7	16.3				
99W-4 (14)	277	0.93	1011	3.7	16.3	7.5	12.8		
99W-5 (BG)	277**	0.93***	475	3.7	16.3	7.5	12.8	9.7	10.5
99W-6 (4)	222	0.73	1356	4.0	16.4				
99W-7 (14)	273	0.89	1052	4.0	16.4	6.7	13.6		
99W-8 (BG)	273	0.89	490	4.0	16.4	6.7	13.6	9.4	11.5
99W-9 (4)	224	0.72	1365	3.3	16.0				
99W-10 (4)	224	0.72	1365	3.3	16.0				
99W-11 (14)	274	0.88	1029	3.3	16.0	6.9	13.4		
99W-12 (BG)	274	0.88	473	3.3	16.0	6.9	13.4	8.0	11.9

*BG = baghouse inlet sampling port
**Combustion rate for BG samples are assumed to equal rate at Port 14
***BG sampling rate is set equal to Port 14 rate; this is not an isokinetic sample

APPENDIX B

Calculations for Composition of Gas for Hg-Ash Fixed Bed Experiments

Table B-1. Calculations for Composition of Gas for Hg-ash Fixed Bed Experiments

Ultimate Analysis	Wyodak			Ohio 5, 6, 7			ND Lignite		
		Required for combustion, lb/lb fuel @ 100% total air			Required for combustion, lb/lb fuel @ 100% total air			Required for combustion, lb/lb fuel @ 100% total air	
	lb/lb fuel	O_2	Total air	lb/lb fuel	O_2	Total air	lb/lb fuel	O_2	Total air
C	0.512	1.362	5.902	0.711	1.890	8.194	0.386	1.026	4.447
H_2	0.036	0.289	1.251	0.048	0.382	1.652	0.026	0.207	0.894
O_2	0.123			0.081			0.125		
N_2	0.007			0.014			0.004		
S	0.003	0.003	0.014	0.026	0.026	0.112	0.006	0.006	0.027
H_2O	0.258			0.023			0.359		
Cl_2	0.000			0.001			0.000		
ASH	0.060			0.097			0.094		
SUM	1.000	1.654	7.167	1.001	2.299	9.959	1.000	1.239	5.368
Less O_2 in fuel		-0.123	0.266		-0.081	0.266		- 0.125	0.266
Required @ 100% total air		1.592	6.901		2.237	9.693		1.177	5.102
Required @120% total air		1.910	8.281		2.684	11.631		1.412	6.122
Excess Air			1.380			1.939			1.020
Excess O_2		0.318			0.447			0.235	

Combustion products	lb/lb fuel	% or ppm (wet basis)	lb/lb fuel	% or ppm (wet basis)	lb/lb fuel	% or ppm (wet basis)
CO_2	1.874	13.8	2.601	14	1.412	13.7
H_20	0.691	12.4	0.605	7.9	0.671	15.8
SO_2	0.006	323 ppm	0.052	1928 ppm	0.013	836 ppm
O_2	0.318	3.1	0.447	3.3	0.235	3.0
N_2	6.379	70.7	8.954	74.7	4.720	67.5
Chlorine as Cl_2	0.000	2 ppm	0.001	58 ppm	0.000	ppm